RECOGNITION OF "MINIMAL" LIGANDS BY ENOLASE SUPERFAMILY ENZYMES

by

Sarah A. E. Aboushawareb

Submitted in partial fulfilment of the requirements
for the degree of Master of Science

at

Dalhousie University
Halifax, Nova Scotia
November 2016

Table of Contents

LIST OF FIGURES

LIST OF SCHEMES

LIST OF TABLES

ABSTRACT

Enolase superfamily (ENS) enzymes share a common half-reaction, the Mg^{2+}-dependent, Brønsted base-catalyzed abstraction of an α-proton from a carboxylic acid substrate to form an enolate. The active site architecture of the ENS enzymes L-talarate/galactarate dehydratase (TGD), D-(-)-tartrate dehydratase (TarD), and *β*-methylaspartate ammonia-lyase (MAL) were probed using the "minimal" ligands, tartronate and 3-hydroxypyruvate (3-HP). Both were weak competitive inhibitors of TarD (K_m = 27 ± 7 μM) with K_i values of 500 ± 100 μM and 1800 ± 400 μM, respectively, and weak inhibitors of TGD (K_m = 900 ± 200 μM) with IC_{50} values of 17 ± 1 mM and 15 ± 1 mM, respectively. MAL (K_m = 980 ± 160 μM) bound tartronate weakly, but bound 3-HP as a good competitive inhibitor (K_i = 1800 ± 200 μM). Mass spectrometry experiments revealed that 3-HP forms a Schiff base with the catalytic Lys in the active sites of all three enzymes, which is not deprotonated as it is with MR. Investigation of the metal ion binding site of TarD revealed that 0.5 M EDTA did not obviate activity as it does for MR.

LIST OF ABBREVIATIONS USED

3-HP	3-hydroxypyruvate
5-KDG	5-keto-4-deoxy-D-glucarate
BSA	bovine serum albumin
EDTA	ethylenediaminetetraacetic acid disodium salt hydrate
ENS	enolase superfamily
Hepes	4-(2-hydroxyethyl)piprazine-1-ethanesulfonic acid
IPTG	isopropyl β-D-1-thiogalactopyranoside
LB	Luria-Bertani
MAL	β-methylaspartate ammonia-lyase
MDH	L-malate dehydrogenase
MLE	muconate lactonizing enzyme
MR	mandelate racemase
m/z	mass-to-charge ratio
NADH	nicotinamide adenine dinucleotide – reduced form
NMR	nuclear magnetic resonance
OD	optical density
PDB	Protein Data Bank
TarD	D (-)-tartrate dehydratase
TGD	L-talarate / galactarate dehydratase
Tris	tris(hydroxymethyl)aminomethane

ACKNOWLEDGEMENTS

First of all, I would like to thank Dr. Bearne, for being a tough yet patient teacher and for being supportive in both my thesis writing as well as engaging in extra-curricular activities. I would also like to extend my thanks to Dr. Jakeman and Dr. Rainey, members of my supervisory committee, for their help and guidance with my project. I would also like to thank Dr. Ewart for her support.

I would like to thank all members of the Bearne lab with whom I have had the pleasure of working, specially Dr. Nagar for his help with the kinetic assays, Gregory McCluskey for his help with the molecular biology aspect of my project (especially the design of the MAL primers), and Dr. Douglas for his help with the NMR experiments as well as for their mentorship. I would like to thank Dr. Cohen for running the mass spectrometry experiments and for his help with the data interpretation. I would also like to thank Dr. Rohde and Dr. Prithiviraj for providing the genomic DNA. I also extend my thanks to the funding agencies: The Natural Sciences and Engineering Research Council of Canada (NSERC) and the Nova Scotia Graduate Scholarship.

I would also like to thank Paul Briggs and Heidi MacKinnon with whom I have worked in the teaching lab. I would also like to thank Roisin, Barb, Chris, Sarah, and Brenda from the department office. I would also like to thank all members of Dalhousie Biochemistry Student Society (DBSS) and Faculty of Medicine Graduate Student Society (FMGSS) with whom I have had the pleasure to work.

It is an honour to receive the 2014/2015 Doug Hogue award and for that I would like to thank both the department and the Hogue family.

It has been a pleasure and a fruitful experience working with Dr. McSweeney to facilitate workshops and discussion sessions at the Center for Teaching and Learning at Dalhousie University.

I have met some of the best people I have known here in Halifax, both inside and outside the department, and so I would like to thank Patricia, Ayah, Saki, Laura, Hayam, Anna, Lisa, Emma, Iman, Hidaya, and Qinyan.

I am very fortunate to have a family that respects and supports my decisions in life, and for that I am very grateful and thankful to my parents, sister, grandmother, aunt and her family, and my best friend Salma.

My undergraduate studies at the German University in Cairo have helped shaping my personality and have provided me with strong scientific background as well as important skills such as time-management, meeting deadlines, and hard work. Thus, I am very grateful to all my professors there specially Dr. Abou Aisha, Dr. El-Azizi, Dr. El-Sharkawy, and Dr. Mansour for their advice, support, and mentorship.

CHAPTER 1 INTRODUCTION

1.1 ENOLASE SUPERFAMILY BACKGROUND

The enolase superfamily (ENS) comprises mechanistically-diverse, but structurally-similar enzymes. Members of the superfamily share a common half-reaction, i.e., the Mg^{2+}-dependent, Brønsted base-catalyzed abstraction of an α-proton from a carboxylic acid substrate to form an enolate intermediate. The members of the superfamily were classified into three main subfamilies according to the Brønsted acid-base catalysts present in the active site. These are the enolase subfamily which has two Lys residues in its active site, the mandelate racemase (MR) subfamily which utilizes a Lys and/or a His residue, and the muconate lactonizing enzyme (MLE) subfamily, which contains only one Brønsted acid-base catalyst, Lys (Babbitt *et al*., 1996). However, as more members of the superfamily were identified, the classification expanded to comprise seven subgroups: enolase, MR, *β*-methylaspartate ammonia-lyase (MAL), D-glucarate dehydratase (GlucD), galactarate dehydratase, MLE, and mannonate dehydratase (Gerlt, Babbitt, Jacobson, & Almo, 2012).

The ENS of enzymes serves as a paradigm to understand the relationship between homologous enzymes in terms of their sequence, structure, and function. Although there are large libraries of sequences and structures of homologous enzymes, the presence of highly-divergent enzymes, such as MAL in the case of the mechanistically-diverse ENS,

presents a challenge for correct assignment of function (Gerlt & Babbitt, 2001;Gerlt, Babbitt, Jacobson, & Almo, 2012).

1.1.1 Mechanistic Diversity

The ENS comprises mechanistically-diverse enzymes that share a common half-reaction, the Brønsted base-catalyzed abstraction of an α-proton from a carboxylic acid substrate to form an enolate intermediate, after which each enzyme catalyzes a different overall reaction. Gerlt and Gassman (1993) reported that, according to Marcus formalism, the abstraction of the α-proton presents both an intrinsic kinetic barrier ($\Delta G^{\ddagger}_{int}$) and a thermodynamic barrier (ΔG°) for the reaction (Gerlt & Gassman, 1993). The intrinsic kinetic barrier ($\Delta G^{\ddagger}_{int}$) (defined as the energy barrier in absence of a thermodynamic barrier) arises from the formation of an enolate intermediate which is energetically unfavorable due to the change of the hybridization of the α-carbon and the formation of a negative charge, after the initial deprotonation, which requires solvent rearrangement (entropic cost). They suggest that MR overcomes this problem by having Glu 317 located at a distance close enough to form a low barrier hydrogen bond with an oxygen of the carboxylate group, thereby overcoming the intrinsic kinetic barrier. Low barrier hydrogen bonds, or short strong hydrogen bonds, form when the distance between two heteroatoms of two groups with similar pK_a values is shorter than the sum of their van der Waals radii; this leads to the equal sharing of the proton between both heteroatoms (Gerlt & Gassman, 1993). The thermodynamic barrier (ΔG°) is due to the high pK_a value of the α-proton of carboxylic acid substrates which is estimated at 22-25 (Babbitt *et al*., 1996; Gerlt, Kozarich, Kenyon, & Gassman, 1991) which is higher than the pK_a of the Brønsted base catalyst in the active site. Gerlt and Gassman (1993) suggested that this barrier is overcome through electrophilic

catalysis by Glu 317 in the active site of MR (Gerlt & Gassman, 1993). Guthrie and Kluger (1993) have suggested that electrophilic catalysis is not sufficient for the stabilization of the intermediate in the active site of MR, and that the enolate intermediate formed in the active site of MR is stabilized through the electrostatic interactions with the essential divalent ion (Guthrie & Kluger, 1993).

1.1.2 Structural Similarity & Active Site Diversity

Most members of the ENS share a common overall structure consisting of two distinct domains, a modified TIM barrel domain where the active site is located and a capping domain formed by the N- and C-termini of the protein or just one of the termini, which contains residues that determine the substrate specificity. Although the enzymes share this fold, there are differences in the identities and locations of the active site residues upon which the enzymes are classified into the seven subgroups. The active site residues interacting with the Mg^{2+} are conserved in all subgroups and are located on the third, fourth, and fifth β-strands of the barrel domain; however, it is the identities of the active site residues and their locations that permit further classification of the enzymes into subgroups (Gerlt *et al*., 2012). Members of the enolase subgroup possess a Lys residue at the end of the sixth β-strand which acts as the Brønsted base that abstracts the α-proton and a Glu residue located at the end of the second β-strand that acts as the Brønsted acid that catalyzes the subsequent dehydration reaction catalyzed by the enzyme. For MAL, the active site Lys residue, located at the end of the sixth β-strand, abstracts the α-proton to form the enolate intermediate, however, a Brønsted acid is not needed in the case of MAL for the subsequent deamination reaction. Two Lys residues are present in the active site of MLE, and are located at the ends of the second and sixth β-strands. In the MR subgroup, the active

site possesses a His/Asp dyad with His and Asp located at the ends of the seventh and sixth β-strands, respectively. In this dyad, the His residue acts as the Brønsted base that abstracts the α-proton in the initial half-reaction. Other Brønsted acid-base catalysts are present at the ends of the second, third, or fifth β-strands. For the GlucD subgroup, a dyad with His and Asp is also present at the ends of the seventh and sixth β-strands, respectively. At the end of the second β-strand, a catalytic Lys is present. However, for GlucD there is an Asn residue that interacts with the Mg^{2+} in the active site that is located at the end of the fifth β-strand (Yew *et al*., 2006). For the D-mannonate dehydratase subgroup, a Tyr residue from a Tyr/Arg dyad present in the 150-180s loop between the second and third β-strands acts as the Brønsted base that abstracts the α-proton, and a His residue located at the end of the third β-strand acts as the Brønsted acid that facilitates the departure of the hydroxyl group (Rakus *et al*., 2007). The seventh subgroup is the galactarate dehydratase subgroup of which the members lack the 20s loop that is typically important for the substrate specificity determination. In addition, a second Mg^{2+} ion is present in the capping domain that actually plays the specificity-determining role of the 20s loop. This Mg^{2+} ion is coordinated by Asp, His, and Thr residues. The canonical Mg^{2+} ion in the barrel domain is coordinated in a non-canonical fashion with one of the three ligands being a His present at the end of the fifth β-strand. Furthermore, the members of this subgroup have a Tyr/Arg dyad at the end of the second β-strand where the Tyr acts as the Brønsted base and two Tyr residues reside on the opposite face, one of which acts as a Brønsted acid (Rakus *et al*., 2009).

According to the aforementioned classifications and from consideration of the x-ray crystal structures, it can be concluded that the active site architectures of enzymes from any given subgroup are similar. Indeed, examination of the crystal structures reveals that

the distances between the Brønsted acid-base catalysts and the α-carbon of ligands as well as that between the Mg^{2+} in the active site and the Brønsted acid-base catalysts are very similar. Thus, the work presented here aims at gaining further insight into the subtle features of the active site architectures of the members of the ENS using the "minimal" ligands, tartronate and 3-hydroxypyruvate (3-HP). Three enzymes were chosen for a detailed study: D-(-)-tartrate dehydratase and L-talarate/galactarate dehydratase, both of which belong to the MR subgroup, and *β*-methylaspartate ammonia-lyase, which belongs to the MAL subgroup. The two small molecule inhibitors, tartronate and 3-HP, are used to interrogate the active site of each of these enzymes.

1.2 MANDELATE RACEMASE SUBGROUP

Based on the identity of active site residues and their positions, as well as the identity of the ligands for the Mg^{2+}, heterofunctional enzymes of the ENS are assigned to the MR subgroup. Only one member of the subgroup (MR) catalyzes a racemization reaction, whereas other members of the subgroup catalyze the dehydration of acid sugars (Gerlt, Babbitt, & Rayment, 2005). The MR subgroup currently comprises nine enzyme types, which include D-arabinonate dehydratase, D-galactonate dehydratase, D-tartrate dehydratase (TarD), gluconate dehydratase, L-fuconate dehydratase, L-galactonate dehydratase, L-talarate/galactarate dehydratase (TGD), mandelate racemase (MR), and rhamnonate dehydratase (Akiva *et al*., 2014).

1.2.1 D (-)-Tartrate Dehydratase

1.2.1.1 TarD from *Bradyrhizobium japonicum*

TarD ((*S,S*)-tartrate hydro-lyase, E.C. 4.2.1.81) catalyzes the Mg^{2+}-dependent dehydration of D-tartrate, an acid sugar, to form oxaloacetate (**Scheme 1.1**) (Yew *et al.*, 2006). The gene encoding a putative TarD (GI:27381841) from *Bradyrhizobium japonicum* was cloned from genomic DNA by Gerlt and co-workers and the protein was then expressed, purified, and assayed to verify its function and to determine the kinetic constants (Yew *et al*., 2006).

1.2.1.2 Structure and Active Site Architecture of TarD

Like other members of the ENS, TarD consists of two domains, a modified TIM-barrel domain and a capping domain. The $(\alpha/\beta)_7\beta$-barrel domain contains the Mg^{2+} ligands, Asp 213, Glu 239, and Glu 265 at the ends of the third, fourth, and fifth β-strands as well as the active site Brønsted acid-base residues, Lys 184 and the His 322/Asp 292 dyad at the ends of the second, seventh, and sixth β-strands, respectively, in the barrel domain. The N- and C- termini of the protein form the capping domain which constitutes the binding site for the substrate, D-tartrate (**Figure 1.1 - B**). The crystal structure shows that the minimal biological unit of TarD is a dimer and that the active site is partially located at the interface between those two dimers, with the presence of an interdigitating loop going from one subunit into the active site of the adjacent subunit (**Figure 1.1 - A**) (Yew *et al*., 2006).

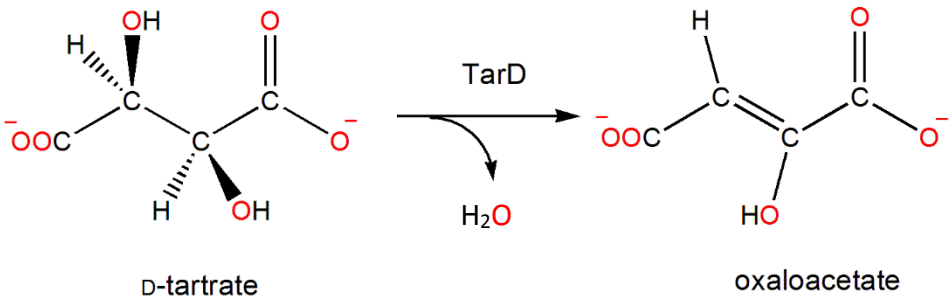

Scheme 1.1 Dehydration reaction catalyzed by TarD. TarD catalyzes the dehydration reaction of D-tartrate to form the enol tautomer of oxaloacetate. (Yew *et al*., 2006)

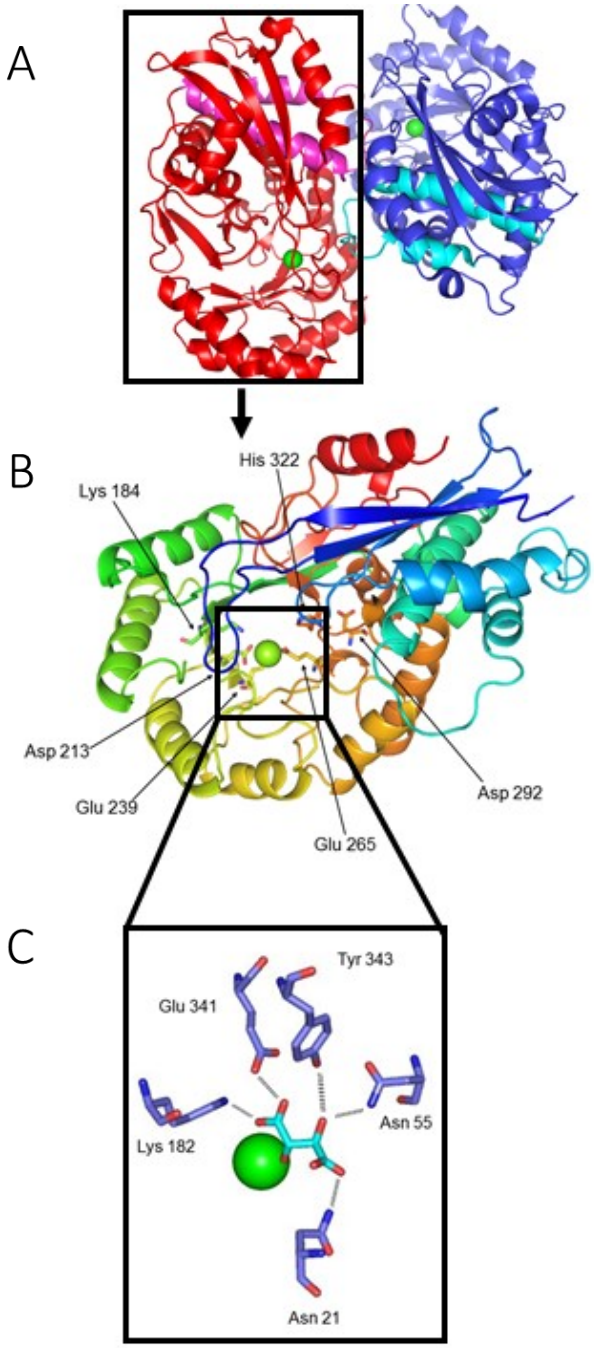

Figure 1.1 Crystal structure of wild-type TarD. (A) TarD exists as a homodimer (red and blue) and each monomer has an interdigitating loop (magenta and cyan) that reaches to the active site of the other monomer. (B) The monomer of TarD consists of a capping domain and a barrel domain where the active site is located. The active site has an essential Mg^{2+} ion that is stabilized through interactions with Asp 213, Glu 239, and Glu 265. The two Brønsted acid-base catalysts, Lys 184 and His 322, are also shown where His exists in a His 322/Asp 292 dyad. (C) The active site of TarD with bound *meso*-tartrate shows the interactions that stabilize the ligand in the active site. Water molecule ligands to Mg^{2+} are not shown (PDB entry 2DW7).

Three crystal structures of TarD are available: (1) wild-type TarD with only Mg^{2+} as a ligand (1TZZ), (2) wild-type TarD with the competitive inhibitor *meso*-tartrate and Mg^{2+} as ligands (2DW7) (**Figure 1.1**) and (**Figure 1.2**), and (3) the K184A mutant of TarD with the substrate D-tartrate and Mg^{2+} as the ligands (2DW6) (**Figure 1.2**). The crystal structure of TarD complexed with *meso*-tartrate and Mg^{2+} (**Figure 1.1 - C**) shows that *meso*-tartrate interacts with the Mg^{2+} through one of the oxygens in the proximal carboxylate group (carboxylate chelating the metal ion). This carboxylate group also forms a hydrogen bond with the ε-ammonium group of the active site Lys 182 located at the end of the second *β*-strand of the barrel domain. A second hydrogen bond is formed between the same carboxylate group through its second oxygen atom and Glu 341 present on the end of the eighth *β*-strand of the barrel domain. The inhibitor also forms hydrogen bonds with Asn 21 in the 20s loop of the capping domain through the distal carboxylate group. The proton on C2 of *meso*-tartrate is oriented towards Lys 184 in the KXK motif, which is on the end of the second *β*-strand in the barrel domain and acts as a Brønsted acid-base catalyst. At the ends of the seventh and sixth *β*-strands are His 322 and Asp 292, which form a catalytic dyad with His 322 acting as a Brønsted acid-base catalyst. Accordingly, the two Brønsted acid-base catalysts in the active site, Lys 184 and His 322, are present on opposite sides of the active site. Unlike the substrate, D-tartrate, which has the (2*S*,3*S*) stereochemistry, *meso*-tartrate has (2*S*,3*R*) stereochemistry. Thus, the hydroxyl group at C3 in *meso*-tartrate appears to form a hydrogen bond with Asn 55 present in the capping domain and with Tyr 343 and His 322 at the ends of the second and seventh *β*-strands, respectively (Yew *et al*., 2006).

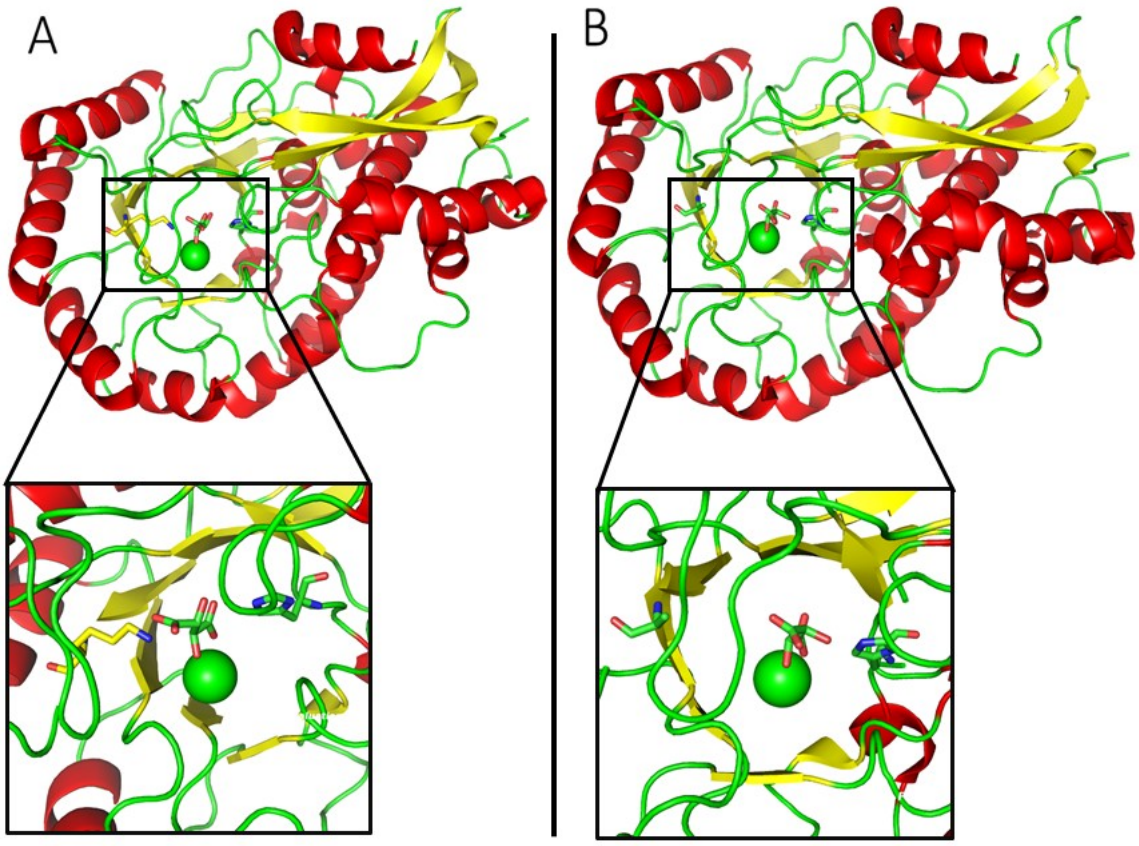

Figure 1.2 Productive binding of the ligand is determined by its geometry. The 3-OH group needs to be orthogonal to the α-proton at C2 to be eliminated in the dehydration reaction and thus, (A) when *meso*-tartrate is bound to wild-type TarD, there is no dehydration (PDB entry 2DW7). (B) D-tartrate bound to TarD K148A mutant where the 3-OH group is in a productive orientation (PDB entry 2DW6).

Comparing the geometry of ligand binding in the crystal structures of TarD K184A mutant with D-tartrate and Mg^{2+} as ligands with that of wild-type TarD with *meso*-tartrate and Mg^{2+} bound at the active site (**Figure 1.2**), it is evident that the hydroxyl group at C3 needs to be orthogonal to the α-proton at C2 to be eliminated in the dehydration reaction with His 322 acting as the Brønsted acid catalyst (Yew *et al*., 2006).

1.2.1.3 Mechanism of the Reaction Catalyzed by TarD

The reaction catalyzed by TarD has been studied in detail by Gerlt and co-workers (Yew *et al*., 2006), and starts with α-proton abstraction followed by the formation of an enediolate intermediate, which is stabilized by the Mg^{2+} ion at the active site. The intermediate can undergo a dehydration reaction through vinylogous *β*-elimination of the C3 hydroxyl group with the help of the Brønsted acid catalyst, His 322. This leads to the formation of the enol tautomer of oxaloacetate as the product (**Scheme 1.2**). Alternatively, the enediolate intermediate may be re-protonated at C2 by the conjugate acid of the Brønsted base leading to the regeneration of the substrate, D-tartrate (**Scheme 1.2**). The occurrence of this latter reaction was confirmed through deuterium exchange experiments in which deuterated buffer was used and the reaction was followed using nuclear magnetic resonance (NMR) spectroscopy. The resulting ^1H NMR spectrum showed a decrease in the signal intensity corresponding to the protons of D-tartrate indicating the formation of the product, oxaloacetate, which has no associated signal due to the rapid exchange of D-tartrate protons with the deuterated solvent. It also showed transient appearance of a signal with an upfield chemical shift corresponding to the C3 proton of D-tartrate, indicating the existence of a competing exchange reaction of the α-proton catalyzed by the polyprotic Brønsted base catalyst Lys184 (Yew *et al*., 2006).

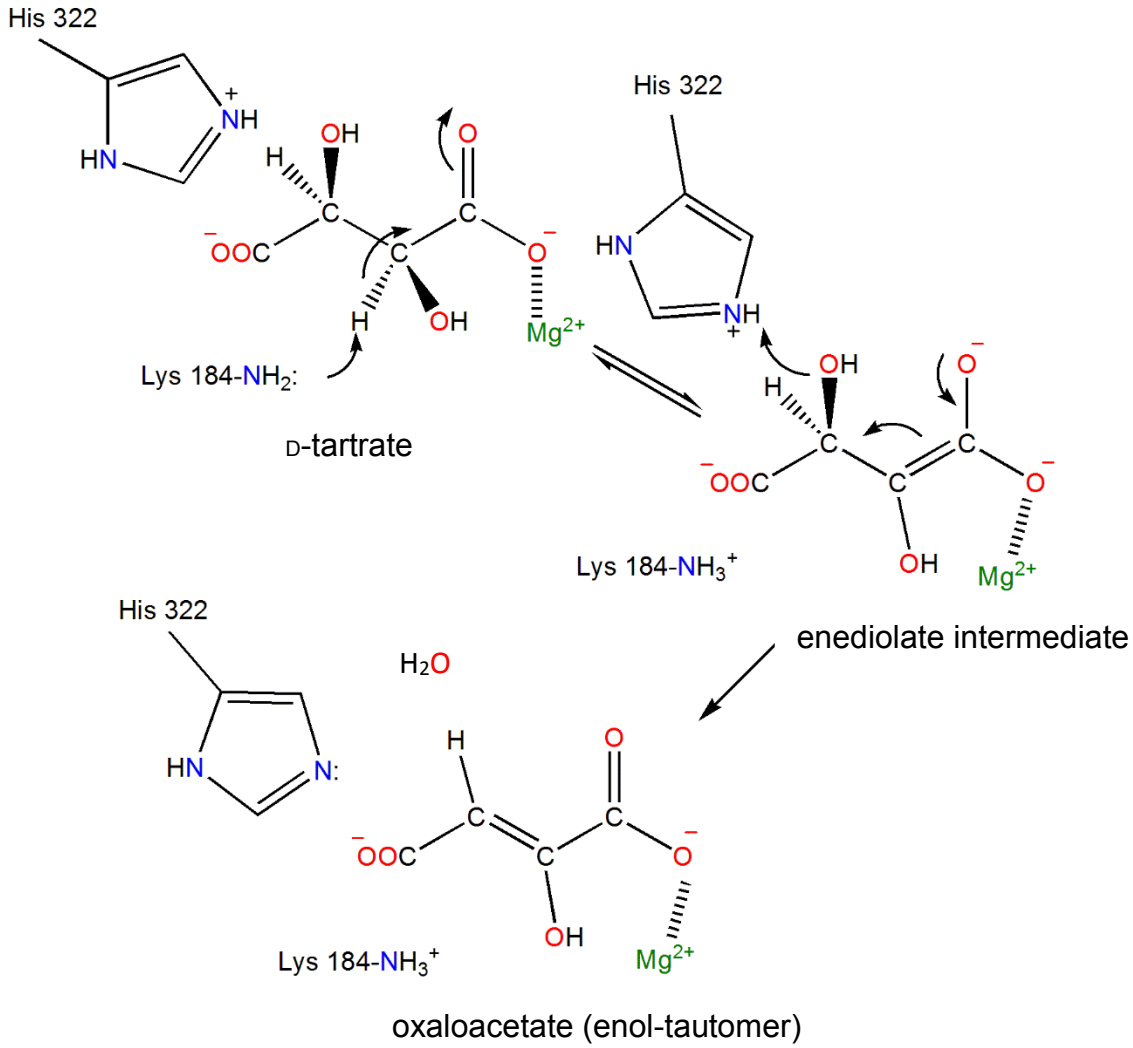

Scheme 1.2 Mechanism of TarD-catalyzed dehydration of D-tartrate. The reaction starts with the initial abstraction of the α-proton to form the enediolate intermediate that is stabilized in the active site by the Mg^{2+} ion. This is followed by the protonation of the hydroxyl leaving group to form the enol tautomer of oxaloacetate. Adapted from (Yew *et al*., 2006)

The dehydration reaction catalyzed by TarD was found to be stereorandom. After the formation of the enediolate intermediate and the Brønsted acid-assisted vinylogous *β*-elimination of the C3 hydroxyl group, the enol-tautomer of oxaloacetate is formed. Keto-enol tautomerism then follows, during which there is protonation from the solvent which can give rise to either retention or inversion of configuration. Detailed deuterium exchange experiments were conducted which ultimately revealed that the product of the dehydration reaction catalyzed by TarD is the enol-tautomer of oxaloacetate which is released from the enzyme and then undergoes nonenzymatic keto-enol tautomerization forming the keto-tautomer of oxaloacetate that serves as the substrate for MDH (**Scheme 1.3**) in the coupled assay (see below).

1.2.1.4 Assay of TarD Activity

Kinetics of the TarD-catalyzed reaction were determined using a continuous coupled assay with MDH as the coupling enzyme, which reduces oxaloacetate to L-malate with concomitant oxidation of NADH to NAD^+, resulting in a decrease in absorbance at 340 nm. The turnover number, k_{cat}, was found to be 7.3 s^{-1}, the Michaelis constant, K_m, was 0.086 mM, and the enzyme efficiency, k_{cat}/K_m, was found to be 8.5×10^4 $M^{-1}s^{-1}$ (Yew *et al*., 2006).

.

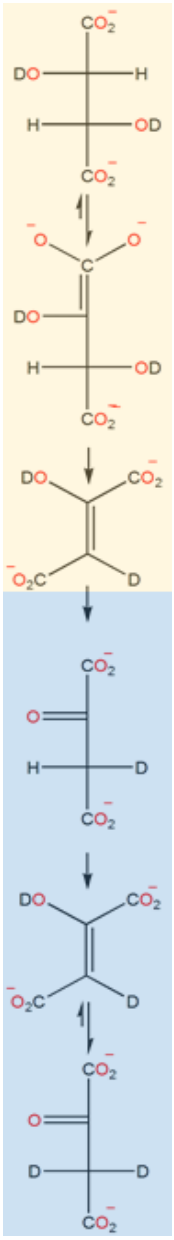

Scheme 1.3 TarD catalyzes the formation of the enol-tautomer of oxaloacetate. The TarD-catalyzed reaction results in the formation of the enol-tautomer of oxaloacetate (highlighted in orange) which then undergoes keto-enol tautomerization nonenzymatically to form the keto-tautomer (highlighted in blue). (Yew *et al*., 2006)

1.2.2 L-Talarate/Galactarate Dehydratase

1.2.2.1 TGD from *Salmonella typhimurium*

TGD (E.C. 4.2.1.156, E.C. 4.2.1.41) catalyzes the Mg^{2+}-dependent dehydration reaction of two substrates, L-talarate or galactarate, to form 5-keto-4-deoxy-D-glucarate (5-KDG) (**Scheme 1.4**). The gene encoding a putative TGD (GI: 16766982) from *Salmonella typhimurium* LT2 has been cloned from genomic DNA and the protein was then expressed, purified, and assayed to verify its function and to determine the kinetic constants (Yew, Fedorov, Fedorov, Almo, & Gerlt, 2007).

1.2.2.2 Structure and Active Site Architecture of TGD

Like other members of the ENS, TGD consists of two domains, an $(\alpha/\beta)_7\beta$-barrel domain and a capping domain. The $(\alpha/\beta)_7\beta$-barrel domain contains the divalent cation ligands, Asp 226, Glu 252, and Glu278, at the ends of the third, fourth, and fifth β-strands as well as the Brønsted acid-base catalysts, Lys 197 at the end of the second β-strand and a dyad of His 328 and Asp 301 at the ends of the seventh and sixth β-strands, respectively (**Figure 1.3- C**). Similar to the active-site architecture in TarD, the arrangement of the two Brønsted acid-base catalysts in TGD places these two residues on opposite sides of the active site. The capping domain is again formed from the N- and C-termini in the of the protein, forming a pocket for binding the substrate, either L-talarate or galactarate. However, in TGD and unlike TarD, the N-terminal residues 3-26 do not contribute to the structure of the capping domain. Instead, these residues wrap around another subunit of an adjacent dimer (**Figure 1.3 – A & B**) (Yew *et al*., 2007).

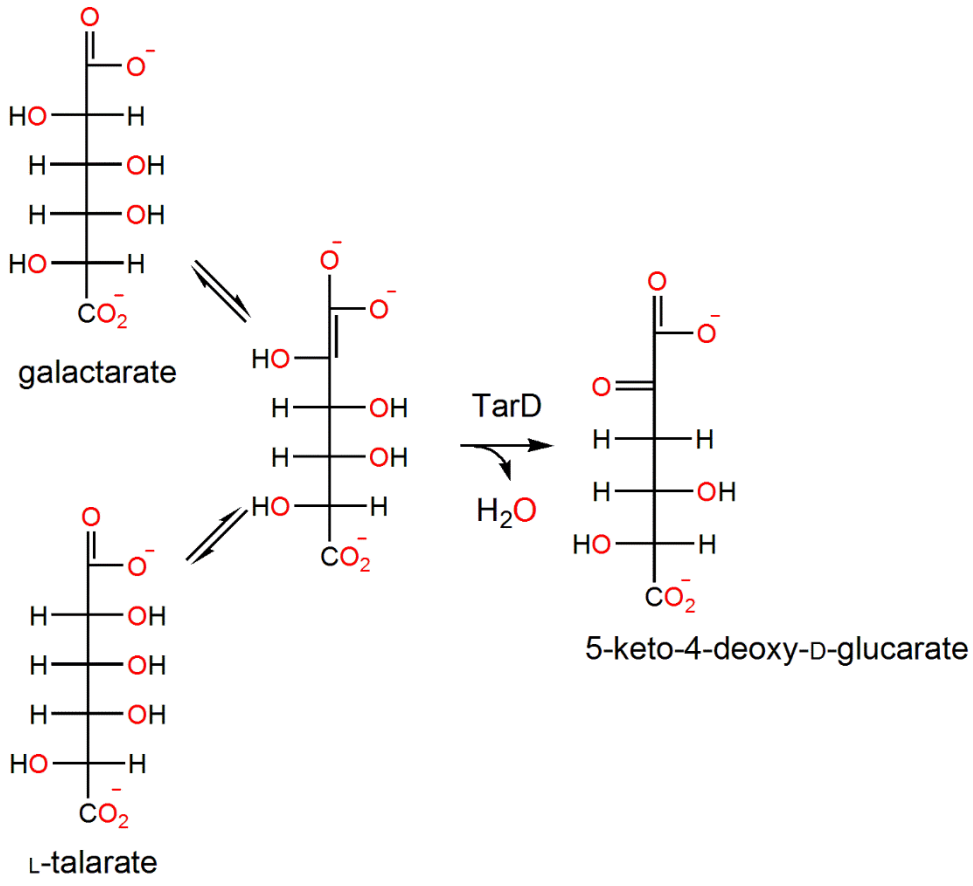

Scheme 1.4 TGD-catalyzed dehydration of galactarate & L-talarate. TGD catalyzes the dehydration of either galactarate or D-talarate to form 5-keto-4-deoxy-D-glucarate (5-KDG). It also catalyzes the epimerization between the two substrates. Adapted from (Yew, Fedorov, Fedorov, Almo, & Gerlt, 2007)

Three crystal structures have been solved for TGD: (1) wild-type TGD with no ligands in the active site (2PP0), (2) wild-type TGD with L-lyxarohydroxamate, an intermediate analogue, and Mg^{2+} as ligands (2PP1) (**Figure 1.3**), and (3) the K197A mutant of TGD with L-glucarate, the C4-epimer of galactarate, and Mg^{2+} as ligands (2PP3). These crystal structures of TGD show the enzyme to be a tetramer of dimers, similar to MR. Two types of dimers, A & B, were identified for TGD. Dimer A comprises two monomers in which the N-terminal residues 116-124 of each monomer reaches between the capping and $(\alpha/\beta)_7\beta$-barrel domains in the other monomer (**Figure 1.3 - A**). Dimer B is comprised of two monomers that are not connected with a crystallographic axis and have their N-terminal residues 3-26 wrapping around the other monomer (**Figure 1.3 - B**). Unlike TarD, TGD does not possess interdigitating loops, and only the N-terminal residues 116-124 described above in dimer A are shared between dimers (Yew *et al*., 2007).

By examining the active-site architecture in the crystal structure of wild-type TGD with L-lyxarohydroxamate and Mg^{2+} as ligands, interactions between residues in the active site and the ligands can be determined (**Figure 1.3 - D)**. L-Lyxarohydroxamate serves as a bidentate ligand for the Mg^{2+} in the active site and interacts with it through its hydroxamate group which replaces a carboxylate group in the substrates, galactarate or L-talarate. It also forms two hydrogen bonds through the oxygens of its distal carboxylate group, one with the guanidinium group of Arg 83 and the other with a water molecule that interacts with carbonyl group of Val 44 and the guanidinium group of Arg 83 through hydrogen bonds. The hydroxyl group at C4 forms two hydrogen bonds as well, one with the carboxyl group

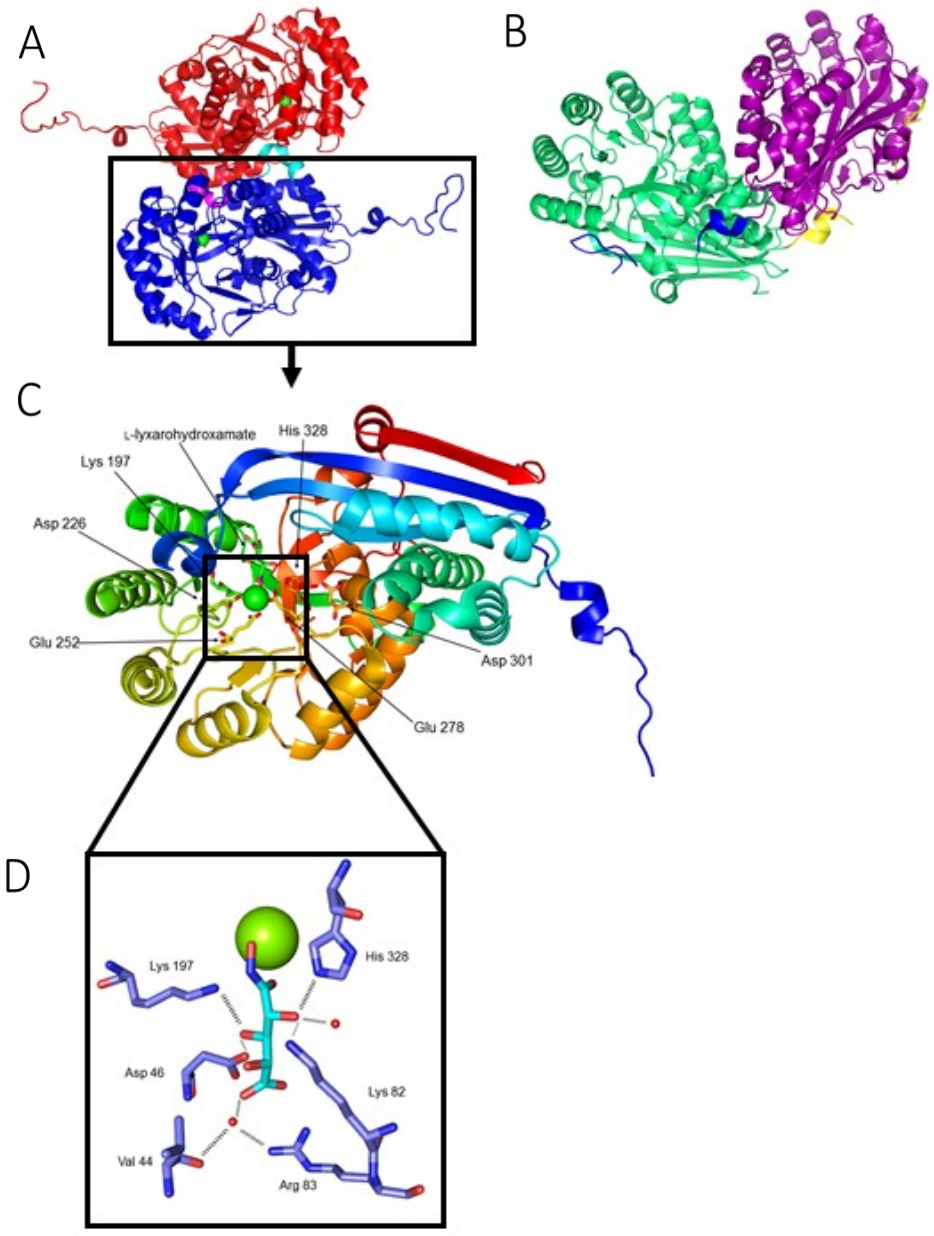

Figure 1.3 Crystal structure of wild type TGD. (A) TGD in dimer A exists as a homodimer (red and blue) and each monomer has an interdigitating loop (magenta and cyan) that reaches to the active site of the other monomer. (B) TGD in dimer B exists as a homodimer (green and purple) where each monomer has a loop that goes around the neighboring one (yellow and blue). (C) The monomer of TGD consists of a capping domain and a barrel domain where the active site is located. The active site has an essential Mg^{2+} ion that is stabilized through interaction with Asp 226, Glu 252, and Glu 278. The two Brønsted acid-base catalysts, Lys 197 and His 328, are also shown where His exists in a His 328/Asp 301 dyad. (D) The active site of TGD with bound L-lyxarohydroxamate shows the interactions that stabilize the ligand in the active site. Water molecule ligands to Mg^{2+} are not shown (PDB entry 2PP1).

of Asp 46 and another with the ε-ammonium group of Lys 197. The hydroxyl group at C3 forms hydrogen bonds with the ε-ammonium group of Lys 82, the imidazolium group of His 328, and a water molecule. This extensive network of hydrogen bonds formed between the ligand and residues of the active site determines the substrate specificity of the enzyme (Yew *et al*., 2007).

1.2.2.3 Mechanism of the Reaction Catalyzed by TGD

TGD catalyzes the Mg^{2+}-dependent dehydration reaction of two substrates, L-talarate and galactarate, which are C2-epimers (**Scheme 1.5**). The dehydration reaction catalyzed by TGD occurs along with a competing epimerization reaction between the two substrates in which the enolate intermediate formed partitions between the two processes. The rate of the epimerization reaction is 30% of the overall rate for dehydration when L-talarate is the substrate; however, there is negligible epimerization observed when galactarate is used as the substrate. This was detected upon comparing the kinetic parameters obtained using a polarimetric assay versus a continuous coupled kinetic assay for the TGD-catalyzed dehydration of L-talarate, in which time-dependence was observed. This was also demonstrated by directly monitoring two substrates and product using ^{1}H NMR spectroscopy (Yew *et al*., 2007).

Lys 197 was found to be the galactarate-specific Brønsted base catalyst while His 328 was found to be the L-talarate-specific Brønsted base. This was first hypothesized based on amino acid sequence alignments and the crystal structure of the active site. It was then further confirmed through deuterium exchange experiments using ^{1}H NMR spectro-

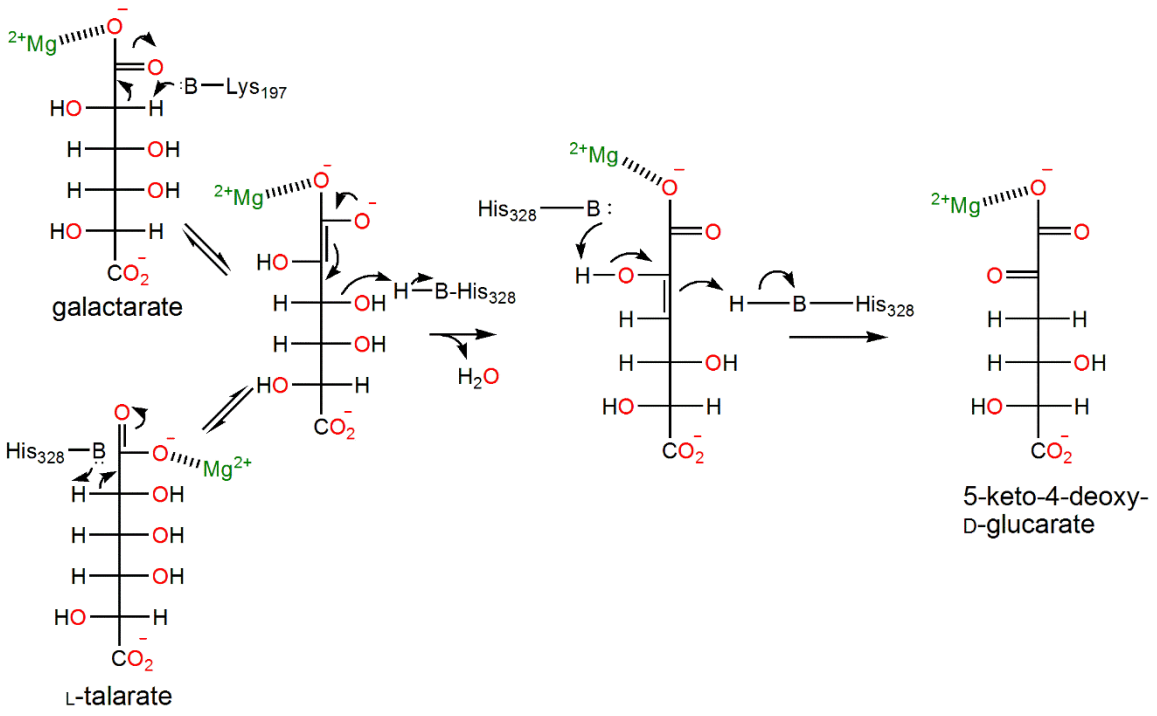

Scheme 1.5 Mechanism of TGD-catalyzed dehydration of galactarate and L-talarate. The TGD-catalyzed dehydration reaction starts with the initial abstraction of the α-proton to yield the enolate intermediate that is stabilized in the active site by the Mg^{2+} followed by protonation of the hydroxyl leaving group to yield 5-keto-4-deoxy-D-glucarate. Adapted from (Yew *et al*., 2007).

scopy. Incubation of L-talarate with wild-type TGD did not result in deuterium exchange which is in good agreement with His 328, a monoprotic base, being the Brønsted base specific for L-talarate. When the same experiment was conducted with galactarate, deuterium exchange was observed through the appearance of an upfield signal in the ^{1}H NMR spectrum corresponding to deuterium exchange at C2 position affecting the resonance of the C3 proton (Yew *et al*., 2007).

Accordingly, the mechanism of the TGD-catalyzed reaction is as follows: when galactarate is the substrate, Lys 197 acts as the Brønsted base that abstracts the α-proton leading to the formation of an enolate intermediate that is stabilized in the active site through interaction with the Mg^{2+}. The intermediate then partitions to a dehydration reaction to form the enol product, where His 328 acts as the Brønsted acid that protonates the C3 hydroxyl leaving group. The resulting enol product is further ketonized to form 5-KDG through the His 328-assisted protonation of the C3 position in a stereospecific manner. The other possibility is for the intermediate to undergo C2 re-protonation either from the same face to yield galactarate or from the opposite face to undergo epimerization and form L-talarate. When L-talarate is the substrate, His 328 acts as the Brønsted base that abstracts the α-proton to form the Mg^{2+}-stabilized enolate intermediate. In this case, the intermediate can also partition between the dehydration reaction through the His 328-catalyzed vinylogous *β*-elimination of the 3-hydroxyl group or it can undergo epimerization through re-protonation at the C2 position. Both ^{1}H and ^{13}C NMR spectroscopy experiments showed that the product exists as the α- and β-furanosyl hemiketals (**Scheme 1.5**) (Yew *et al*., 2007).

1.2.2.4 Assay of TGD Activity

The kinetic parameters of TGD were assessed using a continuous coupled assay that uses two coupling enzymes, 5-KDG aldolase and L-lactate dehydrogenase. The dehydration product, 5-KDG, acts as a substrate for 5-KDG aldolases to produce tartronate semialdehyde and pyruvate, where the latter serves as a substrate for L-lactate dehydrogenase to form L-lactate. The second coupling reaction requires NADH as a cofactor and its oxidation maybe followed at 340 nm using spectrophotometry. When galactarate was used as a substrate, the turnover number, k_{cat}, was found to be 3.6 s^{-1}, the Michaelis constant, K_m, was 0.33 mM, and the enzyme efficiency, k_{cat}/K_m, was found to be 1.1×10^4 $M^{-1}s^{-1}$. When L-talarate was used as the substrate, k_{cat}, was found to be 2.1 s^{-1}, K_m was 0.23 mM, and k_{cat}/K_m, was found to be 9.1×10^3 $M^{-1}s^{-1}$ (Yew *et al*., 2007).

1.3 3-METHYLASPARTATE AMMONIA-LYASE SUBGROUP

The ENS contains seven subgroups, as previously mentioned, and among these is the *β*-methylaspartate ammonia-lyase (3-methylaspartate ammonia-lyase or MAL) subgroup. This subgroup is highly divergent and it contains only one member, which is MAL (Gerlt *et al*., 2005; Rakus *et al*., 2007).

1.3.1 *β*-Methylaspartate Ammonia-Lyase

1.3.1.1 MAL from *Fusobacterium varium*

MAL (E.C. 4.3.1.2) catalyzes the reversible, Mg^{2+}-dependent deamination of *β*-methylaspartate to form mesaconate and ammonia (**Scheme 1.6**). Both (2*S*,3*S*)-3-methylaspartate (or L-*threo*-3-methylaspartate) and (2*S*,3*R*)-3-methylaspartate (or L-*erythro*-3-methylaspartate) serve as natural substrates for MAL (Bearne *et al.* 2001; De

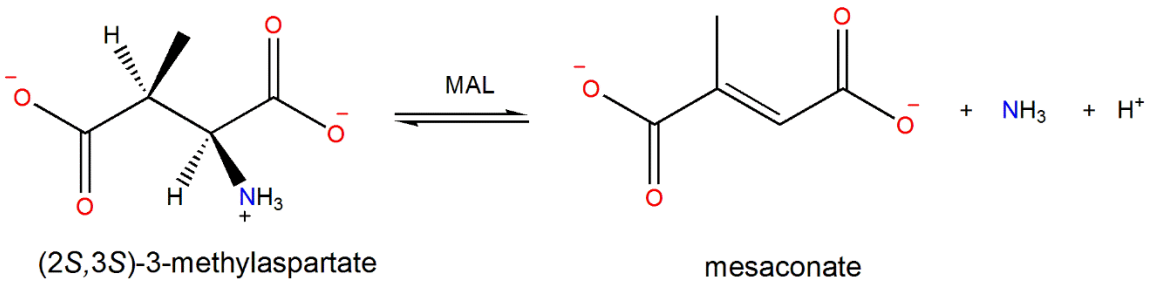

Scheme 1.6 Deamination reaction catalyzed by MAL. MAL catalyzes the deamination reaction of (2*S*,3*S*)-3-methylaspartate to form mesaconate. Adapted from (De Villiers, Veetil, Raj, De Villiers, & Poelarends, 2012).

Villiers *et al.* 2012). MAL from *Fusobacterium varium* has been purified, characterized, and assayed for activity and determination of its kinetic constants (Bearne *et al*., 2001; Ohkusa *et al*., 2003).

1.3.1.2 Structure and Active Site Architecture of MAL

Consistent with other members of the ENS, MAL has two distinct domains, a TIM barrel domain and a capping domain. The acidic residues Asp 238, Glu 273, and Asp 307 serve as ligands for the divalent metal ion, Mg^{2+}, and are located in the barrel domain (**Figure 1.4 – A & B**). MAL has a requirement for a monovalent ion as well, K^{+}, which was not observed through crystallography (Asuncion *et al.*, 2002; Goda, Minton, Botting, & Gani, 1992; Levy *et al*., 2002). Crystal structures of MAL are available from *Citrobacter amalonaticus* (1KKR and 1KKO) and *Clostridium tetanomorphum* (1KCZ, 1KDO, 3ZVI, and 3 ZVH) (Asuncion *et al*., 2002; Levy *et al*., 2002). For the crystal structure of MAL from *C. tetanomorphum*, the substrate was modelled in the active site. No crystal structures are reported for MAL from *Fusobacterium varium*.

The crystal structure for MAL from *C. amalonaticus* with Mg^{2+} and (*2S,3S*)-3-methylaspartic acid as ligands (1KKR) shows that the enzyme exists as a homodimer. In the active site of each monomer, the substrate interacts with the divalent cation through one of the oxygens of its proximal carboxylic acid (**Figure 1.4 – A & C**). The Mg^{2+} ion further interacts with one oxygen atom of each of the acidic residues that act as ligand for

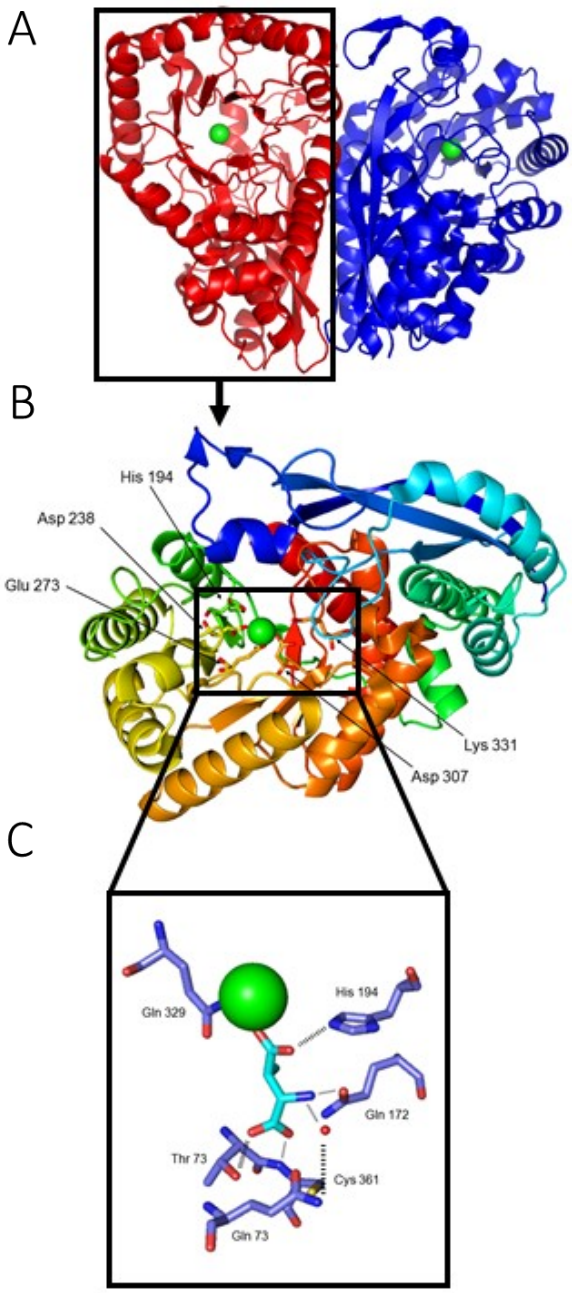

Figure 1.4 Crystal structure of wild type MAL. (A) MAL exists as a homodimer (red and blue). (B) The monomer of MAL consists of a capping domain and a barrel domain where the active site is located. The active site has an essential Mg^{2+} ion that is stabilized through interaction with Asp 238, Glu 273, and Asp 307. The two Brønsted acid-base catalysts, Lys 331 and His 194 are shown. (C) The active site of MAL with bound (2*S*,3*S*)-3-methylasparate shows the interactions that stabilize the ligand in the active site. Water molecule ligands to Mg^{2+} are not shown (PDB entry 1KKR).

the cation, Asp 238, Glu 273, and Asp 307. It also interacts with two water molecules, both of which form hydrogen bonds with the carboxyl oxygens of Glu 308 leading to octahedral coordination of the Mg^{2+} ion in the active site (**Figure 1.4 - B**). In the absence of the substrate in the *C. tetanomorphum* MAL structure, the coordinating carboxyl group is replaced by a water molecule. For the substrate, (2*S*,3*S*)-3-methylaspartate, the electron density map does not definitively show the exact orientation of the bound substrate because the electron density of the 2-amino and the 3-methyl groups are similar. However, electrostatic considerations would suggest that the substrate binds in such a way that the 2-amino group is further from the bound Mg^{2+} ion in the active site and the 3-methyl group closer to it. This orientation is also the more likely possibility since it provides the substrate with several interactions that help its stabilization in the active site of the enzyme where the oxygens of the 4-carboxyl group form hydrogen bonds with the nitrogen in the amide side chain of Gln 329 and the imidazole ring of His 194. The 2-amino group also forms hydrogen bonds with the oxygen in Gln 172 and the nitrogen of Gln 73 through a water molecule (**Figure 1.4- C**). The oxygens of the 1-carboxylate group form hydrogen bonds with the backbone amide of Cys 361, the side chain oxygen of Thr 360, and the side chain nitrogen in Gln 172. Not only does this orientation provide the substrate with an extensive hydrogen bond network within the active site, but it also ensures the packing of the 3-methyl group in a less-solvent-accessible pocket that consists of amino acid residues Leu 384 and Gln 172, in addition to Phe 170 and Tyr 356 in case of *C. tetanomorphum* MAL, which provides additional van der Waals interactions for stabilization. This orients the 2-amino group such that it faces a more solvent-accessible pocket (Asuncion *et al*., 2002;

Levy *et al*., 2002) (**Figure 1.4 - C**), which would also facilitate the release of ammonia, followed by release of mesaconate (Levy *et al*., 2002; Pollard *et al*., 1999).

1.3.1.3 Mechanism of the Reaction Catalyzed by MAL

As a member of the ENS, the MAL-catalyzed reaction is initiated by the abstraction of the α-proton to form the enolate intermediate, which is stabilized by the divalent ion in the active site, followed by a spontaneous deamination to form mesaconate and ammonia. The rate of the *anti*-deamination of the (2*S,*3*S*)-3-methylasparate is higher than that observed for the *syn*-deamination of (2*S,*3*R*)-3-methylaspartate (**Scheme 1.7**). For the reverse reaction, MAL catalyzes the stereoselective and regioselective amination of mesaconate to form (2*S,*3*S*)-3-methylasparate (the *threo*-isomer) as a major product and (2*S,*3*R*)-3-methylaspartate (the *erythro*-isomer) as a minor product. MAL possesses two Brønsted acid-base catalysts in its active site, Lys 331 and His 194, which act as the *S*-specific and *R*-specific bases in the deamination reaction, respectively. The role of Lys 331 was shown by mutagenesis experiments where the K331A mutant was shown to be inactive using ^{1}H NMR spectroscopy. This role was further confirmed by the position of Lys 331 in the active site structure of MAL from *C. amalonaticus* complexed with the substrate, (2*S,*3*S*)-3-methylaspartate. Lys 331 is the closest Brønsted base to the C3 proton on the *S*-face of the substrate (Levy *et al*., 2002; Raj *et al*., 2009). This was also suggested from the log (k_{cat}/K_m) vs. pH profile for both the wild-type MAL and the H194A mutant, which showed the presence of a residue with pK_a value of 7.8 that is active in its deprotonated state when catalyzing the deamination reaction (Raj *et al*., 2009).

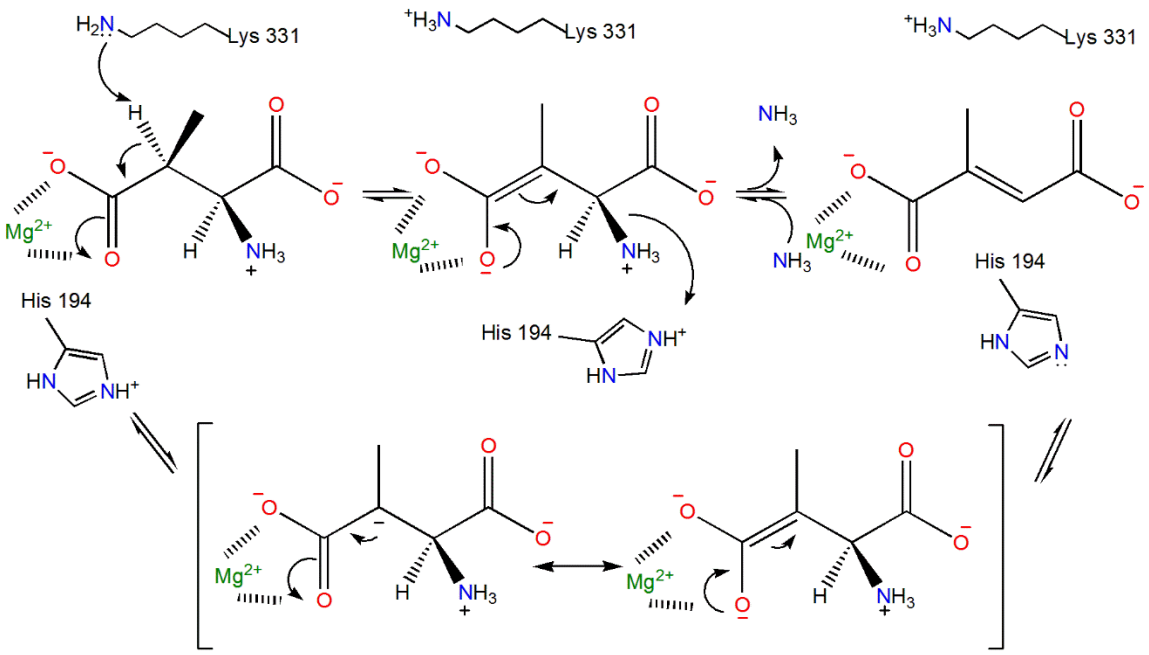

Scheme 1.7 Mechanism of MAL-catalyzed reversible anti-deamination of (2*S*,3*S*)-3-methylaspartate. The MAL-catalyzed reaction starts with the initial abstraction of the α-proton leading to the formation of the enolate intermediate that is stabilized in the active site by the Mg^{2+} ion followed by collapse of the intermediate and generation of ammonia. Adapted from (De Villiers *et al*., 2012).

His 194 was shown to be the *R*-specific acid-base catalyst through mutagenesis experiments where the H194A mutant was found to be inactive in the deamination of (2*S,*3*R*)-3-methylaspartate. However, ^{1}H NMR spectroscopy was used to show that this mutant catalyzes the stereospecific amination of mesaconate to form (2*S,*3*S*)-3-methylaspartate. Modelling the *erythro*-isomer of the substrate into the active site of MAL in the crystal structure of the *C. amalonaticus* enzyme showed that His 194 is positioned such that the nitrogen in the imidazole ring is facing the C3 proton on the *R*-face of the substrate. In addition to its role as a Brønsted acid-base catalyst for the *R*-specific deprotonation, His 194 plays a role as an electrophilic catalyst. His 194 forms a hydrogen bond with one of the oxygen atoms in the C4 carboxylate group of the *threo*-isomer, which, along with the Mg^{2+} ion, may serve to decrease of the pK_a value of the α-proton by stabilizing the enolate intermediate. This possibility was supported by the observation that the H194A mutant exhibited about a 160-fold decrease in the value of k_{cat} for the deamination reaction (Raj *et al*., 2009).

Another residue of importance in the MAL-catalyzed reaction is Gln 329, which forms a hydrogen bond with the C4 carboxylate group of the bound substrate, as is evident from the crystal structure, leading to further stabilization. Thus, it is believed that the divalent cation, His 194, and Gln 329 each play a major role in the stabilization of the enolate intermediate formed during the reaction, where both amino acid residues act as electrophiles (Raj *et al*., 2009).

A point that remains unanswered is why the K331A mutant is unable to catalyze the *syn*-deamination reaction starting from the *erythro*-isomer of the substrate. One of the proposed hypotheses to explain this observation is that an alteration of the orientation of

the imidazole side chain of His 194 is brought about by the mutation which disfavors the His-catalyzed proton abstraction reaction (Raj *et al*., 2009).

1.3.1.4 Assay of MAL Activity

The kinetic parameters of the *F. varium* MAL-catalyzed reaction have been determined using a continuous UV-visible spectroscopic assay where the rate of deamination of (2*S,*3*S*)-3-methylaspartate was determined by following the increase in absorbance at 240 nm corresponding to the formation of mesaconate ($\Delta\varepsilon$ = 3850 $M^{-1}cm^{-1}$). The maximum reaction velocity, V_{max}, was found to be 2.4 mM s^{-1} and the Michaelis constant K_m, was 0.51 mM (Bearne *et al*., 2001). Bearne and co-workers report a specific activity of 137 untis/mg, total units of 2172 μmol/min, and total protein of 15.9 mg, all in a 5 mL total volume of the final purification fraction. From the aforementioned values, the k_{cat} value can be calculated to be equal to 105 s^{-1} and k_{cat}/K_m to be equal to 205 mM^{-1} s^{-1} (Bearne *et al*., 2001).

1.4 OVERVIEW OF THIS WORK

The "minimal" ligands tartronate and 3-HP and their derivatives are used to investigate the active site architecture of three members of the ENS. Tartronate is a ground-state analogue of mandelate, the substrate for MR, that is found to be a competitive inhibitor of MR (K_i = 1.8 mM *c.f.* K_m = 1 mM) (**Figure 1.5**). The x-ray crystal structure of MR with tartronate and Mg^{2+} as ligands shows that tartronate binds to the active site with its glycolate moiety chelating the Mg^{2+} and the 3-carboxylate group bridging the two Brønsted acid-base catalysts, Lys 166 and His 297 (**Figure 1.6 - A**) (Nagar, Lietzan, Maurice, & Bearne, 2014).

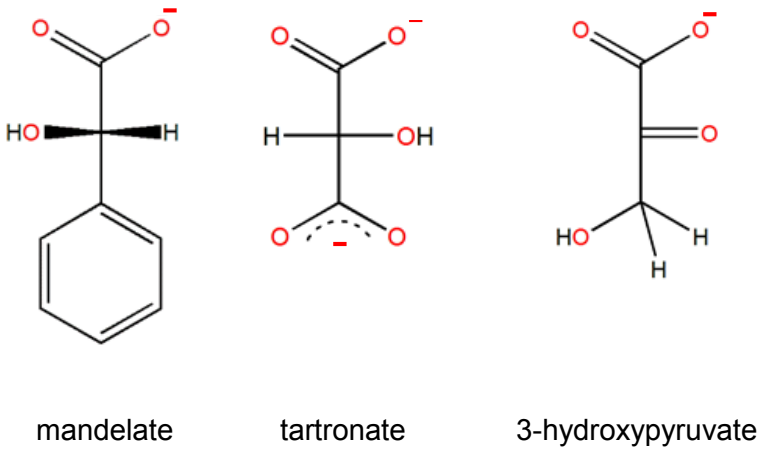

Figure 1.5 Ground-state analogues. Tartronate and 3-HP are ground state analogues of mandelate, as well as other substrates of the ENS enzymes.

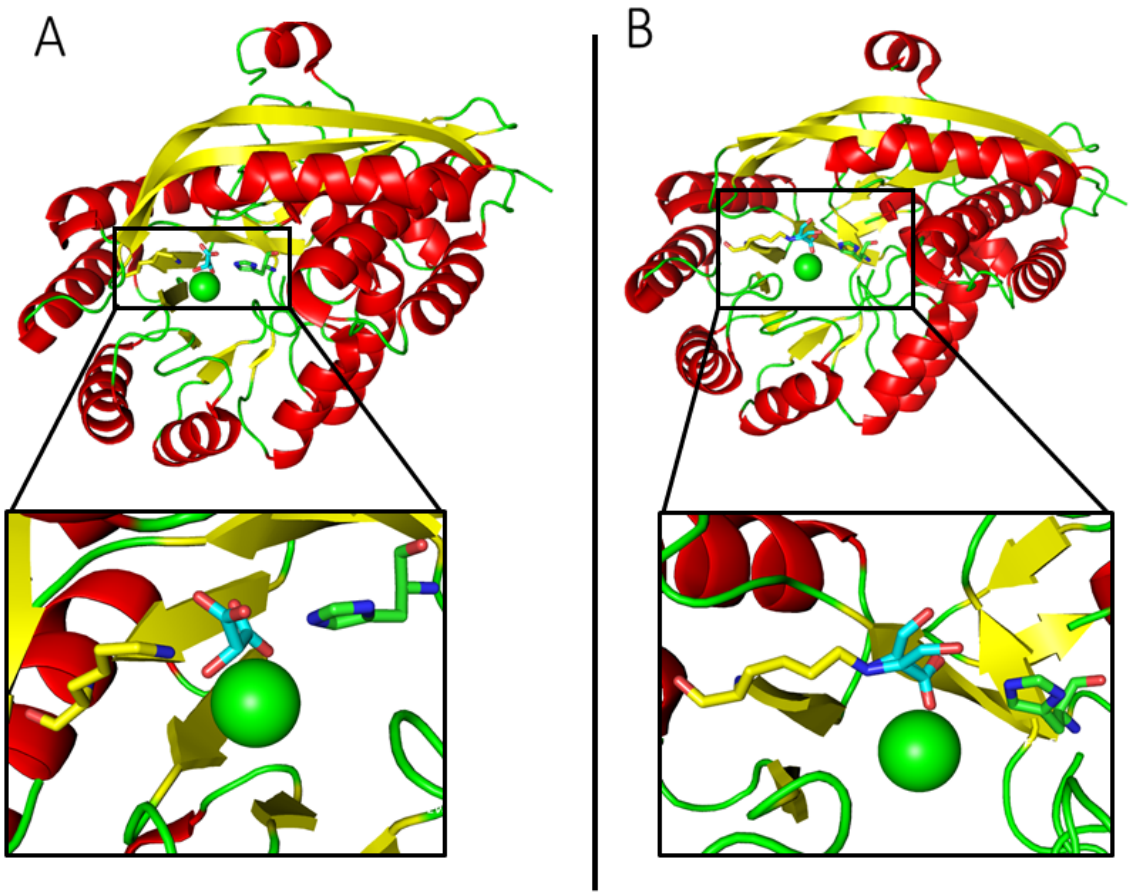

Figure 1.6 Binding of the "minimal" ligands tartronate and 3-HP to the active site of MR. (A) Tartronate is a competitive inhibitor of MR that chelates the Mg^{2+} through its glycolate moiety and bridges the Brønsted acid-base catalysts in the active site with its 3-carboxyl group (PDB entry 4M6U). (B) 3-HP is a time-dependent irreversible inhibitor of MR that forms a Schiff base with the active site Brønsted base catalyst Lys 166 followed by a base-catalyzed deprotonation that "traps" 3-HP in the active site (PDB entry 4X2P).

3-HP is also a ground-state analogue of mandelate and has been found to be a time-dependent irreversible inhibitor (k_{inact}/K_I = 83 $M^{-1}s^{-1}$) (**Figure 1.6 - B**) (Nagar, Wyatt, St. Maurice, & Bearne, 2015). The x-ray crystal structure of MR with 3-HP and Mg^{2+} as ligands shows that 3-HP forms a Schiff-base with the Lys 166 residue in the active site followed by deprotonation by the other Brønsted base catalyst in the active site, predicted to be His 297, to form an aldehyde/ enol(ate) adduct (**Figure 1.6 - B**) (**Scheme 1.8**).

Because both tartronate and 3-HP can also be considered minimal structural analogues of most substrates of ENS enzymes, and appear to recognize the molecular features essential for the α-proton abstraction half-reaction (i.e., chelation of Mg^{2+} via the glycolate moiety, recognition of the Brønsted acid-base catalyst, and/or deprotonation), these two molecules appear to be good candidates to be used as probes of the active site architectures of different members of the ENS. Three enzymes were chosen for the study presented in this thesis: TarD and TGD from the MR subgroup, and MAL from the MAL subgroup. TarD and TGD were chosen because they belong to the MR subgroup and both 3-HP and tartronate were anticipated to interact with these enzymes in a fashion similar to their interactions with MR. On the other hand, 3-HP and tartronate differ structurally from 3-methylaspartate and it was therefore anticipated that they might exhibit different behavior with MAL, an ENS enzyme not from the MR subgroup. Overall, the findings were quite surprising and the "minimal" ligands revealed that there are subtle differences in the architecture of active sites of enzymes even within the MR subgroup, despite no obvious differences being evident in the x-ray structures (**Figure 1.7**).

Finally, since the presence of a Mg^{2+} ion in the active site of members of the ENS is crucial for catalysis, a preliminary investigation of the metal biding site in TarD is also presented.

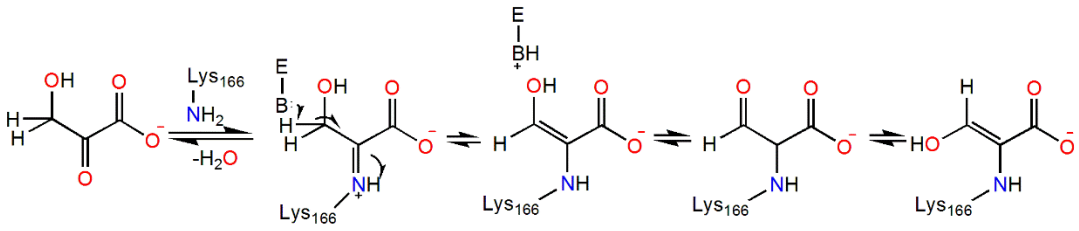

Scheme 1.8 Mechanism of inhibition of MR by 3-HP. 3-HP forms a Schiff-base with the Lys 166 residue in the active site followed by deprotonation by the other Brønsted base catalyst in the active site, predicted to be His 297, to form an aldehyde/ enol(ate) adduct. Adapted from (Nagar, Wyatt, St. Maurice, & Bearne, 2015).

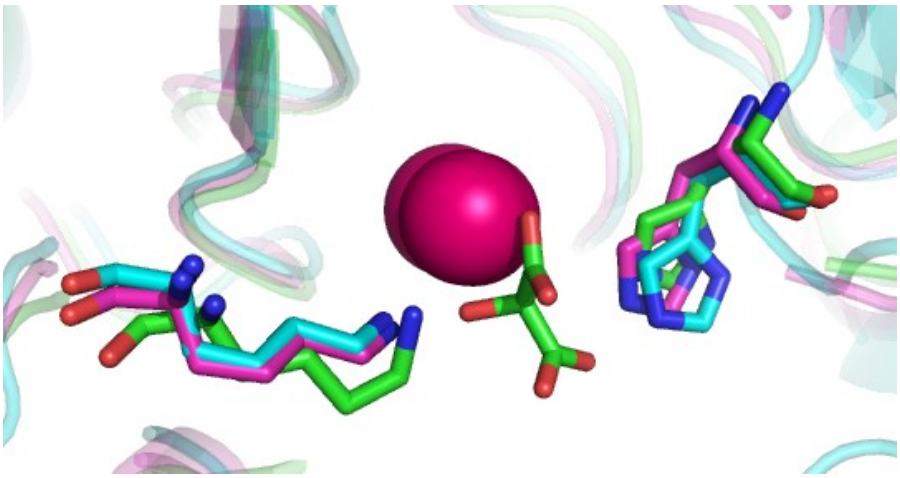

Figure 1.7 Overlay of the x-ray crystal structures of MR, TarD, and TGD from the MR subgroup. The overlay of the x-ray crystal structures of MR (green) (PDB entry 4M6U), TarD (cyan) (PDB entry 2DW7), and TGD (magenta) (PDB entry 2PP1) shows that there are no gross differences in the architecture of the active sites of the three enzymes. The ligand in the active site is tartronate that is co-crystallized with MR.

CHAPTER 2 PROBING THE ARCHITECTURE OF THE ACTIVE SITE OF RECOMBINANT D-TARTRATE DEHYDRATASE

2.1 INTRODUCTION

This chapter discusses obtaining TarD, determining its kinetic constants, and determining its inhibition by tartronate and 3-HP to further investigate its active site architecture. The assay reported to measure TarD activity is a continuous coupled assay, as previously described (**1.2.1.4 Assay of TarD Activity**), where MDH is the coupling enzyme. However, it has been shown that MDH is inhibited by tartronate (Davies & Kun, 1957), which is also shown in this work, and thus, an end-point assay using semicarbazide was developed to measure the kinetics and inhibition by tartronate. The end-point assay was not used for inhibition assays with 3-HP due to the ability of 3-HP to react with semicarbazide and interfere with the measurements. Mass spectrometry experiments were conducted to determine if 3-HP reacts with a Lys residue in the active site, particularly the Brønsted acid-base catalyst Lys 184. Glyceric acid was tested as a competitive inhibitor of TarD and as a partial substrate because of its structural similarity to D-tartrate.

2.2 MATERIALS & METHODS

2.2.1 General

D-Tartrate, *β*-nicotinamide adenine dinucleotide reduced disodium salt (NADH), deutetrium oxide, malic dehydrogenase from porcine heart, semicarbazide hydrochloride, lithium 3-hydroxypyruvate, and sodium cyanoborohydride were purchased from Sigma-Aldrich Canada, Ltd. (Oakville, ON). Tartronic acid was purchased from Alfa Aesar (Ward

Hill, MA). Calcium DL-glycerate hydrate was purchased from TCI America (Portland, OR). Sodium acetate anhydrous was purchased from Fisher Scientific (Ottawa, ON). Assays were conducted using an Agilent 8453 UV-visible spectroscopy system. DNA oligonucleotide primers were purchased from Integrated DNA Technologies (Coralville, IA). Restriction endonucleases were purchased from New England Biolabs (Ipswich, MA). Silver nitrate was purchased from J.T. Baker Chemical Co. (Phillipsburg, NJ). ^{1}H NMR spectroscopy was carried out at the Nuclear Magnetic Resonance Research Resource (NMR^{3}) at Dalhousie University, using a Brüker AV-300 spectrometer and chemical shifts (δ) are in ppm referenced to the HOD peak at 4.8 ppm (Gottlieb, Kotlyar, & Nudelman, 1997). LC-ESI-MS/MS experiments were carried out using HPLC with nanoflow (UltiMate 3000, Dionex) for the liquid chromatography and a hybrid ion trap-orbitrap high resolution tandem mass spectrometer (Velos Pro, Thermoscientific) for the ESI-MS/MS. The instrument was operated in data-dependent acquisition mode (DDA).

2.2.2 Cloning of the TarD Open Reading Frame from Genomic DNA of *Bradyrhizobium japonicum*

The open reading frame encoding TarD (GI: 27381841) was cloned from the genomic DNA of *Bradyrhizobium japonicum* (kindly provided by Dr. Prithiviraj at the Department of Plant, Food, and Environmental Sciences in Faculty of Agriculture at Dalhousie University, NS, Canada) using whole-cell PCR with KAPA HiFi HotStart Ready Mix (KAPA Biosystems, D-Mark Biosciences – Toronto, ON) following the manufacturer's protocol. The forward and reverse primers for amplification of the open reading frame were: forward primer (5' – GGGAAAGTTGAGACCATATGTCCGTCCGCATCGTC – 3') and reverse primer (5' –

CGGCGTGGATCCAATTACTCCGCCAGC – 3'), where the underlined bases correspond to NdeI and BamHI recognition sequences, respectively. The amplification was conducted using an S1000 Thermal Cycler from BIO-RAD Laboratories (Mississauga, ON) and the program was set for initial denaturation at 95 °C for 3 min, 35 cycles of 98 °C for 20 s for denaturation, thermal gradient of 60-70 °C for 75 s for annealing, 72 °C for 72 s for extension, and 72 °C for 144 s for final extension. The PCR product was gel purified using QIAquick Gel Extraction Kit (QIAGEN) (Toronto, ON). NdeI and BamHI endonucleases were then used to cut the PCR product for insertion into the multiple cloning site of the pET-15b vector (Novagen, Madison, WI). The insert and the vector were digested in a stepwise manner in which they were incubated, in separate 1.5-mL Eppendorf tubes, with NdeI for 2 h and then BamHI was added and incubation continued for two more hours at 37 °C according to manufacturer's recommendations. The digestion products were gel purified as previously mentioned. T4 DNA ligase (Invitrogen) was used following the manufacturer's instructions and the ligation reaction was conducted overnight at 16 °C. The pET-15b-*Bj*TarD plasmid encodes a fusion protein with an N-terminal His_6-tag. Chemically-competent *E. coli* DH5α cells were transformed with the pET-15b-*Bj*TarD plasmid using heatshock and glycerol stocks were prepared and stored at –80 °C. The sequence of the insert was verified through commercial DNA sequencing (Robarts Research Institute, London, ON) to ensure full incorporation of the correct insert and the absence of any mutations.

2.2.3 Expression and Purification of TarD Recombinant Protein

Competent *E. coli* BL21 (DE3) cells were also transformed with the pET-15b-*Bj*TarD plasmid and glycerol stocks were prepared and stored at –80 °C. The protein was

then overexpressed by inoculation of two starter cultures, each containing 5 mL sterile LB, 50 μg/mL ampicillin, and 10 μL of the glycerol stock, followed by incubation overnight at 37 °C with continuous shaking at 250 rpm. The starter cultures were then added to 1 L of sterile LB broth containing 50 μg/mL of ampicillin. This was incubated for 48 h (without isopropyl *β*-D-1-thiogalactopyranoside (IPTG) induction) at 37 °C with continuous shaking at 250 rpm (Yew *et al*., 2006). The cells were harvested using centrifugation at 4000 × *g* for 10 min at 4 ºC. The cell pellet was re-suspended in 30 mL of ice-cold binding buffer (1 M NaCl, 20 mM Tris-HCl, 5 mM imidazole, pH 7.9) and then sonicated on ice with 5 × 10 s bursts and 1 min cooling times between bursts, or longer if needed, using a Branson Sonifier 250. The cell lysate was then clarified by ultracentrifugation at 40,000 × *g* for 30 min at 4 °C. The supernatant was subsequently passed through a Ni^{2+}-charged His-bind resin-packed column (10 mL columns packed to 2.5 mL) at 4 °C. The column was subsequently washed with 25 mL binding buffer, 15 mL wash buffer (1 M NaCl, 20 mM Tris-HCl, 60 mM imidazole, pH 7.9), and 7 mL strip buffer (0.5 M NaCl, 20 mM Tris-HCl, 100 mM EDTA, pH 7.9). The purified protein eluted in the strip buffer. Purity was confirmed using 12% acrylamide SDS-PAGE followed by staining with Coomassie blue R-250. The protein was then dialyzed against the assay buffer (50 mM K^+- Hepes, 10 mM $MgCl_2$, pH 7.5) for 18 h at 4 °C with three buffer changes (500 mL each) (Sambrook, 1989; Yew *et al*., 2006).

2.2.4 Kinetic and Inhibition Assays of Recombinant TarD

2.2.4.1 Continuous Coupled Assay

The activity of the recombinant TarD was assayed spectrophotometrically using a continuous coupled assay with MDH as the coupling enzyme and NADH as a cofactor as

described previously by Gerlt and co-workers (Yew *et al*., 2006). The change in absorbance at 340 nm corresponding to the oxidation of NADH (ε_{340} = 6220 $M^{-1}cm^{-1}$) was followed for 40 s. A 1-cm path length quartz cuvette was used and the final volume of the reaction was 1 mL (at 25 °C). The reaction mixture contained a concentration of TarD that gave a linear time course (2.6 ng/μL), as has been reported by Rode & Giffhorn, D-tartrate (0.005-0.800 mM), 50 mM K^+-Hepes (pH 7.5 adjusted by KOH), 10 mM $MgCl_2$, 0.16 mM NADH, and 10 units of MDH (Rode & Giffhorn, 1982; Yew *et al*., 2006). The enzyme concentration was determined by measuring the absorbance at 280 nm using the calculated extinction coefficient of the recombinant protein (57,300 $M^{-1}cm^{-1}$) from the ExPASY ProtParam tool (Gasteiger *et al*., 2003).

Nonlinear regression analysis was used to fit the Michaelis-Menten equation **2.1** to the initial velocity data to obtain V_{max} and K_m values for the recombinant TarD using the program KaleidaGraph v. 4.02 from Synergy Software (Reading, PA) (Segel, 1975). The kinetic assays were conducted in triplicate, and the values are the average and the error reported is the standard deviation.

This assay was used for inhibition studies with 3-HP after verifying that 3-HP does not inhibit the coupling enzyme, MDH. IC_{50} and K_i values were obtained using nonlinear regression analysis to fit equations **2.2** and **2.3** to the relative initial velocities and initial velocities (Segel, 1975), respectively, using KaleidaGraph v. 4.02. The inhibition assays were conducted in triplicate, and values are the averages and the error reported is the standard deviation. The IC_{50} studies were conducted at a substrate concentration equal to the measured K_m from the continuous coupled assay and the 3-HP concentrations used

ranged from 0 to 10.0 mM. For the K_i determination studies, the 3-HP concentrations used were 0, 1.0, 2.0, 5.0, and 8.0 mM.

$$v_o = \frac{V_{max} \cdot [S]}{K_m + [S]} \quad (2.1)$$

$$\frac{v_i}{v_o} = \frac{IC_{50}^n}{IC_{50}^n + [I]^n} \quad (2.2)$$

$$v_i = \frac{V_{max}\,[S]}{K_m\left(1 + \frac{[I]}{K_i}\right) + [S]} \quad (2.3)$$

2.2.4.2 Development of an End-Point Assay

Semicarbazide has been used for the determination of total α-keto acid concentration (Doudoroff & MacGee, 1954). Accordingly, a spectrophotometric end-point assay was developed to determine the activity of the recombinant protein using semicarbazide to measure product formation (**Scheme 2.1**). The assay was conducted in a 1.5-mL Eppendorf tube, D-tartrate (0.005-0.80 mM), and buffer (50 mM K^+-Hepes, 10 mM $MgCl_2$, pH 7.50). The reaction was initiated by addition of a concentration of enzyme that gave a linear time course (2.6 ng/μL), as has been reported by Rode & Giffhorn (1982). The reaction mixture was incubated at 25 °C for 0 (immediately after enzyme addition without incubation), 1, 2, and 4 min followed by transferring 200 μL of the reaction mixture to another 1.5-mL Eppendorf tube containing 200 μL of the stop solution (stock stop solution containing 16 mM semicarbazide hydrochloride and 22 mM sodium acetate) to stop the reaction followed by incubation at 30 °C for 15 min (Doudoroff & MacGee, 1954). After the 15-min incubation time, the mixture (400 μL) was transferred to a 1-cm pathlength quartz cuvette and distilled water (600 μL) was added to dilute the mixture (to

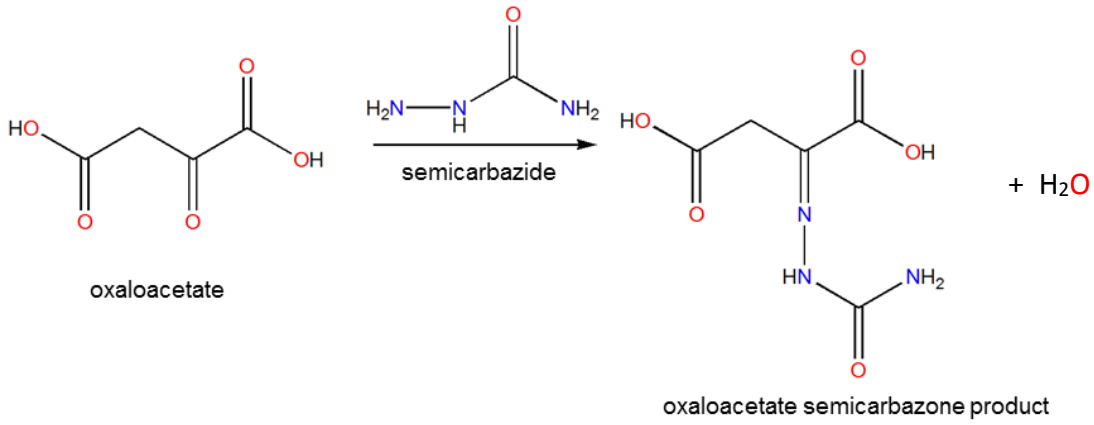

Scheme 2.1 Semicarbazide reaction with the α-keto acid, oxaloacetate. Oxaloactetate forms a Schiff base with semicarbazide to form an oxaloacetate semicarbazone product that can be detected using UV-vis spectrophotometry at 250 nm.

a final volume of 1 mL) and the absorbance was measured at 250 nm (Doudoroff & MacGee, 1954).

The absorbance values were plotted as a function of time at each substrate concentration to give the initial velocity. The Michaelis-Menten equation **2.1** was fit to the initial velocities to obtain V_{max} and K_m values using nonlinear regression analysis with KaleidaGraph v. 4.02 (Segel, 1975). The kinetic assays were conducted in triplicate, and values are the averages and the error reported is the standard deviation.

The molar absorptivity (ε) of the oxaloacetate semicarbazone product was determined experimentally by constructing a calibration curve of the measured absorbance of the semicarbazone product at 250 nm for various concentrations of oxaloacetate (0.01-0.30 mM). The molar absorptivity (ε) was calculated from the slope of the resulting line according to Beer-Lambert law equation **2.4**, where b is the pathlength (1 cm), and c is the concentration.

$$A = \varepsilon\, b\, c \qquad (\mathbf{2.4})$$

This assay was used for inhibition studies with tartronate because tartronate inhibits the coupling enzyme, MDH. IC_{50} and K_i values were obtained using nonlinear regression analysis to fit equations **2.2** and **2.3** to the relative initial velocities and initial velocities, respectively, using KaleidaGraph v. 4.02 (Segel, 1975). The IC_{50} and inhibition assays were conducted in triplicate and duplicate, respectively. The IC_{50} studies were conducted at a substrate concentration equal to the measured K_m value from the end-point assay and the tartronate concentrations used ranged from 0 to 1.0 mM. For the K_i determination

studies, the tartronate concentrations used were 0, 3.0, and 8.0 mM. Values are the averages and the error reported is the standard deviation.

2.2.4.3 Assays with Glyceric Acid

2.2.4.3.1 Inhibition by Glycerate

The end-point assay using semicarbazide was used for inhibition studies with glycerate. Glycerate was purchased as the calcium salt; however, the calcium was exchanged for sodium since calcium inhibits TarD. The exchange was done using AG 50W-X 8 Resin (100-200 mesh) from BIO-RAD Laboratories, Inc. (Hercules, CA) according to the manufacturer's recommended procedure. A summary of the steps is as follows: The column was packed with the resin (100 mL) and washed with 1 M HCl until the eluate was acidic to pH paper. The column was then washed with 3× the bed volume of distilled water and then washed with 1 M NaCl until the eluate was neutral to pH paper. The column was washed again with distilled water to remove any traces of chloride which was assessed by the lack of white precipitate formation between the eluate and a silver nitrate solution. After converting the resin to the Na^+-form, 0.5 g of calcium glycerate was dissolved in 15 mL distilled water, applied to the column, and eluted using distilled water. A volume of 250 mL of eluate was collected in a round-bottom flask, and the water was removed using rotary evaporation at 30 °C until 15-30 mL of solvent was left. The remaining solvent was removed by lyophilization. The lyophilized sample was then dissolved in 5 mL D_2O and an aliquot was analyzed using ^1H NMR spectroscopy to determine the concentration relative to an internal reference of pyrazine. The relative integration of the peaks corresponding to glycerate and pyrazine was used to calculate the concentration of the sodium glycerate in the stock solution.

2.2.4.3.2 Deuterium exchange experiment by glycerate and TarD

A deuterium exchange experiment using ^{1}H NMR spectroscopy was conducted to assess the ability of TarD to catalyze the initial α-proton abstraction using glycerate as a substrate. The experiment was conducted as follows: 5 mL of the buffer (50 mM K^{+}-Hepes and 10 mM $MgCl_2$) was prepared using D_2O as the solvent and then lyophilized three times to ensure deuteration of the exchangeable protonation sites. The pD was adjusted to 7.90 using KOD. The NMR tube contained 26 ng/μL TarD, 10 mM sodium glycerate, and the deuterated buffer to a final volume of 600 μL. ^{1}H NMR spectra were obtained before addition of the enzyme, immediately after addition of the enzyme (3 min), and at 1 h, 6 h, and 24 h with incubation at room temperature.

2.2.5 Mass Spectrometry Experiments with 3-HP

In order to assess the possibility of reaction of 3-HP with the active site Lys residues to form a Schiff base, mass spectrometry experiments were conducted where two samples were prepared and investigated: a control sample that contained TarD and 3-HP and a "trapping" sample that contained TarD, 3-HP, and $NaCNBH_3$. The experiment was conducted as follows: 97.5 μL TarD (5.5 mg/mL) was incubated with 60 μL 3-HP (50 mM) at the reaction temperature, 25 °C, for 30 min for both samples followed by addition of 47.2 μL distilled water to the control sample and 47.2 μL $NaCNBH_3$ (1 M) to the "trapping" sample, the pH was adjusted to 7.50, and both samples were further incubated at 25 °C for 30 min. The final volume of the reaction, after addition of either $NaCNBH_3$ or water was 204.7 μL. Both samples were processed identically throughout the subsequent steps of the experiment.

In-gel digestion was carried out manually with a protocol adapted from Shevchenko and co-workers (Shevchenko, Tomas, Havlis, Olsen, & Mann, 2007). A 10 μL aliquot of each sample was subjected to SDS-PAGE (12%) and the bands corresponding to TarD were cut from the gel and washed with distilled water (1.5 mL). After washing, the gel sections were further cut into ~ 1 mm^3 cubes with a scalpel and they were rinsed again with distilled water (200 μL) before transfer to a 1.5-mL Eppendorf tube. Acetonitrile (50% in water, 200 μL) was added and the sample was vortexed for 5 min. The solvent was then discarded, and the sample was dried for 5 min using vacuum concentration (Speed Vac Concentrator, SDP 111 V-230, Thermo Electron Corp.). The previous step was then repeated, followed by treatment with 10 mM dithiothreitol (100 μL). After incubation for 30 min at 56 °C, the excess liquid was removed, and the sample was cooled to room temperature. Thiol groups were then alkylated using 100 mM iodoacetamide (100 μL), incubated for 30 min at room temperature in the dark, and then excess liquid was removed. This was followed by the addition of acetonitrile (50% in water, 200 μL), and the sample was vortexed for 5 min, solvent discarded, and sample dried for 5 min using vacuum concentration. Enough trypsin was added to cover the gel pieces (12.5 ng/μL, ~ 30 μL) for the digestion of the protein. the mixture was then incubated at 4 °C for 2 h, however, with checking of the sample after 30 min to ensure that the optimal level of trypsin solution was maintained. Ammonium bicarbonate (50 mM) was added until it covered the gel (~ 30 μL) and the mixture was incubated overnight at 37 °C. The peptides were extracted with 100 μL extraction buffer (50% acetonitrile in 5% formic acid in LC-MS-grade water) and vortexed for 30 min at room temperature. The supernatant was transferred to a tube, dried using vacuum concentration, resuspended in 15-30 μL resuspension buffer (3% acetonitrile

in 0.5% formic acid in LC-MS-grade water), sonicated for 15 min, and then transferred to a 300 µL HPLC vial (Shevchenko *et al*., 2007).

For liquid chromatography, a 1 µL sample was injected at a rate of 300 nL/ min through a C18 packed capillary column (4µm, 0.0750 × 500 mm). A fused silica emitter (20 µM inside diameter with a 10 µm ID tip, PicoTip Emitter from New Objective) was used to spray the samples at a voltage of 1.6 kV. A linear gradient from 3 to 35% solvent B (0.1% formic acid in acetonitrile) in solvent A (0.1% formic acid in water) over 30 min was used for the elution. After 30 min, solvent B was increased to 95% over 5 min. Xcaliber from Thermo Fisher was used to acquire raw data. Peptide and protein identification was done using the Proteome Discoverer software v. 1.4 (Thermo Fisher) using the Sequest database search algorithm. Carbamidomethylated cysteine was set as a static modification and oxidized methionine, 3-hydroxypyruvate ($C_3O_3H_2$, delta mass 86.0004), and reduced 3-hydroxypyruvate ($C_3O_3H_4$, delta mass 88.01604) modifications of Lys residues were set as dynamic modifications. High-confidence XCorr threshold values for charged precursors were set at 1.9, 2.3, and 2.6 for doubly, triply, and highly charged precursors, respectively, for the validation of the Peptide to Spectrum Match (PSM).

2.3 RESULTS

2.3.1 Cloning, Expression, and Purification of Recombinant TarD

The recombinant TarD was obtained with high purity as shown by the 12% SDS-polyacrylamide gel (**Figure 2.1**).

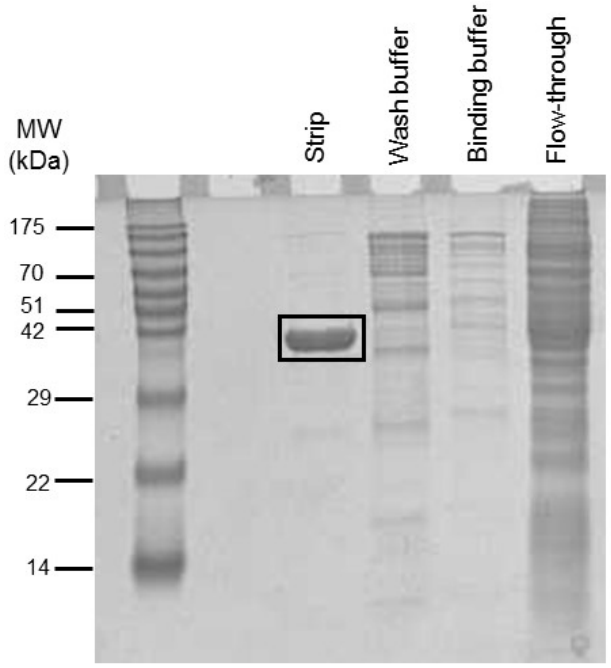

Figure 2.1 The purified recombinant TarD. The gel shows the different fractions resulting from the protein purification. Recombinant TarD elutes in the strip fraction with high purity. The molecular mass of the TarD monomer calculated from the amino acid sequence is 45.6 kDa.

2.3.2 Kinetic and Inhibition Assays of Recombinant TarD

The kinetic parameters of the recombinant TarD were determined using a continuous coupled assay and an end-point assay and are reported in **Table 1**.

These values were obtained from the Michaelis-Menten plots as previously described (**Figure 2.2**). The molar absorptivity (ε) for the formed oxaloacetate semicarbazone product was calculated from the linear equation of the calibration curve (**Figure 2.3**) and found to be 3228 ± 377 M^{-1} cm^{-1}.

Inhibition studies of the coupling enzyme, MDH, in the continuous coupled assay with tartronate and 3-HP showed that tartronate inhibits MDH with an IC_{50} of 6 ± 1 mM. However, 3-HP did not inhibit MDH (**Figure 2.4**). Accordingly, the continuous coupled assay was used to determine the inhibition of TarD by 3-HP. For the inhibition by tartronate, the end-point assay was conducted.

Inhibition by tartronate using the end-point assay resulted in an IC_{50} value of 0.8 ± 0.1 mM. The K_i value can be calculated from equation **2.5** to be equal to 0.4 mM for a competitive inhibitor (**Figure 2.5**) (Segel, 1975).

$$IC_{50} = K_i\left(1 + \frac{[S]}{K_m}\right) \qquad \textbf{(2.5)}$$

Inhibition studies with tartronate showed competitive inhibition with a K_i value of 0.5 ± 0.1 (**Figure 2.5**). The K_i value was determined from a replot of the slope from the Lineweaver-Burk (LB) plot, where the K_i value is equal to the –x-intercept value (equation **2.6**) (Segel, 1975).

$$\frac{K_m^{app}}{V_{max}} = \frac{K_m}{V_{max}} + \frac{K_m}{V_{max}\,K_i}\,[I] \qquad \textbf{(2.6)}$$

Table 1 Kinetic parameters of the recombinant TarD

V_{max}, μM/s	K_m, mM	k_{cat}, s^{-1}	k_{cat}/K_m, $M^{-1} s^{-1}$	Assay type
0.21 ± 0.02	0.018 ± 0.007	3.6 ± 0.4	(22 ± 8) × 10^4	continuous coupled
0.12 ± 0.01	0.035 ± 0.007	2.1 ± 0.1	(5.84 ± 0.03) × 10^4	end-point

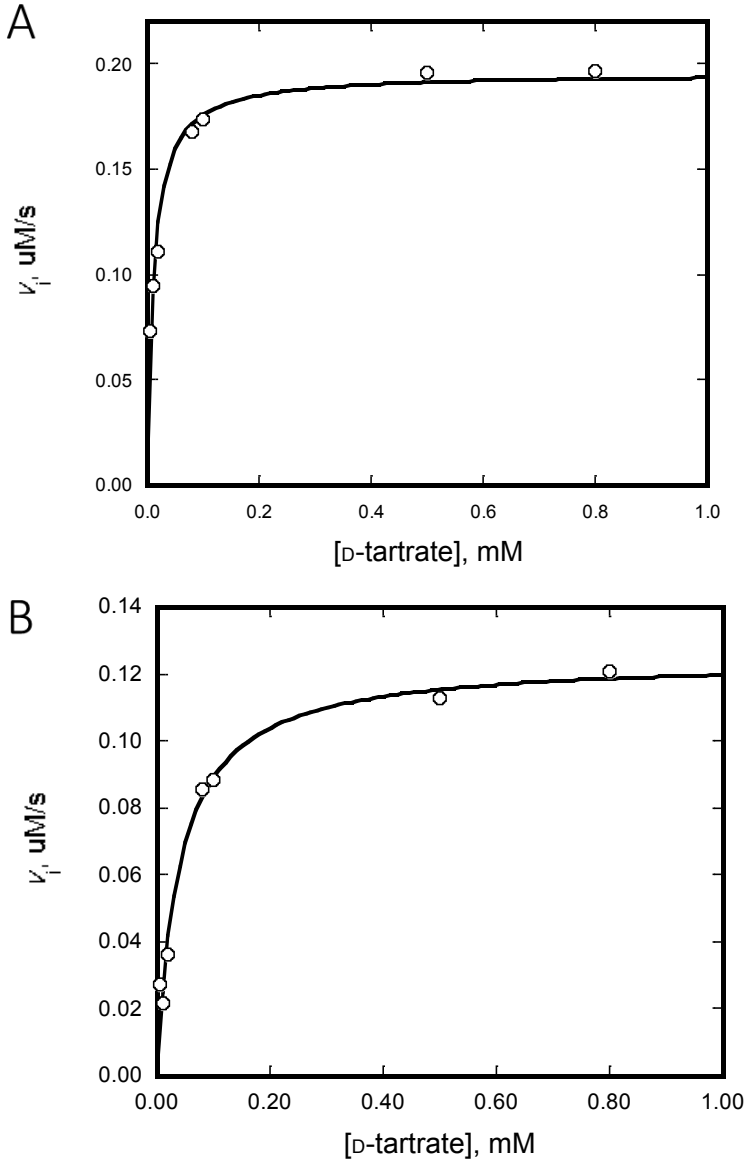

Figure 2.2 Michaelis-Menten plots for TarD. (A) Using the continuous coupled assay, k_{cat} was found to be 3.6 ± 0.4 s^{-1} and K_m to be 0.018 ± 0.007 mM. (B) Using the end-point assay, k_{cat} was found to be 2.1 ± 0.1 s^{-1} and K_m to be 0.035 ± 0.007 mM.

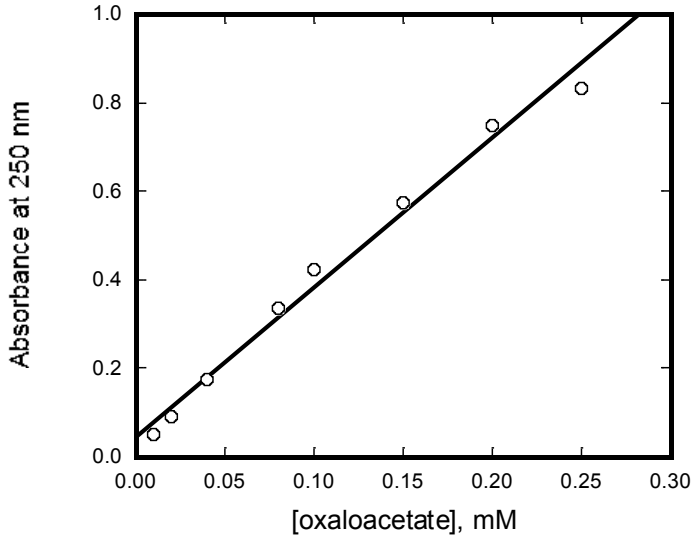

Figure 2.3 Determination of the molar absorptivity of oxaloacetate semicarbazone through constructing a calibration curve. A representative curve of 3 determinations is shown where the molar absorptivity is represented by the value of the slope of the line which was found to be 3228 ± 377 M^{-1} cm^{-1}.

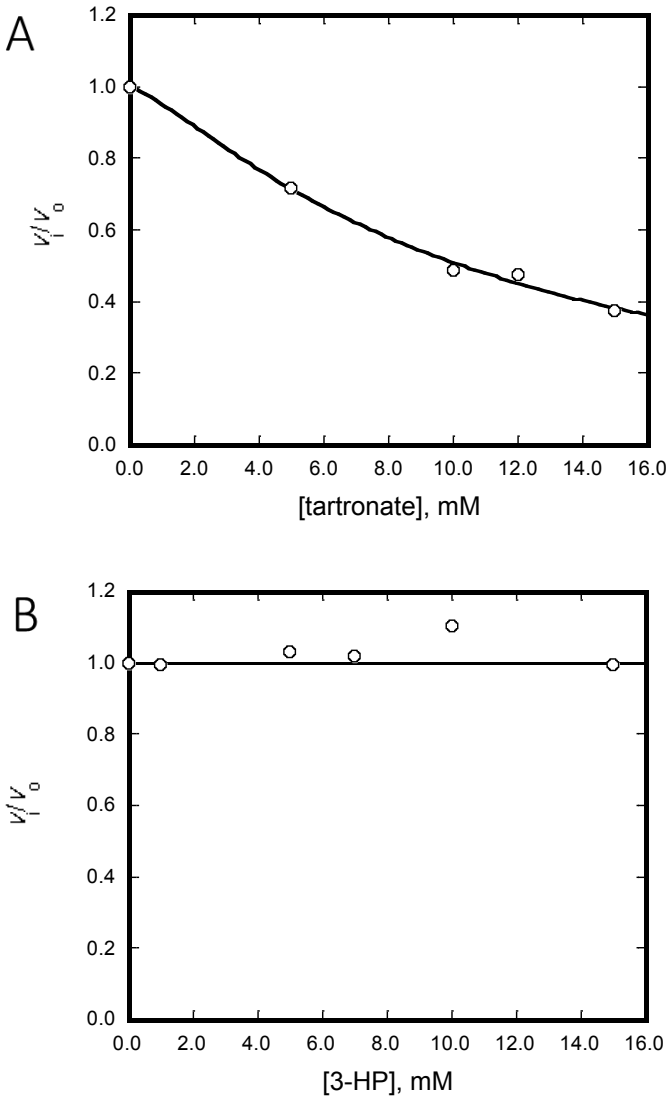

Figure 2.4 IC_{50} studies of the coupling enzyme, malate dehydrogenase, with the minimal ligands. The IC_{50} studies were conducted in K^+-Hepes buffer (50 mM, 7.9), $MgCl_2$ (10 mM), oxaloacetate (0.1 mM), NADH (0.31 mM), and MDH (0.05 units/mL). The initial rate was measured at 340 nm. (A) Tartronate (0-15 mM) inhibits MDH with an IC_{50} value of 6 ± 1 mM and *n* of 0.4 ± 0.1. (B) 3-HP (0-15 mM) does not inhibit MDH.

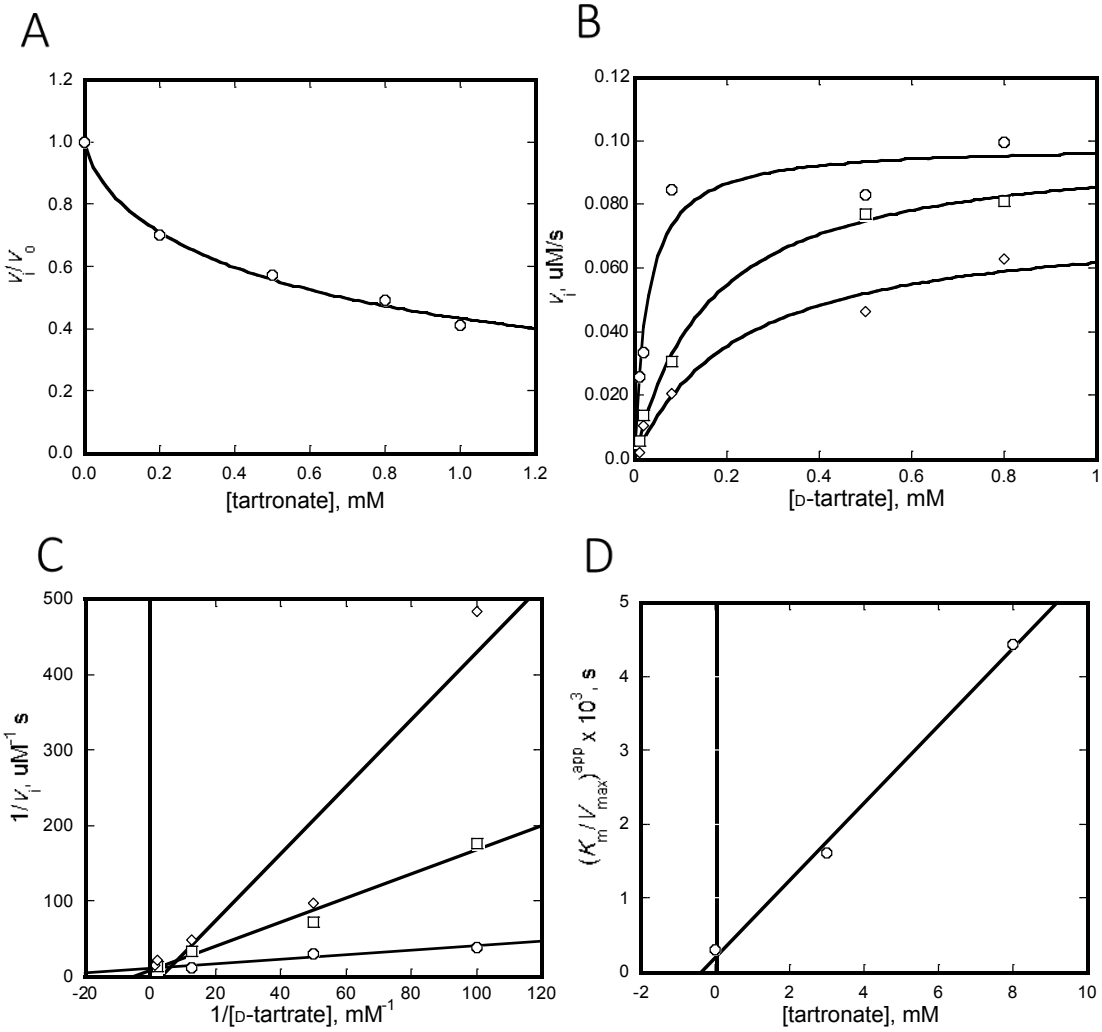

Figure 2.5 Inhibition studies of TarD by tartronate using the end-point assay. (A) A representative IC_{50} plot of TarD inhibition by tartronate. The concentrations used were 0.03 mM for D-tartrate and (0-1.0 mM) for tartronate. The IC_{50} was found to be 0.8 ± 0.1 mM and n = 0.6 ± 0.2. (B) A representative Michaelis-Menten plot for the inhibition of TarD by tartronate. The concentrations of D-tartrate were (0-0.4 mM) and for tartronate were 0 mM (○), 3.0 mM (□), and 8.0 mM (◊). (C) A representative Lineweaver-Burk (LB) plot showing competitive inhibition of TarD by tartronate. Tartronate concentrations used were 0 mM (○), 3.0 mM (□), and 8.0 mM (◊). (D) A representative replot of the LB slope against inhibitor concentration where the x-intercept is $-K_i$. The K_i value was found to be 0.5 ± 0.1 mM.

Inhibition by 3-HP was determined using the continuous coupled assay and gave an IC_{50} value of 3.9 ± 0.2 mM (**Figure 2.6**). The K_i value can be calculated from equation **2.5** to be equal to 0.2 mM for a competitive inhibitor (Segel, 1975).

Inhibition studies with 3-HP showed competitive inhibition with a K_i value of 1.8 ± 0.4 mM. The K_i value was determined from a replot of the slopes from the LB plot, where the K_i value is equal to the –x-intercept value on the replot (equation **2.6**) (Segel, 1975).

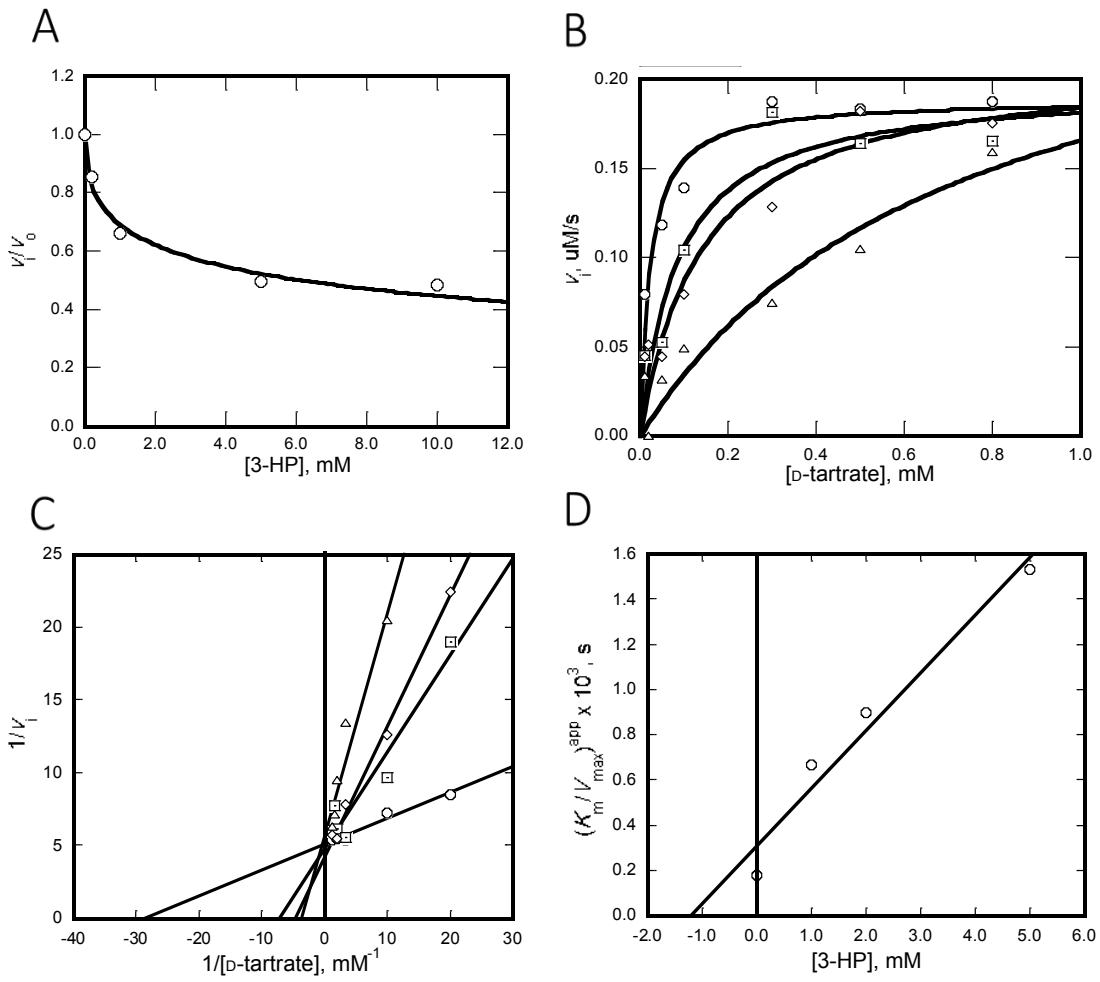

Figure 2.6 Inhibition studies of TarD by 3-HP using the continuous coupled assay. (A) A representative IC_{50} plot of TarD inhibition with 3-HP. The concentrations were 0.02 mM for D-tartrate and (0-10.0 mM) for 3-HP. The IC_{50} was found to be 3.9 ± 0.2 mM and n = 0.7 ± 0.2. (B) A representative Michaelis-Menten plot for the full inhibition study with 3-HP showing competitive inhibition. The concentrations of D-tartrate were (0-0.8 mM) and for tartronate were 0 mM (○), 1.0 mM (□), 2.0 mM (◊), and 5.0 mM. (C) A representative Lineweaver-Burk (LB) plot showing competitive inhibition of TarD with 3-HP. 3-HP concentrations were 0 mM (○), 1.0 mM (□), 2.0 mM (◊), and 5.0 mM. (D) A representative replot of the LB slope against inhibitor concentration where the x-intercept is $-K_i$. The K_i value was found to be 1.8 ± 0.4 mM.

2.3.3 Assays with Glycerate

2.3.3.1 Inhibition with Glycerate

Calcium was found to inhibit TarD with an IC_{50} value of 2.6 mM ± 0.4 (**Figure 2.7**). Sodium glycerate was therefore used instead of calcium glycerate; however, no inhibition was observed with glycerate concentrations up to 20 mM.

2.3.3.2 Glycerate as a Partial Substrate

The ^{1}H NMR spectra collected at various time points showed no significant loss of signal at 4.14 ppm corresponding to the signal of the α-proton (**Figure 2.8**). Consequently, no hydrogen-deuterium exchange was observed for the α-proton of glycerate in the presence of TarD.

2.3.4 Mass Spectrometry Results for Lys Modification

The Brønsted acid-base catalyst Lys 184 (underlined) of TarD is present in the M<u>K</u>IGGAPIEEDR peptide (MK-peptide, residues 183-194). For the control sample, the MK-peptide (monoisotopic, MH^{3+}, *m/z* (mass/charge) = 439.23 Da) showed no modification of the active site Lys 184 (**Figure 2.9**) and (**Figure 2.10**). The "trapping" sample showed two types of modifications of Lys 184: (1) a modification of 86 Da to the MK-peptide (monoisotopic, MH^{2+}, *m/z* = 701.34 Da), corresponding to a covalent modification by 3-HP due to the formation of a Schiff base followed by a base-catalyzed proton abstraction (**Figure 2.9**) (**Figure 2.11**). (2) A modification of 88 Da to the MK-peptide (monoisotopic, MH^{3+}, *m/z* = 468.57 Da), corresponding to a covalent modification due to the reduction of the formed Schiff base with $NaCNBH_3$ (**Figure 2.9**) and (**Figure 2.12**).

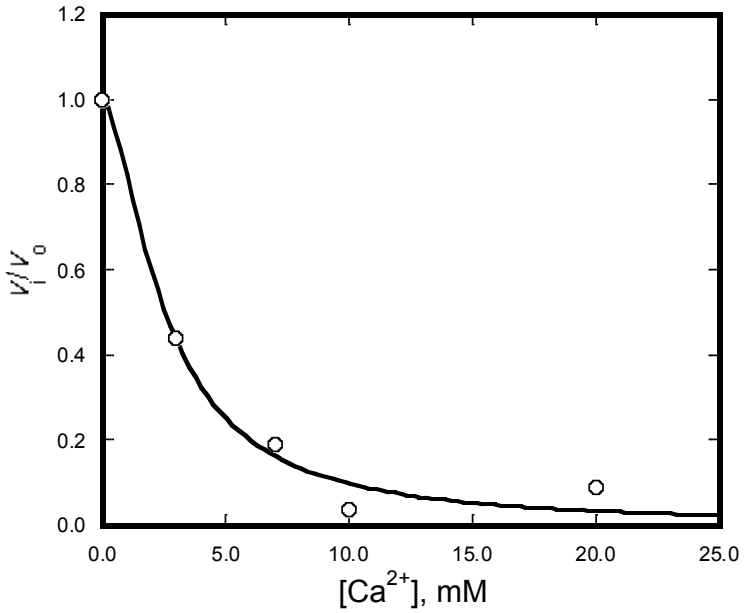

Figure 2.7 Inhibition of TarD by Ca^{2+}. IC_{50} study was conducted using the end-point assay in K^+-Hepes buffer (50 mM, pH 7.5), $MgCl_2$ (10 mM), D-tartrate (0.03 mM), and $CaCl_2$ (0-20.0 mM). The IC_{50} was found to be 2.6 ± 0.4 mM and n = 1.6 ± 0.3.

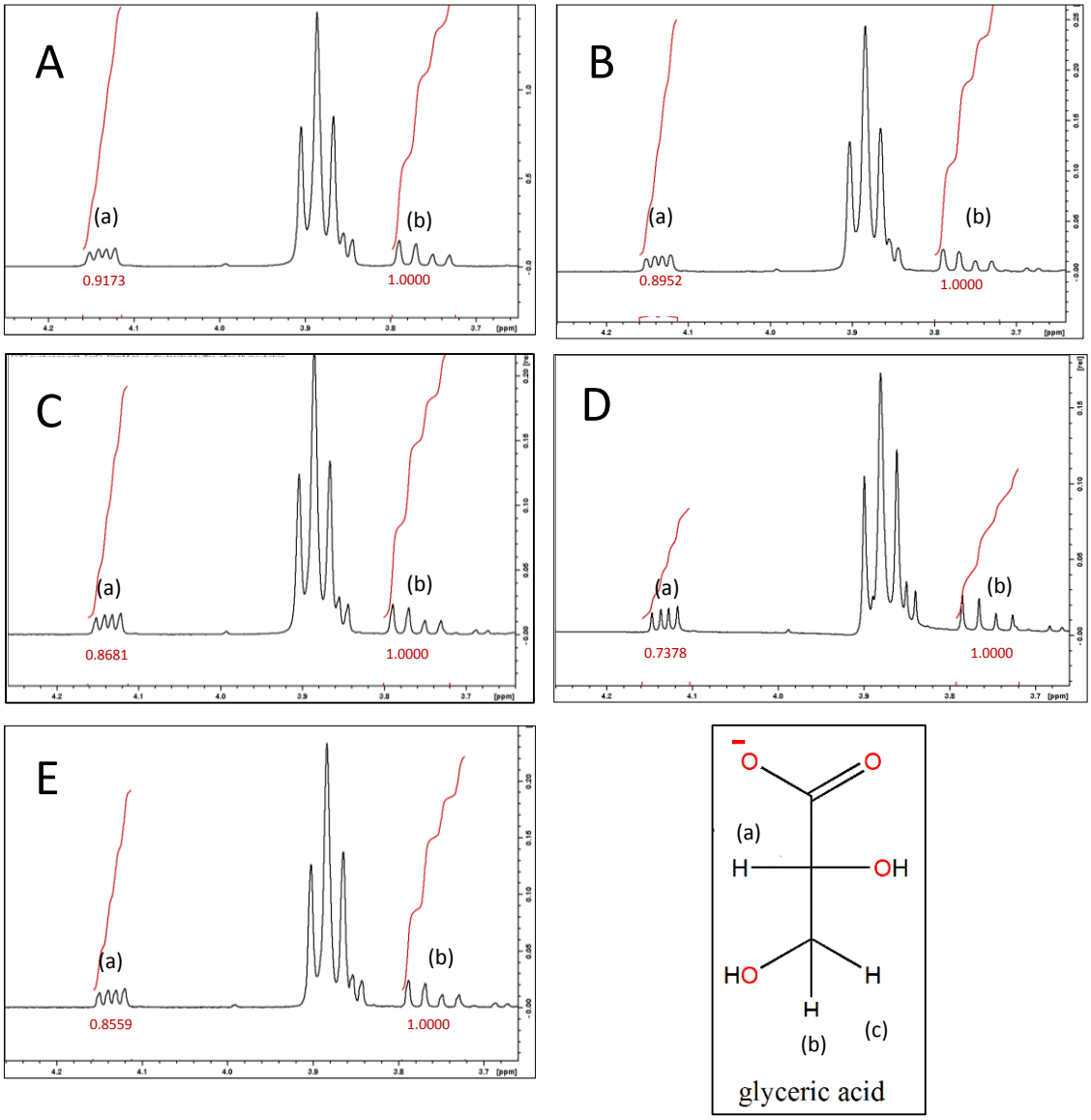

Figure 2.8 Glycerate as a "minimal" substrate for TarD. ^{1}H NMR spectra for the deuterium exchange experiment with glycerate and TarD. (A) The spectrum before TarD addition. Spectra obtained at different incubation periods after addition of TarD (26 ng/µL): (B) 3 min, (C) 1 h, (D) 6 h, (E) 24 h. The values for integrations show ~ 6% conversion occurring either due to deuterium exchange or product formation indicating that glyceric acid is a very poor substrate, if a substrate at all. The integration of the α-proton (a) at 4.14 ppm are relative to proton (b) at 3.75 ppm, which was calibrated to 1.000 and (c) is under the buffer peak at 3.88 ppm.

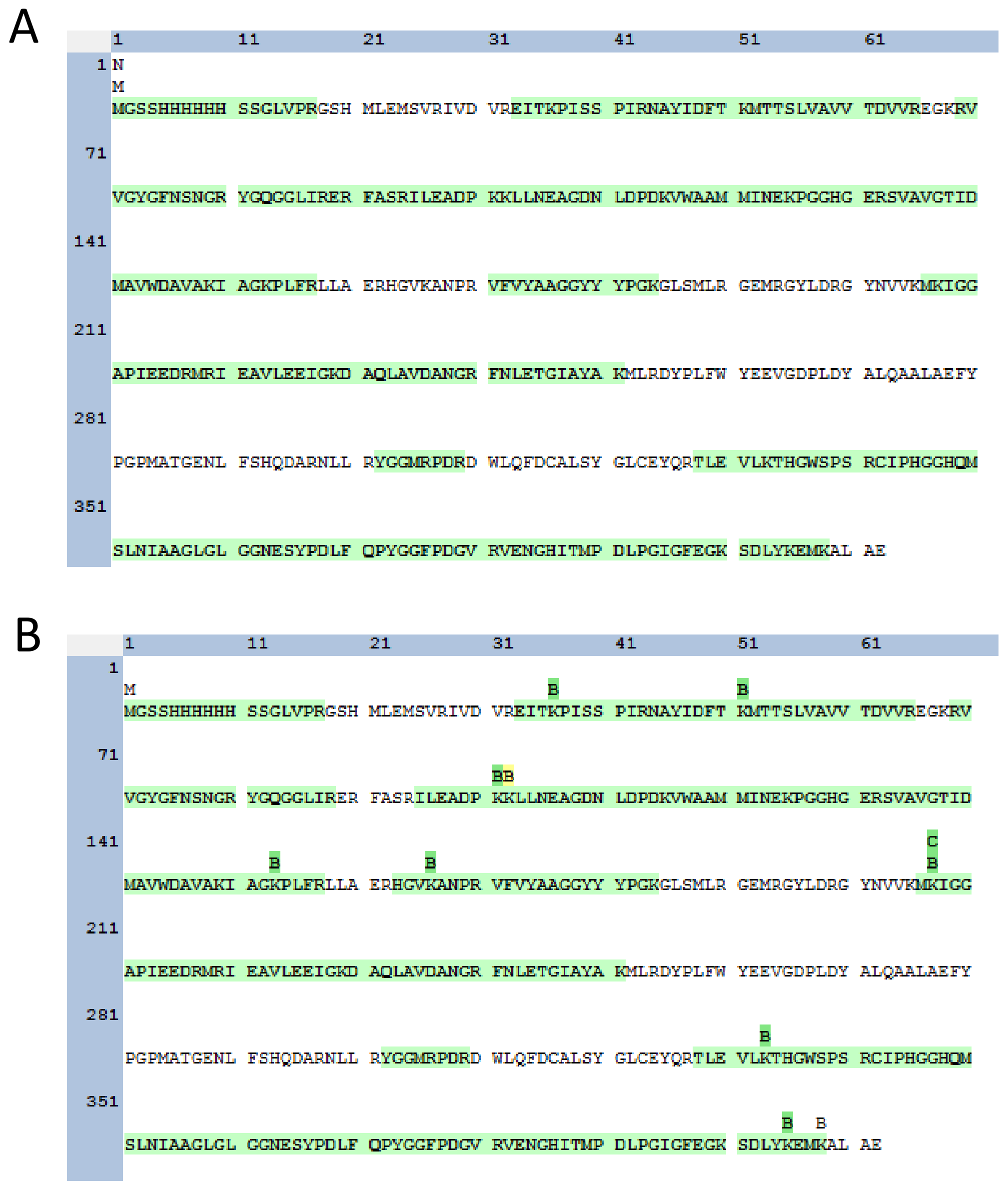

Figure 2.9 The sequence of the recombinant TarD as identified by MS. The figure shows the full sequence of the recombinant TarD bearing the N-terminal His$_6$-tag. The highlighted residues show the coverage of the polypeptide from the mass spectrometry analysis. The modified residues have letters above them, where B indicates modification by 3-HP (88 Da adduct), C indicates modification by 3-HP (86 Da adduct), M indicates Met-loss and acetylation (N-terminus), and N indicates Met-loss (N-terminus). The highlight color of these letters indicates the modification site probability, where green is 100%-99%, light green is 99%-75%, and yellow is 75%-45%. (A) The sequence of recombinant TarD from the control sample shows no modification of Lys 184 in the active site. (B) The sequence of recombinant TarD from the "trapping" sample shows two modifications of Lys 184 by 3-HP forming an 86 and an 88 Da adduct. Off-target and surface modifications by 3-HP forming 88 Da adducts are also present. (The first 23 amino acid residues correspond to the His$_6$-tag and linker region.)

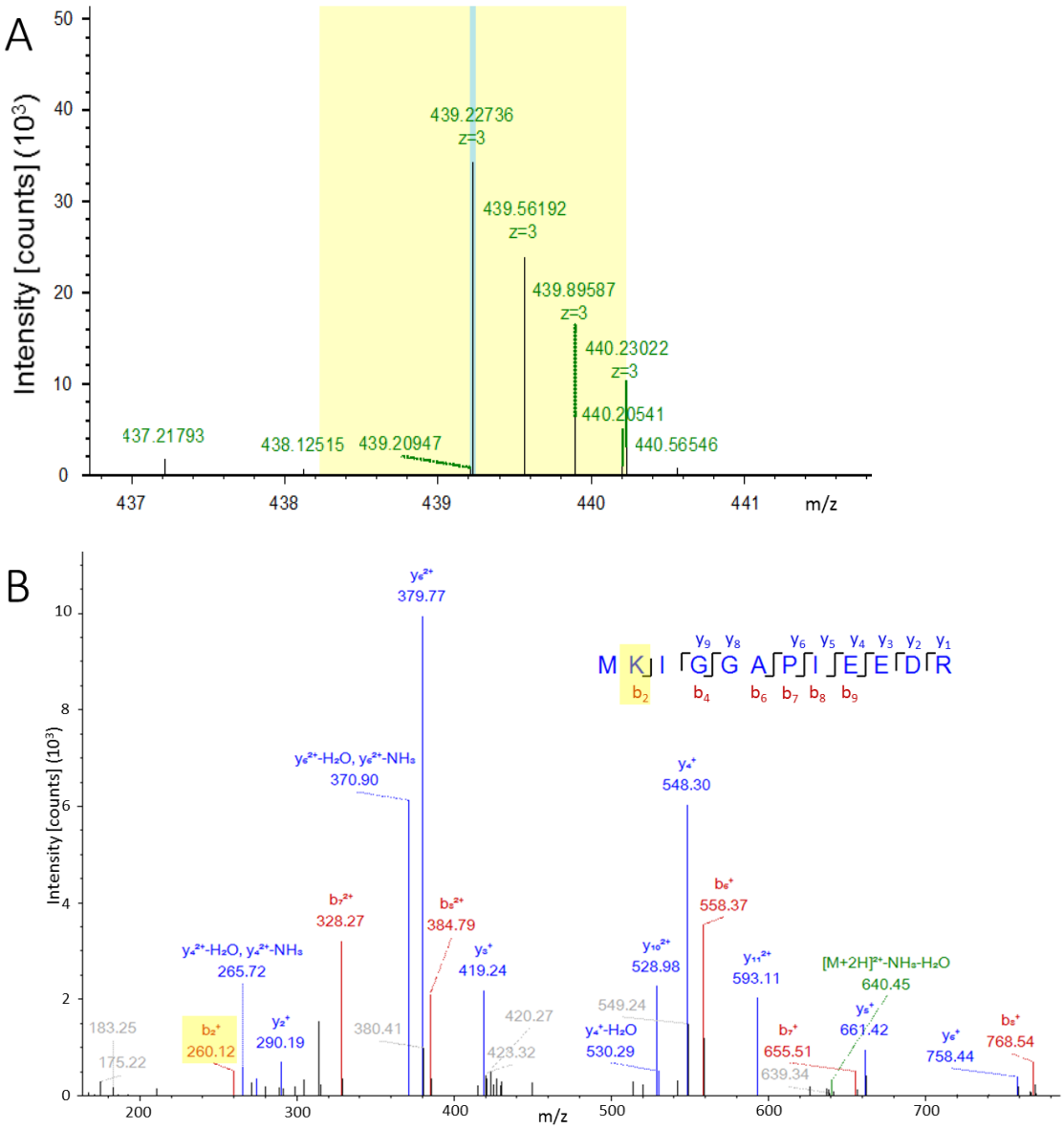

Figure 2.10 Mass spectrometry results for the control sample. (A) The precursor isotope pattern spectrum (MS1 spectrum) for the control sample of TarD shows no modification of the MK-peptide by 3-HP (monoisotopic, MH^{3+}, m/z = 439.23 Da). (B) The fragment match spectrum (MS/MS spectrum) shows no modification of Lys 184 present in the b_2 ion.

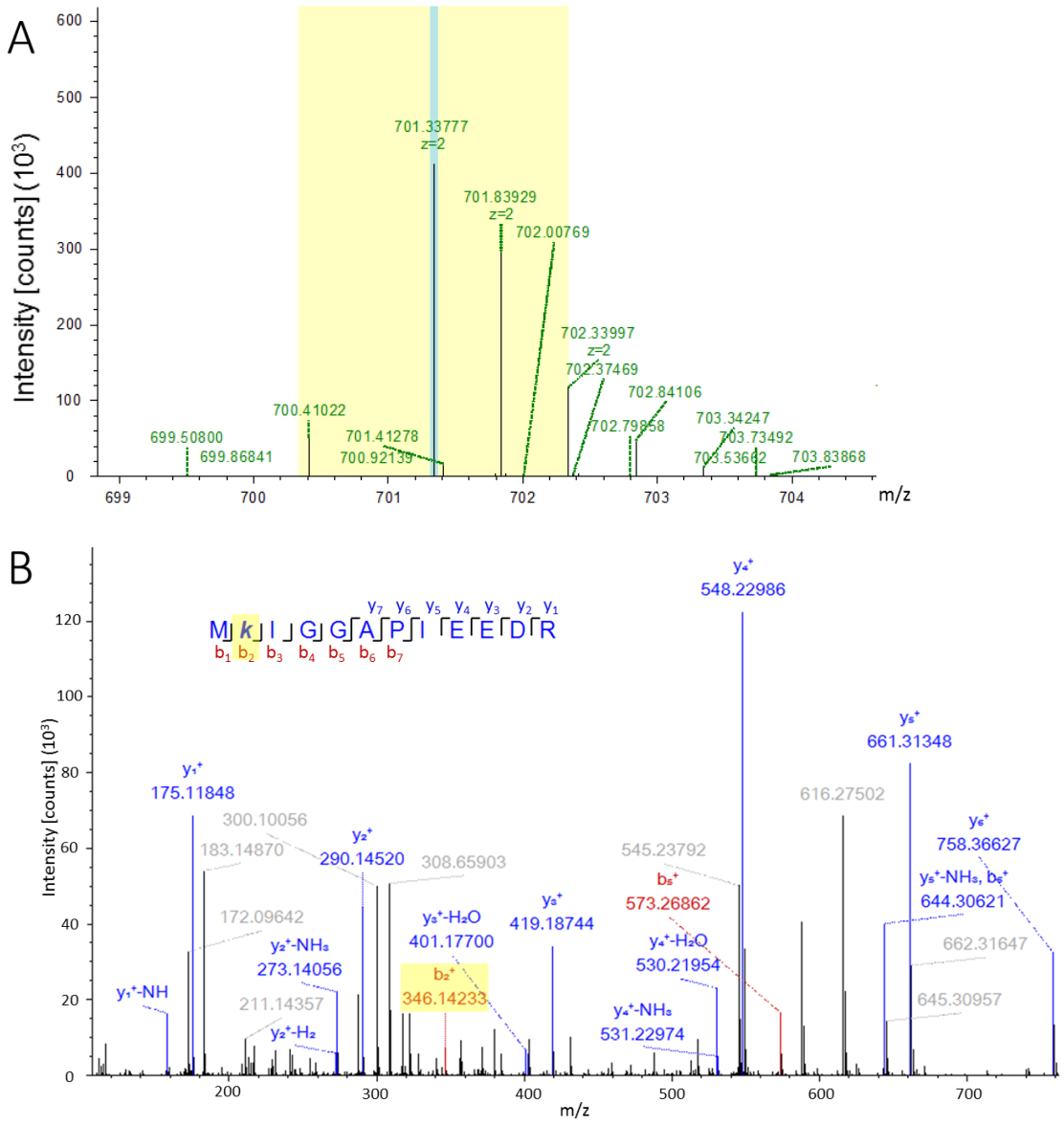

Figure 2.11 Mass spectrometry results for the "trapping" sample showing an 86 Da adduct with Lys 184. (A) The precursor isotope pattern spectrum (MS1 spectrum) for the "trapping" sample shows a modification of 86 Da by 3-HP (monoisotopic, MH^{2+}, *m/z* = 701.34 Da). (B) The fragment match spectrum (MS/MS spectrum) shows an 86 Da modification of Lys 184 present in the b_2 ion. (The modified residue is italicized.)

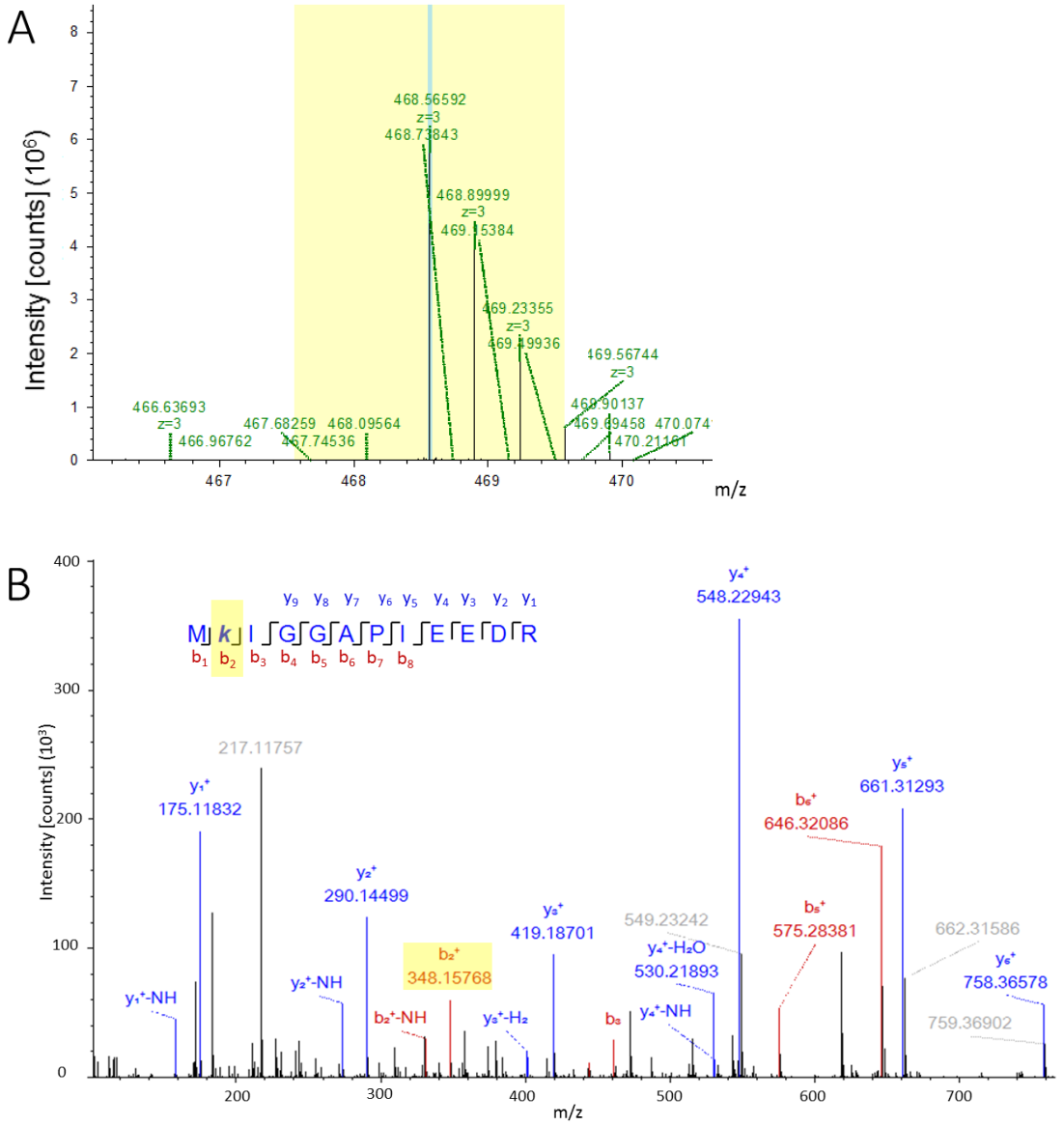

Figure 2.12 Mass spectrometry results for the "trapping" sample showing an 88 Da adduct with Lys 184. (A) The precursor isotope pattern spectrum (MS1 spectrum) for the "trapping" sample showing a modification of 88 Da with 3-HP (monoisotopic, MH^{3+}, m/z = 468.57 Da). (B) The fragment match spectrum (MS/MS spectrum) shows an 88 Da modification of Lys 184 present in the b_2 ion. (The modified residue is italicized.)

2.4 DISCUSSION

The open reading frame encoding TarD was successfully cloned into the pET-15b vector and protein expression was carried out without IPTG induction because the pET-15b is a "leaky" vector where there is a basal level of T7 RNA polymerase expression at low sugar levels, and because of the long expression time of 48 h. This observation is similar to that of Gerlt and co-workers who used the same expression system (Yew *et al*., 2006). SDS-PAGE showed that the recombinant TarD was obtained in high purity, however, the protein migrated farther than predicted, yielding a lower molecular weight (~41 kDa) than calculated from the amino acid sequence (45.6 kDa) (**Figure 2.1**). This could be attributed to incomplete unfolding of the protein, thereby maintaining some of its globular nature, or the possibility that more SDS bound to the protein than is typical, resulting in increased negative charge on the protein and enhanced migration.

As previously mentioned in section **2.1 Introduction**, tartronate inhibits the coupling enzyme, MDH, thus, there was a need to develop an alternative assay to carry out the inhibition assays with tartronate. It must be noted that an end-point assay with semicarbazide in the stop solution would not have been suitable for inhibition assays with 3-HP, an α-keto acid, which could result in a high background and a mixture of semicarbazone products. The inhibition of MDH by tartronate arises because tartronate is a substrate for MDH in the presence of NAD^+ (Davies & Kun, 1957).

Kinetic constants determined by either the continuous coupled (K_m = 0.018 ± 0.007 mM and k_{cat} = 3.6 ± 0.4 s^{-1}) or the end-point (K_m = 0.035 ± 0.007 mM and k_{cat} = 2.1 ± 0.1 s^{-1}) assays appear to be on the same order of magnitude as those reported in the literature (K_m = 0.086 mM and k_{cat} = 7.3 s^{-1}), indicating that the obtained recombinant enzyme

is active and can be used for the inhibition assays. However, the values obtained experimentally using the two different assays are not experimentally equal, which might be attributed to the presence of the coupling enzyme (MDH) in the final reaction mixture of the continuous coupled assay affecting the activity of TarD.

Inhibition of TarD by tartronate revealed that tartronate is a competitive inhibitor of TarD with a binding affinity (K_i = 0.5 ± 0.1 mM) 17× lower than the affinity of the substrate (K_m = 0.03 ± 0.01 mM). This observation is in contrast to what was observed for the inhibition of MR by tartronate, which was bound with an affinity (K_i = 1.8 mM) only ~ 2× lower than that of the substrate (K_m = 1 mM) (Nagar *et al*., 2014). Inhibition of MR by tartronate involves chelation of the Mg^{2+} in the active site, as well as bridging of the two Brønsted acid-base catalysts. Possibly, the lower affinity TarD shows for tartronate arises from the difference in the position of one of the Brønsted acid-base residues in the active site. All enzymes of the ENS catalyze the same initial half reaction, the α-proton abstraction; however, the enzymes go on to catalyze different overall reactions, which, in the case of a dehydratase, requires that the Brønsted acid catalyst in the active site be properly positioned to protonate the hydroxyl leaving group. On the other hand, for a racemase, this Brønsted acid must be positioned to protonate the carbanionic carbon of the intermediate (**Scheme 2.2**). Thus, tartronate may be very sensitive to this positioning of the Brønsted acid catalyst. In other words, the minimal ligand, tartronate, is able to recognize the active site architecture of members of the enolase superfamily, but is sensitive to the presence of subtle structural differences.

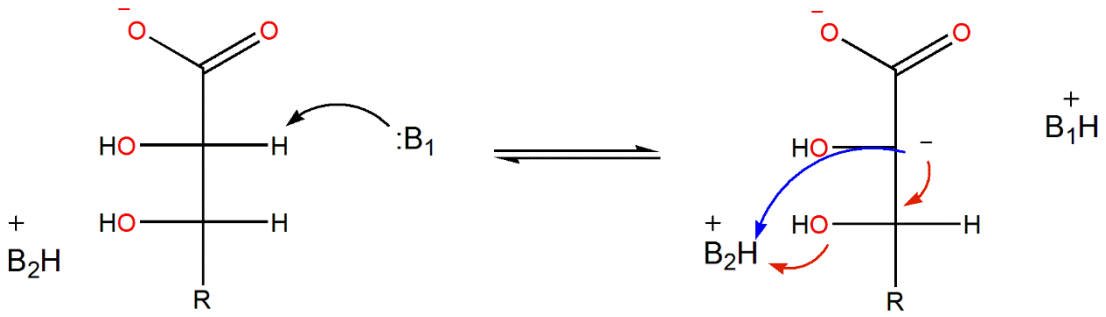

Scheme 2.2 The position of the Brønsted acid catalyst may depend on the overall reaction catalyzed by the enzyme. Although all members of the ENS catalyze the same initial deprotonation reaction, they then catalyze different overall reactions. Accordingly, the Brønsted acid catalyst in the active site may adjust its position to catalyze either the protonation of a carbanion for the racemization reaction (blue) or the protonation of a leaving group to catalyze dehydration (red). Tartronate proves to be very sensitive to such a subtle difference in the active site architecture of the enzymes.

Inhibition assays with tartronate using the end-point assay to determine the K_i value suffered from several problems. It is time-consuming, which limited the number of the different tartronate concentrations used for the K_i determination. In addition, for accurate distinction of the Michaelis-Menten plots obtained at different tartronate concentrations in the K_i determination assays, the concentration used had to be 3.0 mM apart or more.

Inhibition of TarD by 3-HP revealed that 3-HP is a competitive inhibitor of TarD with a binding affinity (K_i = 1.8 ± 0.4 mM) ~ 60× lower than the affinity for D-tartrate (K_m = 0.03 ± 0.01 mM). This result is quite different from what was observed with MR where 3-HP was found to be an irreversible inhibitor, forming a Schiff base with the Brønsted acid-base catalyst Lys 184 residue in the active site followed by a deprotonation reaction catalyzed by the second Brønsted acid-base catalyst in the active site (Nagar *et al*., 2015). Thus, 3-HP was capable of undergoing the initial half-reaction catalyzed by MR. However, this was not observed in the case of TarD.

Mass spectrometry experiments were conducted to determine if 3-HP formed a Schiff base at the active site of TarD with the Brønsted acid-base catalyst Lys 184 as well as other Lys residues. 3-HP exists in equilibrium with tartronate semialdehyde (**Scheme 2.3**), which can also form a Schiff base. It must be noted that tartronate semialdehyde can also bind through chelation of the Mg^{2+} ion by its glycolate moiety, but this cannot be verified through mass spectrometry. Two samples were prepared, a control sample, containing TarD and 3-HP, and a "trapping" sample, containing TarD, 3-HP, that was then treated with $NaCNBH_3$. The purpose of the "trapping" sample was to selectively reduce

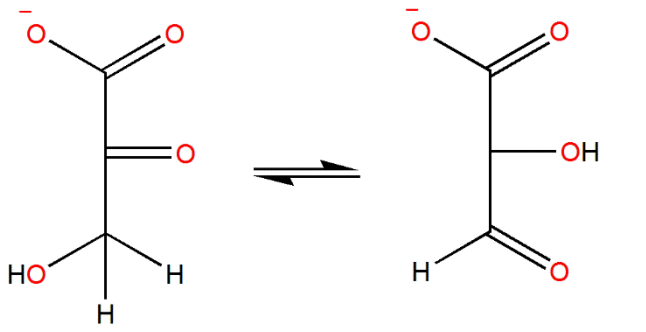

3-HP tartronate semialdehyde

Scheme 2.3 Different forms of 3-HP in solution. 3-HP exists at equilibrium with tartronate semialdehyde, which could either form a Schiff base with a Lys residue in the active site or chelate the Mg^{2+} ion through its glycolate moiety.

("trap") the imine formed with 3-HP and detect it using mass spectrometry. Three possibilities were anticipated: (1) Detection of an 86 Da adduct with Lys 184 corresponding to the formation of a Schiff base followed by a Brønsted base-catalyzed proton abstraction that leads to the formation of the *E*- and *Z*-isomers of the 86 Da adduct (which could occur in either the control sample, the "trapping" sample, or both). (2) Detection of an 88 Da adduct with Lys 184, corresponding to formation of a Schiff base followed by $NaCNBH_3$-catalyzed reduction of the imine (expected to occur only in the "trapping" sample) (**Scheme 2.4**). (3) Modification of other Lys residues in the active site, e.g., Lys 182, or surface Lys residues. The control sample showed no modification by 3-HP whereas the "trapping" sample showed formation of multiple adducts, including an 86 Da adduct and an 88 Da adduct with Lys 184, indicating that 3-HP is indeed able to access the active site and react with Lys 184. While formation of an 88 Da adduct in the "trapping" sample was anticipated due to the treatment with $NaCNBH_3$, detection of an 86 Da adduct was surprising. If the enzyme is able to catalyze the proton abstraction from the Schiff base adduct with 3-HP to give rise to the 86 Da adduct, then this should have been detected in the control sample as well. However, the apparent absence of an 86 Da adduct in the control sample does not completely rule out the possibility of its formation and, possibly, inability to detect it using mass spectrometry. Comparison of the extracted ion chromatograms (XIC) reveals that the signal from the 88 Da adduct was 8× higher than that arising from the 86 Da adduct (**Figure 2.13**), suggesting that the deprotonation reaction could be a minor side reaction. However, it must be noted that the mass spectrometry experiment described here is not quantitative, it is rather qualitative; thus, intensity comparisons may be regarded as merely rough estimates of relative ion abundance.

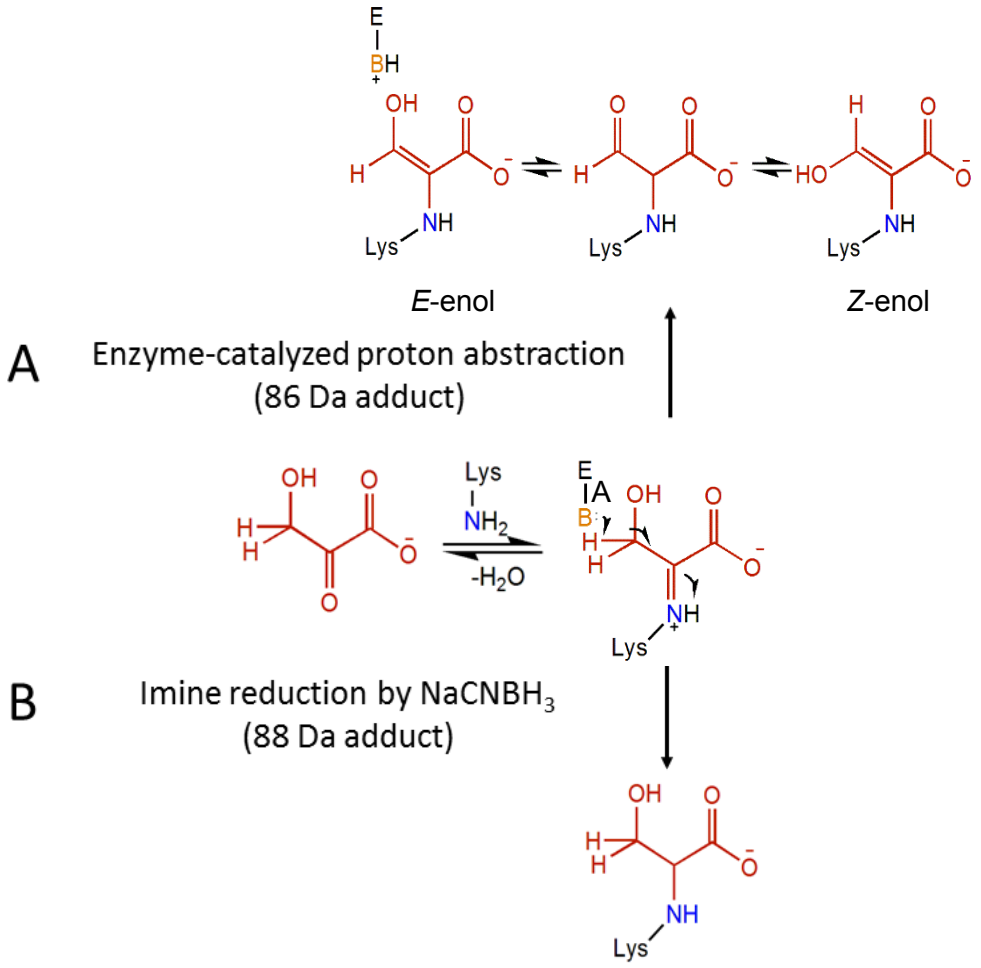

Scheme 2.4 Possible Lys adducts formed by reaction with 3-HP. Following Schiff base formation, two possibilities exist: (A) formation of an 86 Da adduct due to enzyme-catalyzed proton abstraction or (B) formation of an 88 Da adduct due to reduction of the imine by $NaCNBH_3$.

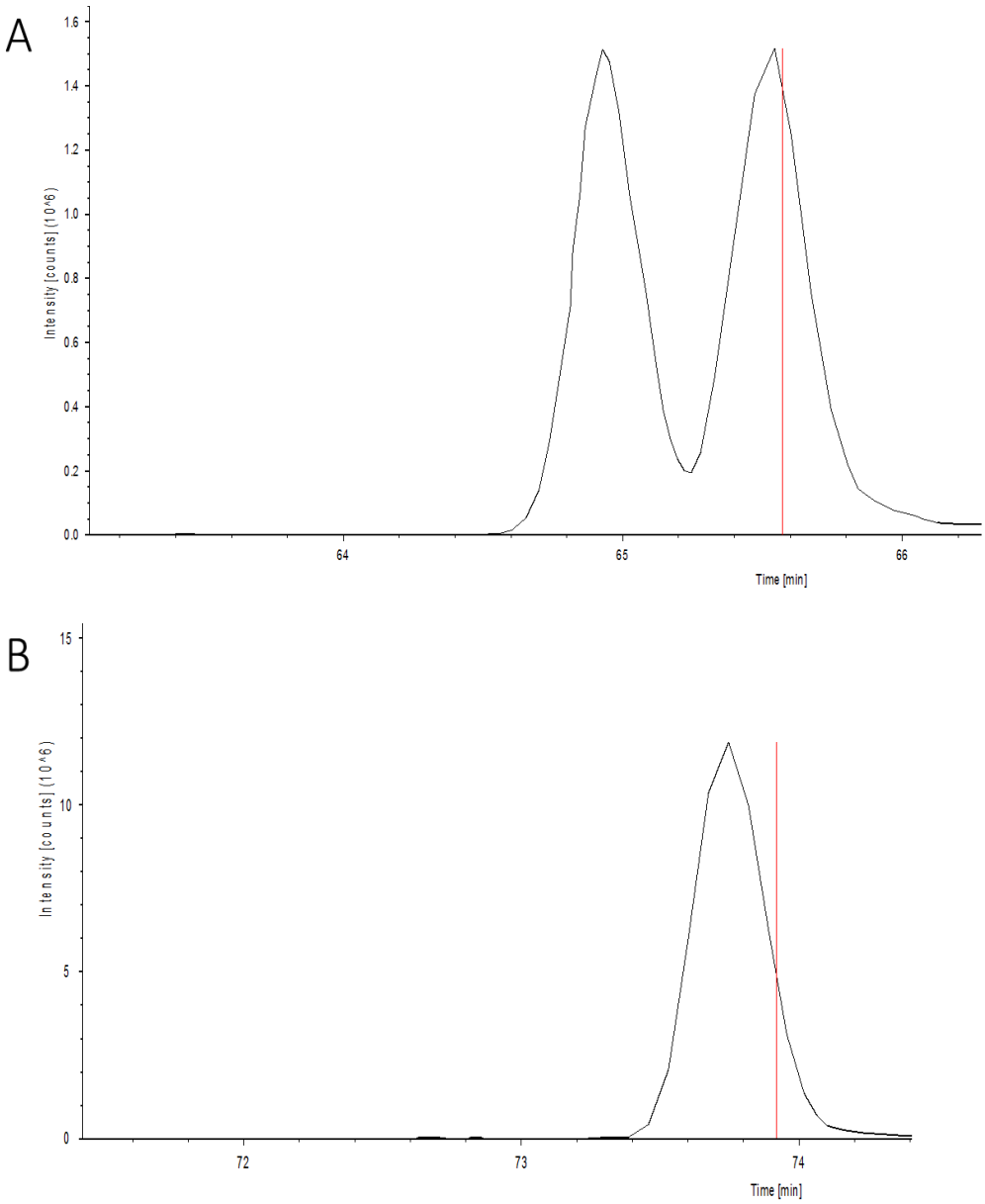

Figure 2.13 Extracted Ion Chromatograms (XIC) for the two adducts formed in the "trapping" sample. (A) XIC for the 86 Da adduct shows a peak intensity of ~ 1.5 × 10^6. Two peaks exist which could arise from the elution of the *Z*- and *E*- enol forms of the adduct. (B) XIC for the 88 Da adduct shows a peak intensity of ~ 12 × 10^6, approximately 8-fold that of the 86 Da adduct.

Calcium was found to inhibit TarD activity with an IC_{50} value of 2.6 ± 0.4 mM, which can be attributed to competition of calcium for the magnesium ion binding site in the active site of TarD. It seems that the presence of Ca^{2+} in the active site does not compensate for the absence of Mg^{2+}, i.e., it is not able to stabilize the intermediate in the active site as well as Mg^{2+}, giving rise to the observed inhibition. Alternatively, inhibition by Ca^{2+} might be due to substrate depletion through complex formation between D-tartrate and Ca^{2+}, where the dissociation constant for this complex was found previously to be equal to 15.9 mM (Cannan & Kibrick, 1938).

Glyceric acid was anticipated to be a minimal ligand for TarD and possibly a substrate, where dehydration would form pyruvate. Alternatively, glyceric acid might only undergo the initial α-proton abstraction half reaction (**Figure 2.14**) (**Scheme 2.5**). In both cases, glycerate should act as an inhibitor of TarD. However, based on the IC_{50} studies, no binding of glycerate to TarD was observed. In addition, the integrations from the ^1H NMR spectra that show only ~ 6% conversion occurring either due to deuterium exchange or product formation (**Figure 2.8**), indicating that glyceric acid is a very poor substrate, if a substrate at all.

By examining tartronate and 3-HP as minimal ligands of TarD, the following observations were made: (1) Tartronate was bound weakly, suggesting, that if the binding mode to TarD is similar to that observed in MR, a suboptimal interaction exists between the Brønsted acid-base catalysts and the 3-carboxylate group. (2) 3-HP formed a Schiff base with Lys 184 in the active site. (3) Glycerate does not appear to bind to TarD. The aforementioned observations suggest that the presence of the two carboxylate groups on tartronate, mimicking the substrate, is crucial for the binding to the active site of TarD and

that the chelation of the Mg^{2+} by the glycolate moiety only, as in the case of glyceric acid, is not sufficient for binding.

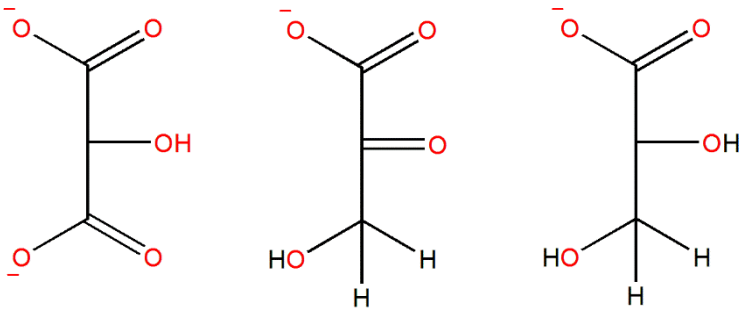

Figure 2.14 The proposed "minimal" ligands for TarD. Tartronate, 3-HP, and glyceric acid are proposed to serve as minimal ligands of TarD.

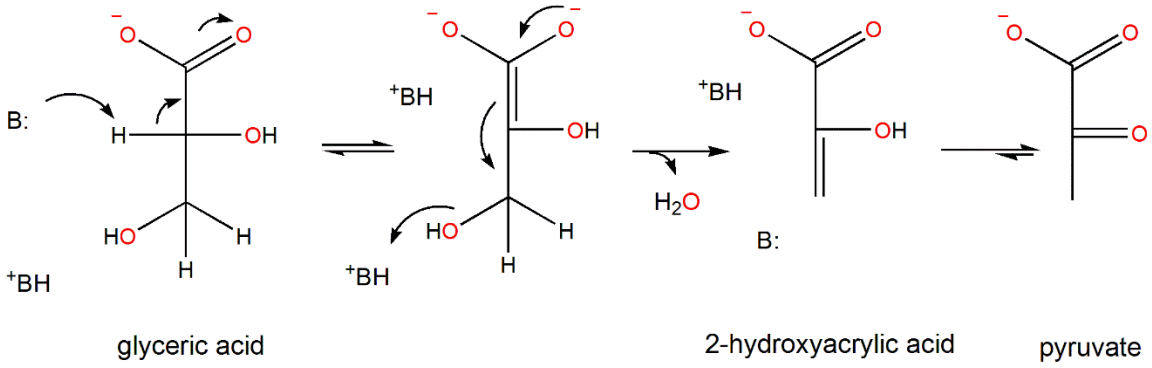

Scheme 2.5 Proposed mechanism for the dehydration of glyceric acid. Glyceric can undergo a dehydration reaction through the abstraction of the α-proton, formation of an enolate intermediate that is predicted to be stabilized by the Mg^{2+} ion in the active site, followed by formation of 2-hydroxyacrylic acid that will predominantly exist as its keto form, pyruvate.

CHAPTER 3 PROBING THE ARCHITECTURE OF THE ACTIVE SITE OF RECOMBINANT L-TALARATE/GALACTARATE DEHYDRATASE

3.1 INTRODUCTION

To examine the effects of the "minimal" ligands tartronate and 3-HP on TGD activity, suitable assays must be employed. Typically, a coupled continuous assay using two coupling enzymes, KDG aldolase and L-lactate dehydrogenase, as previously mentioned in section **1.2.2.4 Assay of TGD Activity**, is used to measure TGD activity (Yew *et al*., 2007). A polarimetric assay was also used previously to follow the time course for dehydration of galactarate using TGD (Rakus *et al*., 2009). There are two problems in the use of the coupled assay for the purposes of this thesis. First, KDG aldolase is not commercially available, although it was characterized previously by Gerlt and co-workers (Yew *et al*., 2007). Second, it is possible that tartronate, 3-HP, and other related molecules could inhibit one of the coupling enzymes. Thus, it was necessary to develop a direct continuous assay for the enzyme. In this chapter, I report the development of a direct assay using circular dichroism (CD) spectroscopy. The assay takes advantage of the fact that galactarate, the substrate, has a plane of symmetry making it a *meso* compound. Following the TGD-catalyzed dehydration reaction, there is a loss of two optical centers, forming the optically active 5-KDG. In addition, I describe the use of tartronate and 3-HP to investigate the active site architecture of TGD. Mass spectrometry experiments were conducted to determine if 3-HP reacts with a Lys residue in the active site. Other structurally-related ground-state analogues, glyceric acid and arabinonic acid, were also assessed for the possibility of their being either full or partial substrates for TGD, where TGD was

anticipated to be inhibited by the analogues or to catalyze the initial α-proton abstraction, in each respective case.

3.2 MATERIALS & METHODS

3.2.1 General

Mucic acid (galactarate), semicarbazide hydrochloride, lithium 3-hydroxypyruvate, and sodium cyanoborohydride were purchased from Sigma-Aldrich Canada, Ltd. (Oakville, ON). Tartronic acid was purchased from Alfa Aesar (Ward Hill, MA). Calcium DL-glycerate hydrate was purchased from TCI America (Portland, OR). Calcium D-arabinonate was purchased from Toronto Research Chemicals Inc. (Toronto, ON). Assays were conducted using a JASCO J-810 spectropolarimeter (Jasco Inc., Easton, MD). UV measurements were conducted using an Agilent 8453 UV-visible spectroscopy system. DNA oligonucleotide primers were purchased from Integrated DNA Technologies (Coralville, IA, USA). Restriction endonucleases were purchased from New England Biolabs (Ipswich, MA, USA). ^{1}H NMR spectroscopic analyses were conducted at the Nuclear Magnetic Resonance Research Resource (NMR^{3}) at Dalhousie University using a Brüker AV-300 spectrometer and the chemical shifts (δ) for ^{1}H spectra are in ppm referenced to HOD peak at 4.8 ppm (Gottlieb, Kotlyar, & Nudelman, 1997). LC-ESI-MS/MS experiments were carried out using HPLC with nanoflow (UltiMate 3000, Dionex) for the liquid chromatography and a hybrid ion trap-orbitrap high resolution tandem mass spectrometer (Velos Pro, Thermoscientific) for the ESI-MS/MS. The instrument was run in a data-dependent acquisition mode (DDA).

3.2.2 Cloning of the TGD Open Reading Frame from Genomic DNA of *Salmonella typhimurium*

The open reading frame encoding TGD (GI: 16766982) was cloned from genomic DNA of *Salmonella typhimurium* (kindly provided by Dr. John Rohde at the Department of Microbiology and Immunology at Dalhousie University, NS, Canada) using Phusion High-Fidelity DNA Polymerase from New England Biolabs (Ipswich, MA) for the PCR amplification following the manufacturer's protocol. The PCR amplification reaction was conducted as reported by Grelt and co-workers (Yew *et al*., 2007). The primers used were: forward (5'-GTGATTATCAGGAGAAAACATATGGCTTTAAGCGCGAATTCCG–3') and reverse (5' - GATTCCCGCCAGGATCCTTAAGGGCGTTTGCCAAATTCAC -3') where the underlined bases correspond to NdeI and BamHI recognition sites, respectively. The amplification was conducted using an S1000 Thermal Cycler from BIO-RAD Laboratories (Mississauga, ON) and the parameters were adapted from those reported by Gerlt and co-worker as follows: initial denaturation at 98 °C for 30 s, 40 cycles of 94 °C for 60 s for denaturation, thermal gradient of 45-60 °C for 75 s for annealing, 68 °C for 120 s for extension, and 72 °C for 144 s for final extension and the PCR product was gel purified using QIAquick Gel Extraction Kit (QIAGEN) (Toronto, ON). NdeI and BamHI endonucleases were then used to cut the PCR product for insertion into the multiple cloning site of the pET-15b vector (Novagen, Madison, WI). The insert and the vector were digested in a stepwise manner by incubation, in separate 1.5-mL Eppendorf tubes, with NdeI for 2 h followed by BamHI and further incubation for two hours at 37 °C according to the manufacturer's recommendations. The digestion products were then gel purified as described previously in **2.2 Materials & Methods**. T4 DNA ligase (Invitrogen) was used following the manufacturer's instructions and the ligation reaction was conducted

overnight at 16 °C. The pET-15b-*St*TGD plasmid encodes a fusion protein with an N-terminal His_6-tag. Competent *E. coli* DH5α cells were transformed with the pET-15b-*St*TGD plasmid and glycerol stocks were prepared and stored at –80 °C. The sequence of the insert was verified through commercial DNA sequencing (Robarts Research Institute, London, ON) to ensure full incorporation of the correct insert and the absence of any mutations.

3.2.3 Expression and Purification of TGD Recombinant Protein

Competent *E. coli* BL21 (DE3) cells were transformed with the pET-15b-*St*TGD plasmid, and glycerol stocks were prepared and stored at –80 °C. The protein was then overexpressed by inoculation of two starter cultures, each containing 5 mL sterile LB, 50 μg/ mL ampicillin, and 10 μL of the glycerol stock, followed by incubation overnight at 37 °C with continuous shaking at 250 rpm. The starter cultures were then added to 1 L of sterile LB broth containing 50 μg/mL of ampicillin. This was incubated for 48 h (without induction by isopropyl *β*-D-1-thiogalactopyranoside (IPTG) induction) at 37 °C with continuous shaking at 250 rpm (Yew *et al*., 2007). The cells were then harvested using centrifugation at 4000 × *g* for 10 min at 4 °C. The cell pellet was re-suspended in 30 mL of ice-cold binding buffer (1 M NaCl, 20 mM Tris-HCl, 5 mM imidazole, pH 7.9) and then sonicated on ice with 5 × 10 s bursts and 1 min cooling times between bursts, or longer if needed, using a Branson Sonifier 250 at power setting 5. The cell lysate was then clarified by ultracentrifugation at 40,000 × *g* for 30 min at 4 °C. The supernatant was subsequently passed through a Ni^{2+}-charged His-bind resin-packed column (10 mL columns packed to 2.5 mL) at 4 °C. The column was subsequently washed with 25 mL binding buffer, 15 mL wash buffer (1 M NaCl, 20 mM Tris-HCl, 60 mM imidazole, pH 7.9), and 7 mL strip buffer

(0.5 M NaCl, 20 mM Tris-HCl, 100 mM EDTA, pH 7.9). The purified protein eluted in the strip buffer. Purity was confirmed using 12% acrylamide SDS-PAGE with protein detection by staining with Coomassie blue R-250. The protein was then dialyzed against the assay buffer (50 mM Tris-HCl, and 10 mM $MgCl_2$, pH 8.0) for 18 h at 4 °C with three buffer changes (500 mL each) (Sambrook, 1989; Yew *et al*., 2007).

3.2.4 Kinetic and Inhibition Assays of Recombinant TGD

3.2.4.1 Development of a Circular Dichroism Assay

A direct, continuous assay was developed to determine the activity of TGD using circular dichroism (CD) spectroscopy. In order to find the appropriate wavelength for following the reaction, CD spectra (wavelength range: 200 – 600 nm) were obtained for galactarate (3.3 mM in assay buffer), TGD (0.05 μg/μL), and then for a mixture of TGD with galactarate for periods of 0, 10, 20, 30, and 40 min. An 0.5-cm pathlength quartz cuvette was used and the final volume of the reaction was 1 mL (at 25 °C).

The activity of TGD was then measured using CD where the change in ellipticity was followed at 316 nm for 3 min (at 25 °C). To determine the TGD concentration that gives a linear time course, the assay was conducted at galactarate concentrations of 0.1 mM and 6.0 mM and varying enzyme concentrations were used (0.01-0.20 μg/μL). For routine assay, the reaction mixture contained a concentration of TGD that gave a linear time course (0.05 μg/μL), galactarate (0.1-6.0 mM), 50 mM Tris-HCl buffer (pH 8.0), and 10 mM $MgCl_2$. The enzyme concentration was determined by measuring the absorbance at 280 nm using the calculated extinction coefficient of the recombinant protein (59,930 $M^{-1}cm^{-1}$) obtained using the ExPASY ProtParam tool (Gasteiger *et al*., 2003).

Nonlinear regression analysis was used to fit the Michaelis-Menten equation **2.1** to the initial velocity data to obtain V_{max} and K_m values for the recombinant TGD using the program KaleidaGraph v. 4.02 from Synergy Software (Reading, PA) (Segel, 1975). The kinetic assays were conducted in triplicate, and the values are the average and the error reported is the standard deviation.

Galactarate (6.0 mM) was incubated with TGD (0.05 μg/μL) in 50 mM Tris-HCl buffer (10 mM $MgCl_2$, pH 8.0) and the reaction was followed for 40 min at 316 nm and 25 °C in an 0.5-cm pathlength quartz cuvette. The molar ellipticity for 5-KDG was determined by constructing a calibration curve through incubation of galactarate (2.0-6.0 mM) with TGD (0.05 μg/μL) in 50 mM Tris-HCl buffer (10 mM $MgCl_2$, pH 8.0) for 20 min at 25 °C in an 0.5-cm pathlength quartz cuvette and measuring the ellipticty. The molar ellipticity was calculated according to equation **3.1** where [Θ] is the molar ellipticity in deg cm^2 $dmol^{-1}$, Θ is the ellipticity in deg, c is the concentration in M, and b is the pathlength in cm. The molar ellipticity determination experiment was conducted twice and the reported error is the standard deviation.

$$\Theta = [\Theta] \, c \, b \qquad \textbf{3.1}$$

3.2.4.2 Inhibition Assays

The CD assay was used to determine IC_{50} values for the inhibition of TGD by tartronate, 3-HP, glyceric acid, and D-arabinonate. Values were obtained using nonlinear regression analysis to fit equation **2.2** to the relative initial velocities (v_i/v_o) using KaleidaGraph v. 4.02 (Segel, 1975). The inhibition assays were conducted in triplicate, and values are the averages, and the error reported is the standard deviation. The IC_{50} studies

were conducted at a substrate concentration equal to the measured K_m from the CD assay and the inhibitor concentrations ranged from 0 to 20.0 mM.

Ion exchange of the Ca salts of glyceric acid and D-arabinonic acid with Na was carried out as described in section **2.2.4.3.1 Inhibition by Glycerate**.

3.2.5 Mass Spectrometry Experiments with 3-HP

To assess the possibility of 3-HP reacting with active site Lys residues to form a Schiff base, mass spectrometry experiments were conducted where two samples were prepared and investigated: a control sample that contained TGD and 3-HP and a "trapping" sample that contained TGD and 3-HP that was then treated with $NaCNBH_3$. The experiment was conducted as follows: 72.8 µL TGD (5.5 mg/mL) was incubated with 80 µL 3-HP (20 mM) at 25 °C for 30 min for both samples followed by addition of 47.2 µL distilled water to the control sample and 47.2 µL $NaCNBH_3$ (1 M) to the "trapping" sample, the pH was adjusted to 8.0, and both samples were further incubated at 25 °C for 30 min. The final volume of the reaction, after addition of either water or $NaCNBH_3$, was 200 µL. Both samples were processed identically throughout the subsequent steps of the experiment as described in section **2.2.5 Mass Spectrometry Experiments with 3-HP**.

3.3 RESULTS

3.3.1 Cloning, Expression, and Purification of TGD

The recombinant TGD was obtained with high purity as shown by the 12% SDS-polyacrylamide gel (**Figure 3.1**).

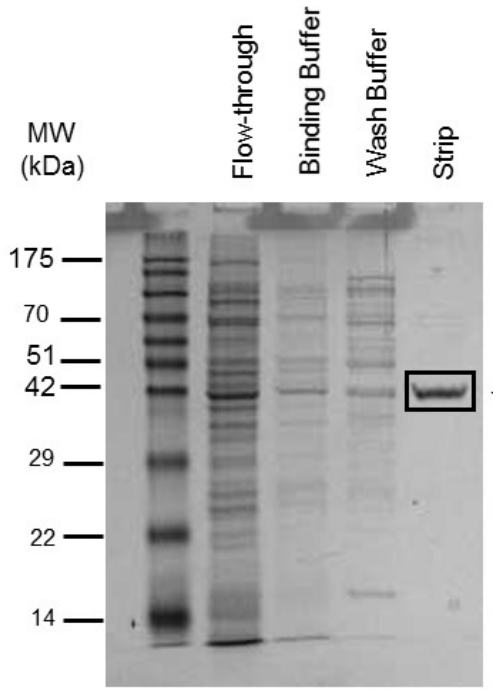

Figure 3.1 Purified recombinant TGD. The gel shows the different fractions resulting from the protein purification. Recombinant TGD elutes in the strip fraction with high purity. The molecular mass of the TarD monomer calculated from the amino acid sequence is 46.6 kDa.

3.3.2 Kinetic and Inhibition Assays of TGD

3.3.2.1 Development of a Circular Dichroism Assay

The CD spectra of galactarate and TGD do not show significant ellipticity between 250-550 nm (**Figure 3.2**). The spectra obtained after incubation of galactarate with TGD for various times showed that the reaction goes to completion within 10 min and that there is a maximal change in ellipticity over a wavelength range of 310-330 nm; thus, a wavelength of 316 nm was chosen to follow the TGD-catalyzed reaction (**Figure 3.3**). The enzyme concentration that gave a linear time course at the highest and lowest substrate concentrations, 0.1 and 6.0 mM, respectively, was determined to be 0.05 μg/μL (**Figure 3.4**). The molar ellipticity [Θ] of 5-KDG at 316 nm was determined to be 148 ± 1 deg cm^2 $dmol^{-1}$ (**Figure 3.5**). The kinetic parameters of the recombinant TGD were determined using the direct CD assay and V_{max} was found to be 8.9 ± 0.8 μM/s, k_{cat} to be 8.2 ± 0.7 s^{-1}, and K_m to be 0.9 ± 0.2 mM (**Figure 3.6**).

3.3.2.2 Inhibition Assays with Tartronate and 3-HP

Inhibition by tartronate gave an IC_{50} value of 17 ± 1 mM. Assuming competitive inhibition, the K_i value can be calculated from equation **2.5** to be equal to 8.5 mM (**Figure 3.7**) (Segel, 1975). Inhibition by 3-HP gave an IC_{50} value of 15 ± 1 mM. Assuming competitive inhibition, the K_i value can be calculated from equation **2.5** to be equal to 7.5 mM (Segel, 1975). Calcium was also found to inhibit TGD with an IC_{50} value of 0.073 ± 0.006 mM (**Figure 3.8**). Both glyceric acid and D-arabinonate showed no inhibition of TGD.

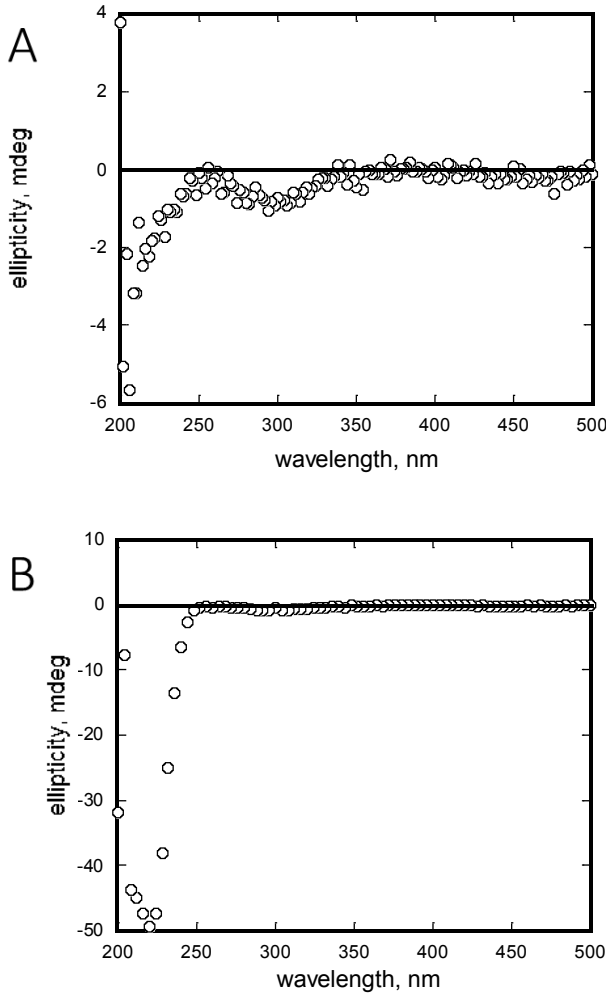

Figure 3.2 CD spectra required for the development of the TGD assay. The CD spectra of (A) galactarate (3.3 mM) in 50 mM Tris-HCl buffer (10 mM $MgCl_2$, pH 8.0) and (B) TGD (0.05 μg/μL) in 50 mM Tris-HCl buffer (10 mM $MgCl_2$, pH 8.0) were obtained.

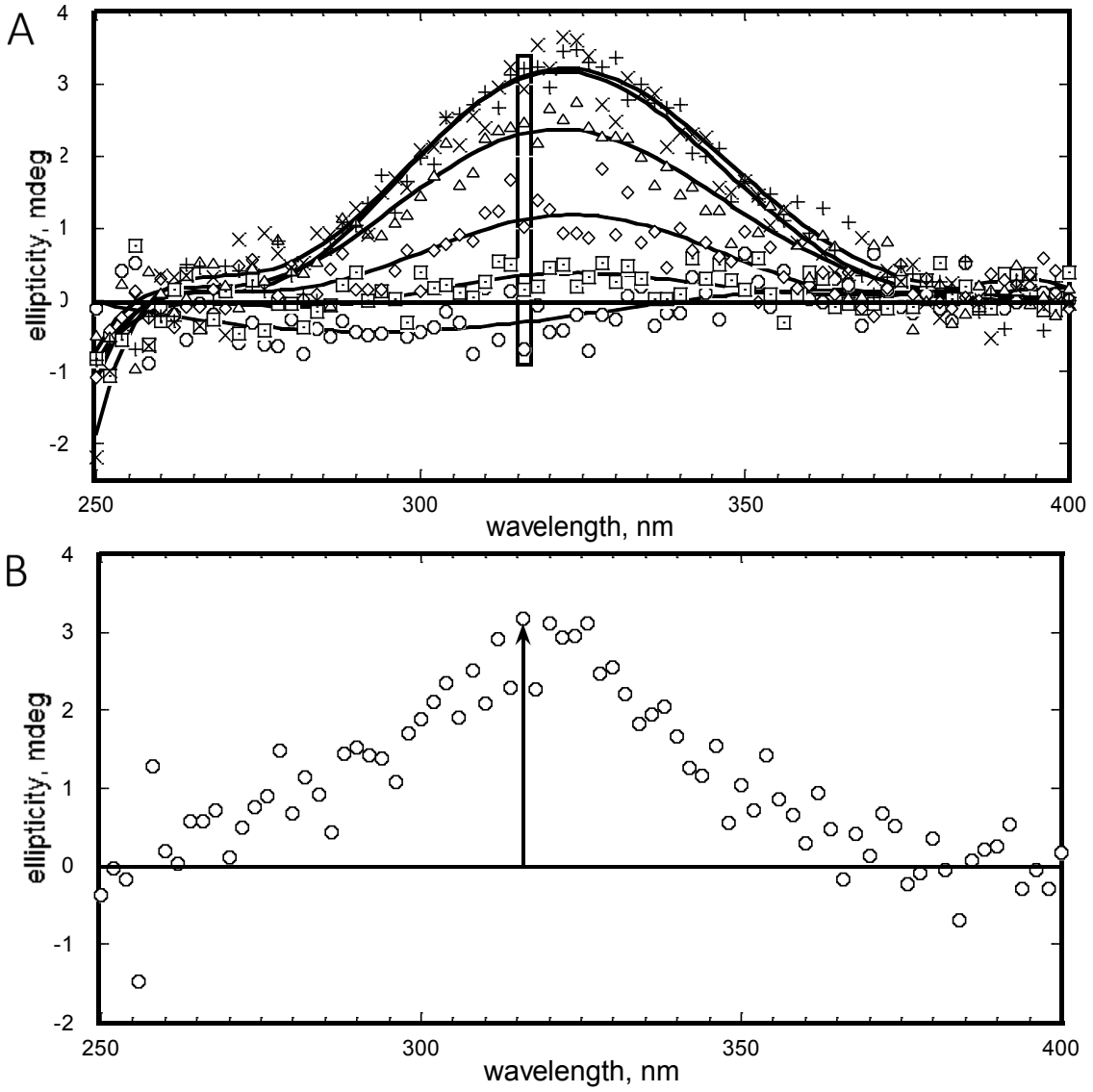

Figure 3.3 Determination of the wavelength at which to follow the TGD-catalyzed reaction. (A) CD spectra of the reaction mixture at the following time points: before addition of TGD (○), at 0 time i.e. right after TGD addition (0.05 μg/μL) (□), after 3 min (◊), after 6 min (Δ), after 10 min (×), and after 15 min (+) of incubation with galactarate (6.0 mM) at 25 °C. This shows that a range of wavelengths between 310-330 nm is suitable for following the TGD-catalyzed reaction. (B) The difference spectrum between measurements after 6 min incubation with TGD (panel A (Δ)) and before TGD addition (panel A (○)) shows that the reaction can be followed at 316 nm.

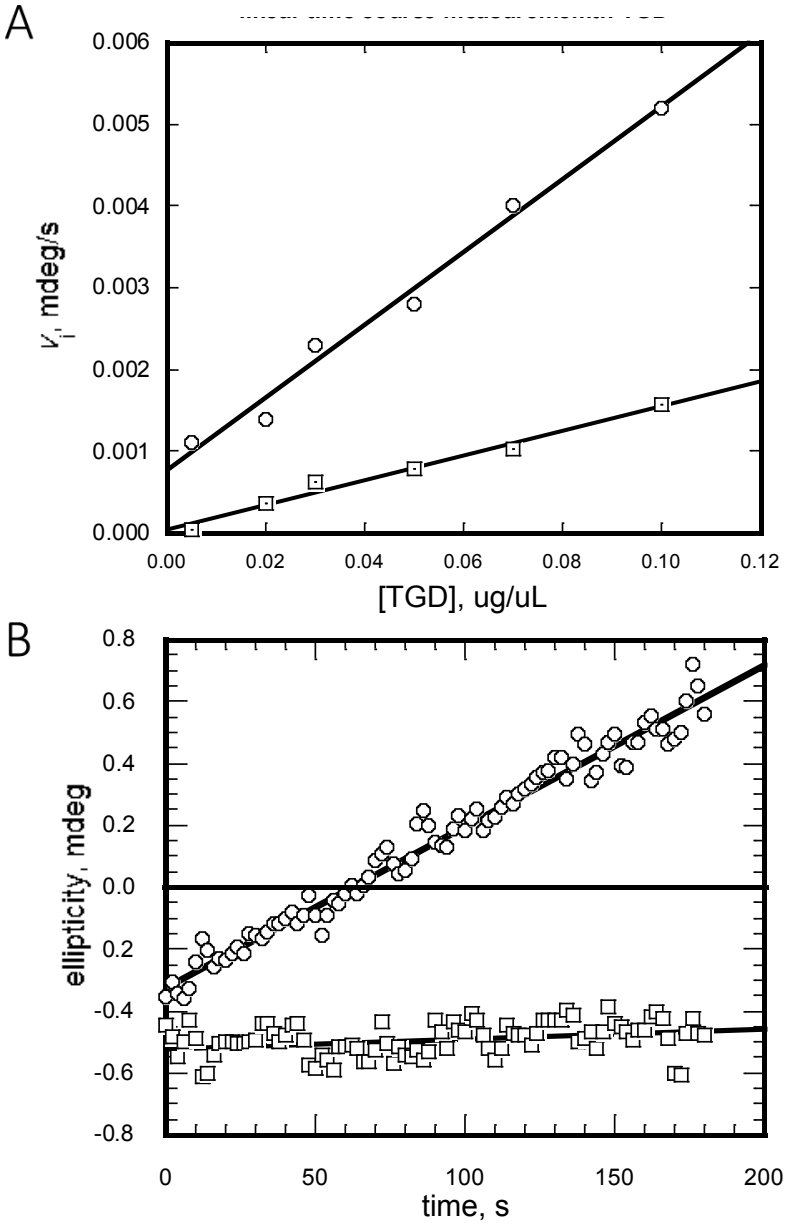

Figure 3.4 Determination of the TGD concentration that gives a linear time course. (A) The TGD-catalyzed reaction was measured at different TGD concentrations (0.100-0.005 μg/μL) at galactarate concentrations of 6.0 mM (○) and 0.1 mM (□). (B) A TGD concentration of 0.05 μg/μL was used at galactarate concentrations of 6.0 mM (○) and 0.1 mM (□). A TGD concentration of 0.05 μg/μL was found to give a linear time course.

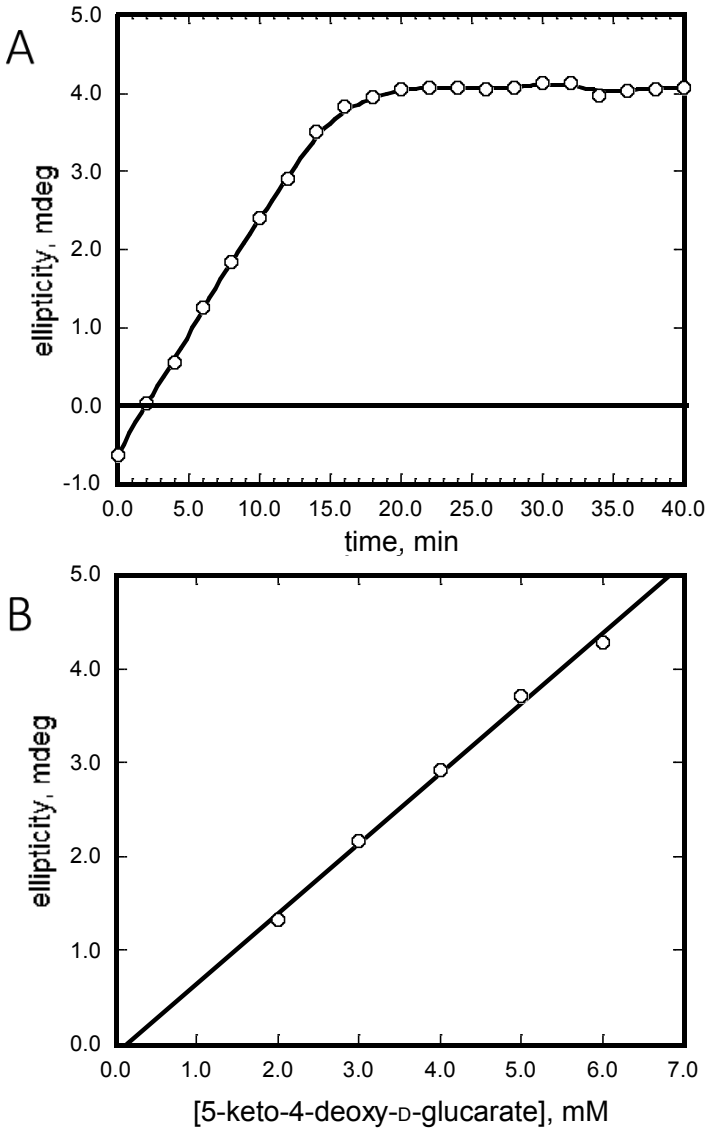

Figure 3.5 Determination of the molar ellipticity of 5-KDG. (A) Time course for the TGD-catalyzed reaction. The graph shows that the reaction goes to completion after 18 min of incubation of TGD (0.05 µg/µL) with galactarate (6.0 mM) in 50 mM Tris-HCl (10 mM $MgCl_2$, pH 8.0) at 25 °C and 316 nm. (B) Calibration curve for the determination of the molar ellipticity of 5-KDG at 316 nm through incubation of galactarate (2.0-6.0 mM) with TGD (0.05 µg/µL) in 50 mM Tris-HCl buffer (10 mM $MgCl_2$, pH 8.0) for 20 min at 25 °C. The molar ellipticity was obtained from the slope of the line and was found to be 148 ± 1 deg cm^2 $dmol^{-1}$.

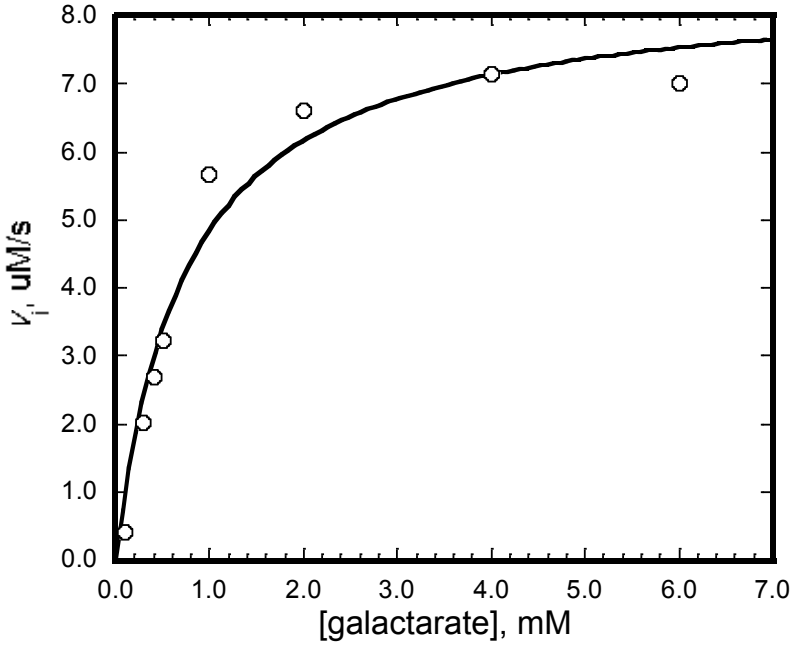

Figure 3.6 Michaelis-Menten plot for TGD. The kinetic parameters for the recombinant TGD were determined using the CD assay where V_{max} was found to be 8.9 ± 0.8 μM/s and K_m to be 0.9 ± 0.2 mM

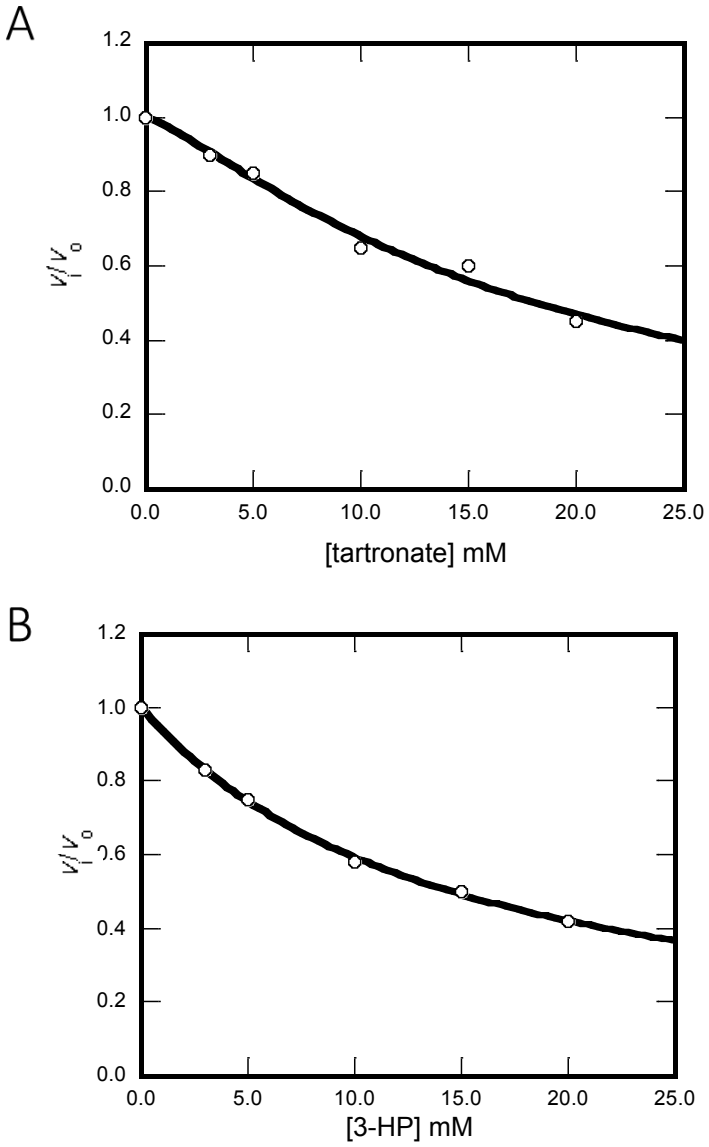

Figure 3.7 IC_{50} determination for TGD with tartronate and 3-HP. (A) Representative plot for IC_{50} study with tartronate where the IC_{50} value was found to be 17 ± 1 mM and n = 1.1 ± 0.2. (B) Representative plot for IC_{50} study with 3-HP where the IC_{50} value was found to be 15 ± 1 mM and n = 1.1 ± 0.1.

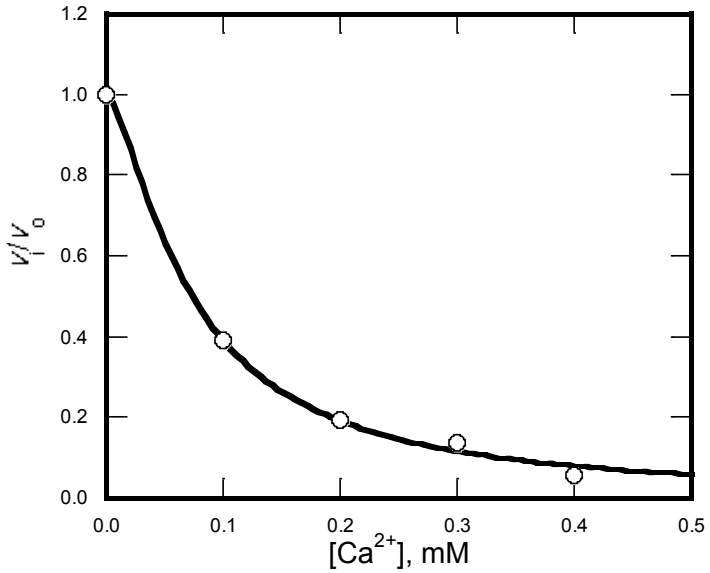

Figure 3.8 Inhibition of TGD with Ca^{2+}. Ca^{2+} was found to inhibit the recombinant TGD with an apparent IC_{50} value of 0.073 ± 0.006 mM and n = 1.4 ± 0.1.

3.3.3 Mass Spectrometry Results for Lys Modification

The active site Brønsted acid-base catalyst Lys 197 (underlined) is present in the LKVGQPNCAEDIR peptide (LK-peptide, residues 96-208). For the control sample, the LK-peptide (monoisotopic, MH^{3+}, *m/z* = 500.59 Da) showed no modification of Lys 197 (**Figure 3.9**) and (**Figure 3.10**). The "trapping" sample showed a modification of 88 Da to the LK-peptide (monoisotopic, MH^{3+}, *m/z* = 529.93 Da), corresponding to a covalent modification to Lys 197 in the active site due to formation of Schiff base with 3-HP and the subsequent reduction of the imine by $NaCNBH_3$ (**Figure 3.9**) and (**Figure 3.11**).

A

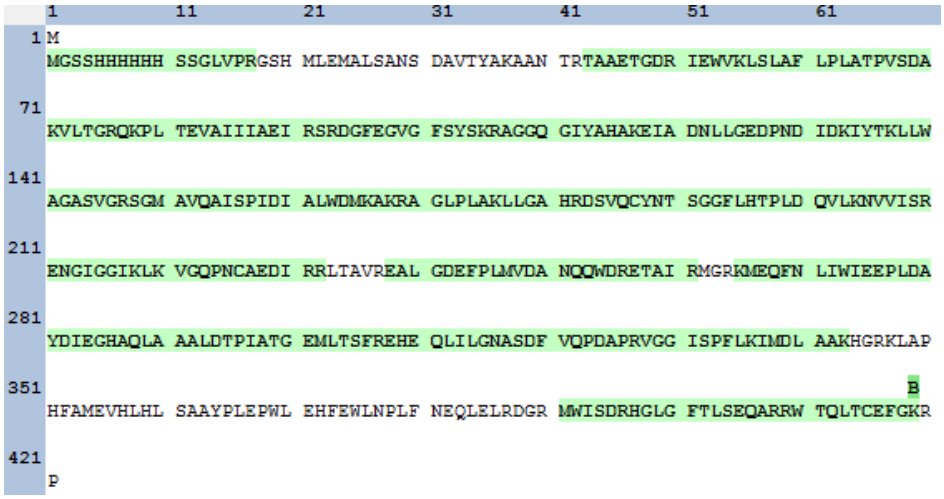

B

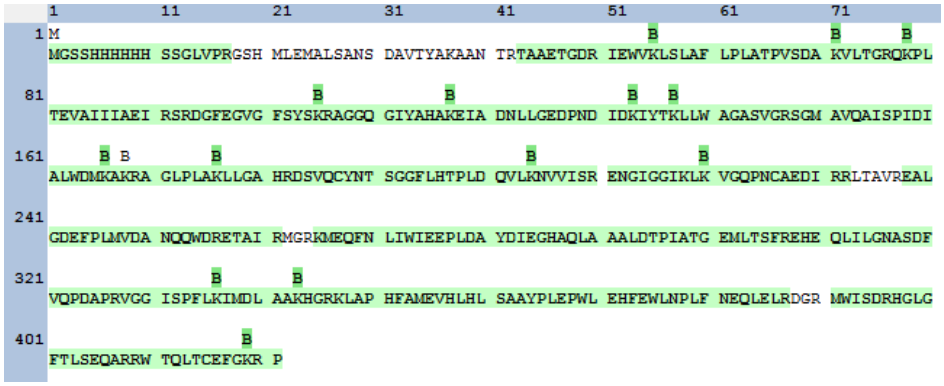

Figure 3.9 The amino acid sequence for the recombinant TGD as identified by MS. The figure shows the full sequence of the recombinant TGD fusion protein with an N-terminal His_6-tag. The highlighted residues are those that were identical to the database search to determine the identity of the protein. The modified residues have letters above the sequence, where B indicates modification by 3-HP (88 Da adduct), and M indicates Met-loss and acetylation (N-terminus). The highlight color of these letters indicates the modification site probability, where green is 100%-99%. (A) The sequence of recombinant TGD from the control sample shows no modification of the Lys 197 in the active site and only modification of Lys 420. (B) The sequence of recombinant TGD from the "trapping" sample shows that 3-HP forms an 88 Da adduct with Lys 197. It also shows off-target and surface modifications by 3-HP forming 88 Da adducts as well. (The first 23 amino acid residues correspond to the His_6-tag and linker region.)

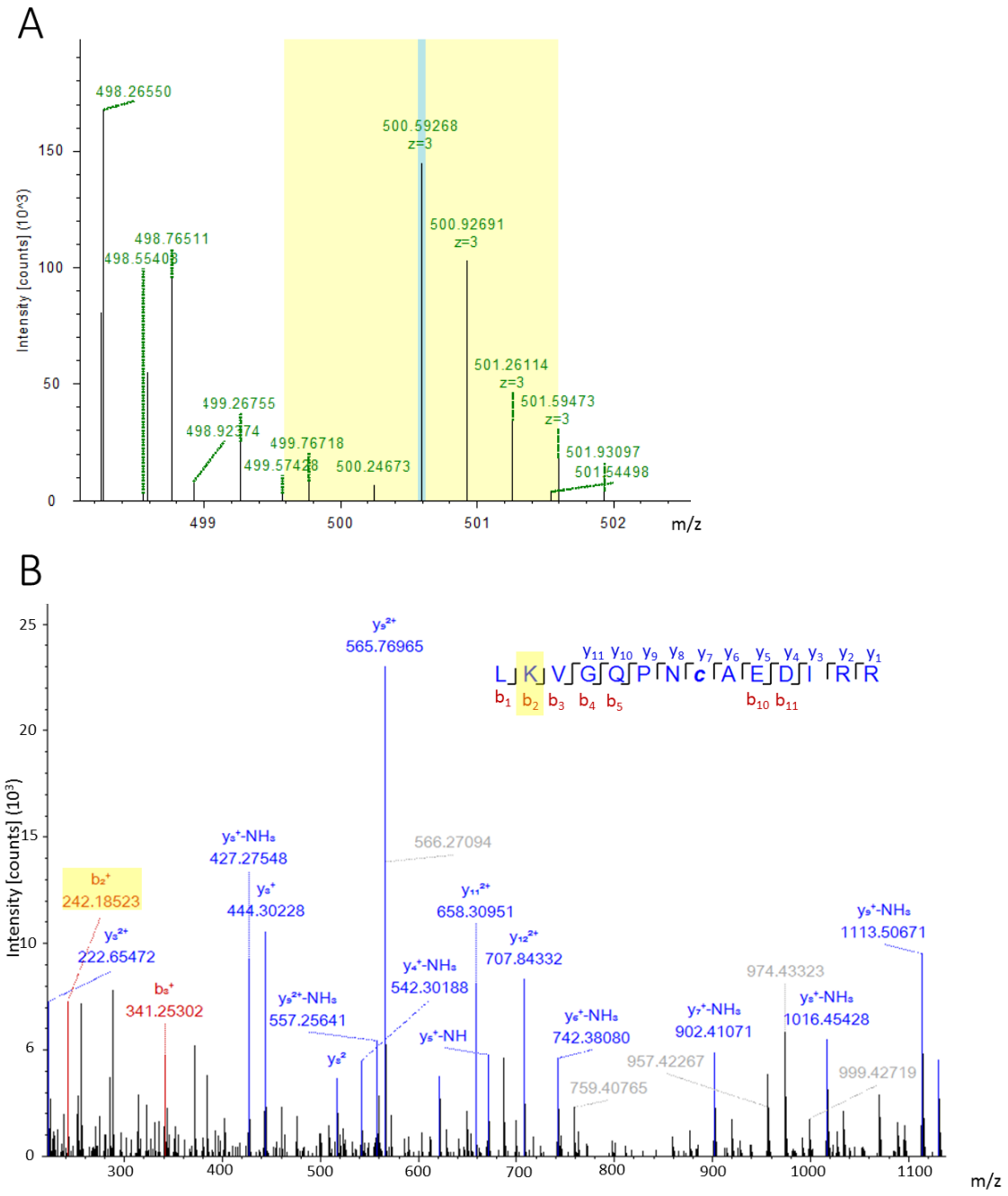

Figure 3.10 Mass spectrometry results for the control sample. (A) The precursor isotope pattern spectrum (MS1 spectrum) for the control sample shows no modification of the LK-peptide by 3-HP (monoisotopic, MH^{3+}, *m/z* = 500.59 Da). (B) The fragment match spectrum (MS/MS spectrum) shows no modification of Lys 197 present in the b_2 ion.

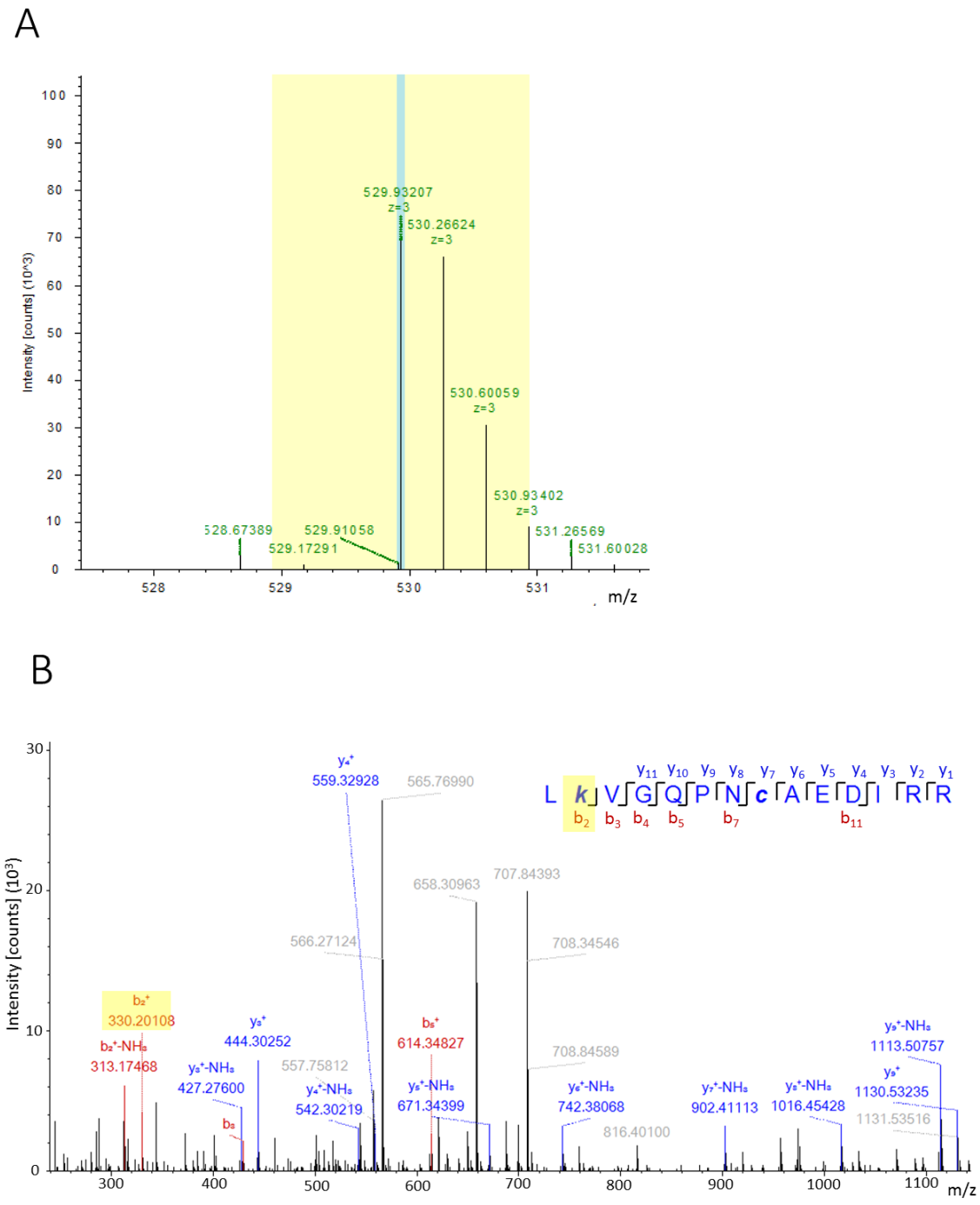

Figure 3.11 Mass spectrometry results for the "trapping" sample. (A) The precursor isotope pattern spectrum (MS1) shows an 88 Da modification by 3-HP (monoisotopic, MH^{3+}, $m/z = 529.93$ Da). (B) The fragment match spectrum (MS/MS spectrum) shows an 88 Da modification of Lys 197 present in the b_2 ion (the modified residue is italicized.)

3.4 DISCUSSION

The open reading frame encoding TGD was successfully cloned into the pET-15b vector and protein expression was carried out without IPTG induction because the pET-15b vector is a "leaky" vector as previously mentioned in section **2.4 Discussion**. SDS-PAGE showed that the recombinant TGD was obtained in high purity, however, the position of the protein corresponds to a molecular weight (~ 41 kDa) that was lower than that calculated from the amino acid sequence (47 kDa). Although this may arise for similar reasons to those mentioned in section **2.4 Discussion**, it is interesting that TGD appears to migrate faster than expected much like TarD. This may be due to the structural similarity of these two enzymes.

As previously mentioned in section **3.1 Introduction**, a direct assay was essential for the purposes of this work and thus, a CD assay was developed by taking advantage of the optical inactivity of the substrate, galactarate, and the production of an optically-active product, 5-KDG. Although TGD catalyzes a competing epimerization reaction between the two substrates galactarate and L-talarate along with the dehydration reaction, galactarate was chosen as the substrate because Gerlt and co-workers had previously reported that 30% of L-talarate undergoes epimerization to form galactarate, whereas epimerization of galactarate to L-talarate is negligible (Yew *et al*., 2007). In addition, galactarate is commercially available. The recombinant TGD was found to be active and the CD assay was found to be adequate for following the TGD-catalyzed reaction. The K_m value obtained (0.9 ± 0.2 mM) is on the same order of magnitude as that previously reported by Gerlt and co-workers (0.33 ± 0.07 mM) (Yew *et al*., 2007). Also, the k_{cat} value obtained (8.2 ± 0.7 s^{-}

^{1}) is on the same order of magnitude of that reported by the same group (3.6 ± 0.2 s^{-1}) (Yew *et al.*, 2007).

Only IC_{50} values were determined for tartronate and 3-HP since the inhibition by both compounds was weak. These values indicated that TGD binds tartronate with an affinity (K_i value of 8.5 mM assuming competitive inhibition) that is ~10× lower than the binding affinity of the substrate (K_m = 0.9 ± 0.2 mM), assuming competitive inhibition. The observed low binding affinity of TGD with tartronate likely arises from the loss of many of the binding determinants as compared to the substrate, galactarate (**Figure 3.12**); however, it is more meaningful to compare the binding of tartronate between ENS enzymes. This result is different from the behavior of tartronate with MR (Nagar *et al*., 2014), in which the compound was bound with only ~ 2× less affinity than that of the substrate, (*R*)-mandelate (K_i value of 1.8 mM *c.f.* K_m value of 1 mM). As mentioned in section **2.4 Discussion**, since the mode of inhibition of MR by tartronate is through chelation of the Mg^{2+} in the active site as well as bridging the two Brønsted acid-base catalysts, it is possible that the lower binding affinity with TGD arises from the difference in the position of the Brønsted acid catalyst that protonates the hydroxyl leaving group. Thus, as was observed with TarD, tartronate appears to be sensitive to the positioning of the Brønsted acid-base catalysts. An x-ray crystal structure of TGD with bound tartronate would be required to verify this supposition.

Inhibition of TGD by 3-HP revealed that TGD binds 3-HP with an affinity (K_i value of 7.5 mM assuming competitive inhibition) that is ~ 8× lower than the binding affinity to the substrate (K_m = 0.9 ± 0.2 mM). This is in contrast to what was observed for MR where 3-HP was found to be an irreversible inhibitor (Nagar *et al*., 2015). As previously discussed

in section **2.4 Discussion**, in the case of MR, 3-HP underwent the initial half-reaction (Nagar *et al*., 2015). Mass spectrometry experiments were carried out to determine if 3-HP reacts with Lys 197, or other Lys residues to form a Schiff base as previously discussed in (**2.4 Discussion**) (**Scheme 2.3**). The control sample showed no modification by 3-HP, whereas the "trapping" sample showed formation of an 88 Da adduct with Lys 197, indicating that 3-HP is able to access the active site and form a Schiff base with Lys 197, followed by reduction of the imine by $NaCNBH_3$ present in the "trapping" reaction (**Scheme 2.4**). This observation is consistent with the inhibition results and suggests a difference in the mode of inhibition of TGD by 3-HP as compared to that observed for MR. Based on the mechanistic studies of Gerlt and co-workers (Yew *et al*., 2007), it seems reasonable to propose that His 328, the L-talarate-specific Brønsted base, is protonated when the galactarate is used as a substrate and that Lys 197, the galactarate-specific Brønsted base, is the one that catalyzes the initial α-proton abstraction. Possibly, the binding of galactarate or the Lys 197-catalyzed proton abstraction induces a conformational change that alters the active site architecture, shifting the equilibrium towards protonation of His 328. Similarly, when 3-HP forms a Schiff base with Lys 197 in the active site, His 328 may become protonated, thereby preventing the proton abstraction reaction, which, in the case of MR, "traps" 3-HP in the active site. Thus, 3-HP appears to be able to detect subtle changes in the protonation state of the Brønsted acid-base catalysts in the active sites of members of the enolase superfamily. The modified cysteine residue in the LK-peptide is carbamidomethylated due to the initial treatment of the dithiothreitol-reduced tryptic peptides with iodoacetamide.

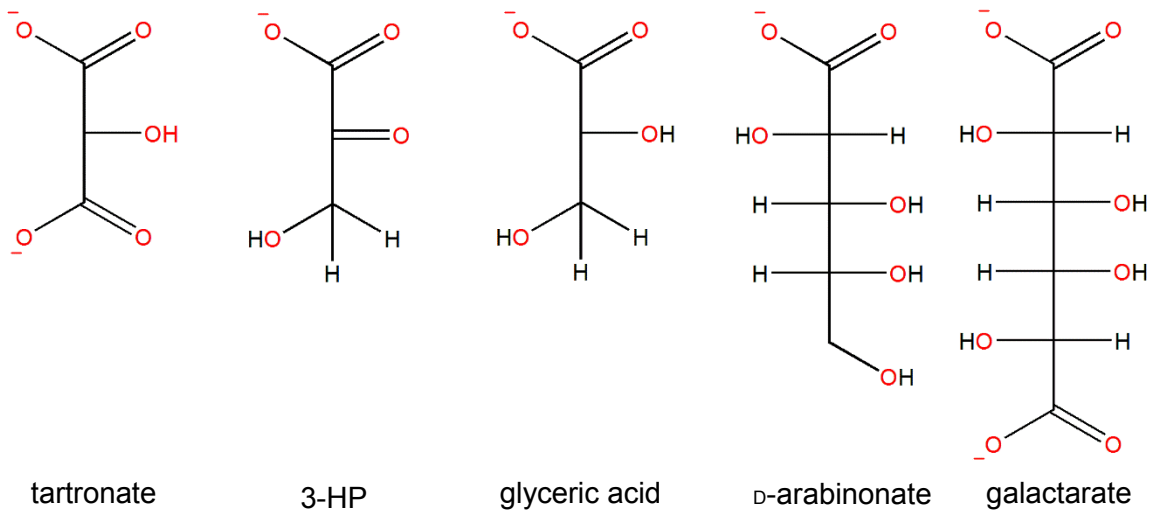

Figure 3.12 The proposed "minimal" ligands for TGD. Tartronate, 3-HP, and glyceric acid are proposed to serve as "minimal" ligands for TGD. The structures of D-arabinonate and galactarate are shown for comparison.

Calcium was found to inhibit TGD activity with an IC_{50} value of 0.073 ± 0.006 mM, which can be attributed to competition of calcium for the magnesium ion binding site in the active site of TGD. From the observed IC_{50} value, it seems that the presence of Ca^{2+} in the active site does not compensate for the absence of Mg^{2+}, i.e. is not able to stabilize the intermediate in the active site as well as Mg^{2+}, if at all.

Glyceric acid was anticipated to be a minimal substrate of TGD, wherein TGD could possibly catalyze either its dehydration to form pyruvate or the initial α-proton abstraction. In both cases, glycerate was expected to inhibit TGD activity. However, IC_{50} studies revealed that TGD does not bind glyceric acid (**Scheme 2.5**). This lack of binding may be due to the loss of many of the binding determinants relative to the substrate, galactarate.

D-Arabinonic acid was also anticipated to serve either as a partial substrate or an inhibitor of TGD (**Figure 3.12**). These two possibilities may depend on the binding orientation of D-arabinonic acid in the active site. If D-arabinonate bound in a "productive" orientation with its glycolate moiety chelating the Mg^{2+} ion in the active site, then it could possibly undergo a dehydration reaction in addition to the deprotonation reaction. However, if it bound in the reverse orientation, then the only possibility would be inhibition. However, the IC_{50} studies showed no inhibition and, thus, no binding. This can be attributed to the difference in the stereochemistry around C4 where, in case of the substrate, galactarate, it has an *S* configuration while as for D-arabinonic acid, it has an *R* configuration. This was not foreseen as a major problem at first, since the active site of TGD might be able to accommodate this difference.

By examining the minimal ligands of TGD, the following are observed: (1) Tartronate was bound weakly, suggesting, if the binding mode to TarD is similar to that observed in MR, that there is a suboptimal interaction between the Brønsted acid-base catalysts and the 3-carboxylate group. (2) 3-HP formed a Schiff base with Lys197 in the active site. (3) Neither glycerate nor D-arabinonate are bound by TGD. The aforementioned suggests that the presence of carboxylate groups at positions 1 and 3, mimicking the substrate, is crucial for the binding to the active site of TarD and that the presence of a Mg^{2+} chelating glycolate moiety only, as in the case of glyceric acid and D-arabinonate, is not sufficient for binding. Loss of many of the binding determinants as in the case of glycerate is also a major contributor to absence of binding. The stereochemistry of the substrate plays a crucial role in substrate binding to TGD, as observed in the lack of binding with D-arabinonate.

CHAPTER 4 PROBING THE ARCHITECTURE OF THE ACTIVE SITE OF RECOMBINANT 3-METHYLASPARTATE AMMONIA LYASE

4.1 INTRODUCTION

The previous two chapters explored the interaction of two enzymes from the mandelate racemase subgroup of the ENS with tartronate and 3-HP. In the present chapter, these potential ligands are used to interrogate the active site architecture of MAL, which is a member of the MAL subgroup of the ENS. The cloning of the putative open reading frame encoding MAL from the genome of *Fusobacterium varium* into a pET-15b expression vector, determination of its kinetic constants, and inhibition by tartronate, oxalate, and 3-HP are described. For inhibition by 3-HP, mass spectrometry experiments were conducted to determine if 3-HP reacts with the Lys residue in the active site and the mode of its reaction.

4.2 MATERIALS & METHODS

4.2.1 General

DL-*threo*-*β*-Methylaspartic acid, lithium 3-hydroxypyruvate, and sodium cyanoborohydride were purchased from Sigma-Aldrich Canada, Ltd. (Oakville, ON). Tartronic acid was purchased from Alfa Aesar (Ward Hill, MA). Sodium oxalate was purchased from The British Drug Houses (VWR, Mississauga, ON). Assays were conducted using an Agilent 8453 UV-visible spectroscopy system. DNA oligonucleotide primers were purchased from Integrated DNA Technologies (Coralville, IA, USA). Restriction endonucleases were purchased from New England Biolabs (Ipswich, MA,

USA). LC-ESI-MS/MS experiments were carried out using HPLC with nanoflow (UltiMate 3000, Dionex) for the liquid chromatography and a hybrid ion trap-orbitrap high resolution tandem mass spectrometer (Velos Pro, Thermoscientific) for the ESI-MS/MS. The instrument was operated in a data-dependent acquisition mode (DDA).

4.2.2 Cloning of the MAL Open Reading Frame from Genomic DNA of *Fusobacterium varium*

The open reading frame encoding MAL (GI: 654687733) was cloned from genomic DNA of *Fusobacterium varium* using KAPA HiFi HotStart Ready Mix (KAPA Biosystems, D-Mark Biosciences – Toronto, ON) following the manufacturer's protocol. The forward and reverse primers for amplification of the open reading frame were: forward primer (5' - AGGATTACATATGAAAATTGTAGATGTAGTATGTTC – 3') and reverse primer (5' - TTAAAGGATCCCTATTTTTTTCTTCTGTTTAC –3'), where the underlined bases correspond to NdeI and BamHI recognition sequences, respectively. The amplification was conducted using an S1000 Thermal Cycler from BIO-RAD Laboratories (Mississauga, ON) with initial denaturation at 95 °C for 3 min, 35 cycles of 98 °C for 20 s for denaturation, 50 °C for 15 s for annealing, 72 °C for 1 min for extension, and 72 °C for 2 min for final extension, and the PCR product was gel purified using QIAquick Gel Extraction Kit (QIAGEN) (Toronto, ON). NdeI and BamHI endonucleases were then used to cut the PCR product for insertion into the multiple cloning site of the pET-15b vector (Novagen, Madison, WI). The insert and the vector were digested in a stepwise manner in which they were incubated, in separate 1.5-mL Eppendorf tubes, with NdeI for 2 h and then BamHI was added and incubation continued for two more hours at 37 °C, according to the manufacturer's recommendations. The digestion products were gel purified, as

previously mentioned. T4 DNA ligase (Invitrogen) was used following the manufacturer's instructions and the ligation reaction was conducted overnight at 16 °C. The pET-15b-*Fv*MAL plasmid encodes a fusion protein with an N-terminal His_6-tag. Competent *E. coli* DH5α cells were transformed with the pET-15b-*Fv*MAL plasmid and glycerol stocks were prepared and stored at –80 °C. The sequence of the insert was verified through commercial DNA sequencing (Robarts Research Institute, London, ON) to ensure full incorporation of the correct insert and the absence of any mutations.

4.2.3 Expression and Purification of MAL Recombinant Protein

Competent *E. coli* BL21 (DE3) cells were also transformed with the pET-15b-*Fv*MAL plasmid and glycerol stocks were prepared and stored at –80 °C. The protein expression from 3 different colonies was examined with and without IPTG induction and for incubation periods of 4, 6, and 8 h to find the optimal expression conditions. The protein was then overexpressed by inoculation of two starter cultures, each containing 5 mL sterile LB, 50 μg/ mL ampicillin, and 10 μL of the glycerol stock, followed by incubation overnight at 37 °C with continuous shaking at 250 rpm. The starter cultures were then added to a 1 L sterile LB broth containing 50 μg/ mL of ampicillin. This was incubated for 7 h after induction with 1 M IPTG (1 mL/ 1 L LB media) at 37 °C with continuous shaking at 250 rpm. The cells were harvested afterwards by centrifugation at 4000 × *g* for 10 min at 4 °C. The cell pellet was re-suspended in 30 mL of ice-cold binding buffer (1 M NaCl, 20 mM Tris-HCl, 5 mM imidazole, pH 7.9) and then sonicated on ice with 5 × 10 s bursts and 1 min cooling times between bursts, or longer if needed, using a Branson Sonifier 250. The cell lysate was then clarified by ultracentrifugation at 40,000 × *g* for 30 min at 4 °C. The supernatant was subsequently passed through a Ni^{2+}-charged His-bind resin-packed

column (10 mL columns packed to 2.5 mL) at 4 °C. The column was subsequently washed with 25 mL binding buffer, 15 mL wash buffer (1 M NaCl, 20 mM Tris-HCl, 60 mM imidazole, pH 7.9), and 7 mL strip buffer (0.5 M NaCl, 20 mM Tris-HCl, 100 mM EDTA, pH 7.9). The purified protein eluted in the strip buffer. Purity was confirmed using 12% acrylamide SDS-PAGE followed by staining with Coomassie blue R-250 (Sambrook, 1989). The protein was then dialyzed against the dialysis buffer (50 mM potassium phosphate, pH 7.5) for 18 h at 4 °C with three buffer changes (500 mL each) (Bearne *et al*., 2001).

Attempts to cleave off the N-terminal His-tag were carried out using a Thrombin Cleavage Capture Kit, Novagen (Billerica, MA) where different thrombin dilutions were used according to the manufacturer's recommendations and the mixture was incubated for 15 min, 30 min, 1 h, and overnight at room temperature. Cleavage trials were assessed using 10% acrylamide SDS-PAGE followed by staining with Coomassie blue R-250 (Sambrook, 1989).

4.2.4 Kinetic & Inhibition Assays of Recombinant MAL

A direct UV-vis spectrophotometric assay was used to determine the kinetic parameters of MAL, as described in section **1.3.1.4 Assay of MAL Activity**. Briefly, the rate of the reaction was measured by following the increase in absorbance at 240 nm corresponding to mesaconate formation ($\Delta\varepsilon$ = 3850 $M^{-1}cm^{-1}$) at 25 °C. The reaction mixture contained a concentration of MAL that gave a linear time course (0.15 ng/µL; see **4.3 Results** section), DL-*threo*-*β*-methylaspartic acid (0.3-10.0 mM, pH adjusted to 9.7 using NaOH), 50 mM ethanolamine-HCl (pH 9.7), 10 mM KCl, and 1 mM $MgCl_2$. The

enzyme was diluted using dialysis buffer (50 mM potassium phosphate, pH 7.5) containing bovine serum albumin (1% w/v). The enzyme concentration was determined by measuring the absorbance at 280 nm using the calculated extinction coefficient of the recombinant protein (30,370 $M^{-1}cm^{-1}$) obtained using the ExPASY ProtParam tool (Gasteiger *et al*., 2003).

IC_{50} studies were conducted with tartronate, oxalate, and 3-HP using a substrate concentration equal to the measured K_m value and the inhibitor concentrations used were 0-18.0 mM for both tartronate and oxalate and 0-3.0 mM for 3-HP. Assays for the determination of the K_i values were conducted using substrate concentrations of 0.3-10.0 mM and 3-HP concentrations of 0, 1.0, 2.0, and 4.0 mM.

Nonlinear regression analysis was used to fit the Michaelis-Menten equation **2.1** to the initial velocity data to obtain V_{max} and K_m values for the recombinant MAL using the program KaleidaGraph v. 4.02 from Synergy Software (Reading, PA) (Segel, 1975). Nonlinear regression was also used to obtain the IC_{50} and K_i values where equations **2.2** and **2.3** were fit to the relative initial velocities and initial velocities, respectively. All studies were conducted in triplicate, and the values are the averages and the reported error is the standard deviation.

4.2.5 Mass Spectrometry Experiments with 3-HP

In order to determine if 3-HP reacted with the active site Lys residues to form a Schiff base, mass spectrometry experiments were conducted where two samples were prepared and investigated: a control sample that contained MAL and 3-HP and a "trapping" sample that contained MAL, 3-HP, and $NaCNBH_3$. The experiment was conducted as

follows: 37 μL MAL (10.8 mg/mL) was incubated with 60 μL 3-HP (50 mM) at the reaction temperature, 25 °C, for 30 min for both samples followed by addition of 47.2 μL distilled water to the control sample and 47.2 μL $NaCNBH_3$ (1 M) to the "trapping" sample, the pH was adjusted to 9.7, and both samples were further incubated at 25 ^oC for 30 min. The final volume of the reaction, after addition of either water or $NaCNBH_3$, was completed 200 μL using the buffer. Both samples were processed identically throughout the subsequent steps of the experiment as described in section **2.2.5 Mass Spectrometry Experiments with 3-HP**.

4.3 RESULTS

4.3.1 Cloning, Expression, and Purification of MAL

The recombinant MAL was obtained with high purity as shown by the 12% SDS-polyacrylamide gel (**Figure 4.1**). The N-terminal His_6-tag appeared to be resistant to thrombin cleavage (**Figure 4.2**), although some evidence of cleavage was evident after incubation overnight.

4.3.2 Kinetic and Inhibition Assays of MAL

The enzyme concentration that gives a linear time course was determined to be 0.15 ng/μL (**Figure 4.3**). The kinetic parameters of the recombinant MAL were determined using the direct UV-vis spectrophotometric assay and k_{cat} was found to be 250 ± 22 s^{-1}, K_m to be 0.98 ± 0.16 mM, and k_{cat}/K_m to be 261 ± 41 $mM^{-1}s^{-1}$ (**Figure 4.4**).

Inhibition by tartronate yielded an IC_{50} value of ~ 54 mM obtained by extrapolation (**Figure 4.5**). Assuming competitive inhibition, the K_i value can be calculated from

equation **2.5** to be equal to 27 mM (Segel, 1975). Similarly, an IC_{50} value was obtained for oxalate by extrapolation (**Figure 4.5**). It was found to be ~ 70 mM, and assuming competitive inhibition, the K_i value can be calculated to be ~ 35 mM. On the other hand, inhibition with 3-HP yielded an IC_{50} value of 4 ± 1 mM (**Figure 4.6**). Assuming competitive inhibition, the K_i value can be calculated from equation **2.5** to be equal to 2 mM (Segel, 1975). This value is in agreement with the value of 1.8 ± 0.2 mM obtained by a full inhibition analysis (**Figure 4.6**). The K_i value was determined from the replot of the K_m/V_{max} values against concentration of inhibitor, where according to equation **2.6**, the K_i value is equal to the –x-intercept value (**Figure 4.6**) (Segel, 1975).

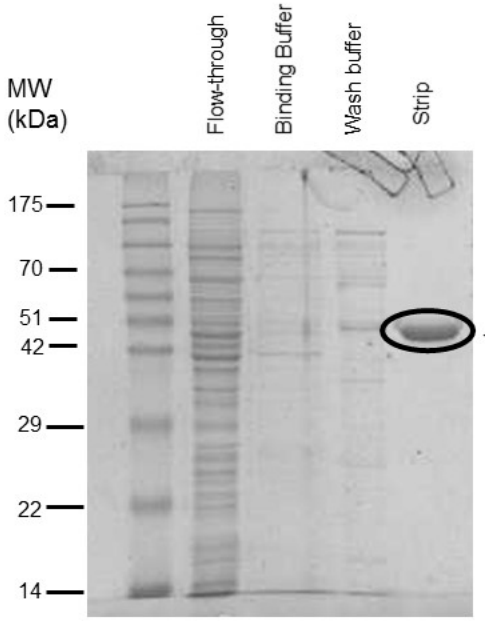

Figure 4.1 The purified recombinant MAL. The gel shows the different fractions resulting from the purification. Recombinant MAL elutes in the strip fraction with high purity. The molecular mass calculated from the amino acid sequence is 47.8 kDa which agrees well with the observed band migration.

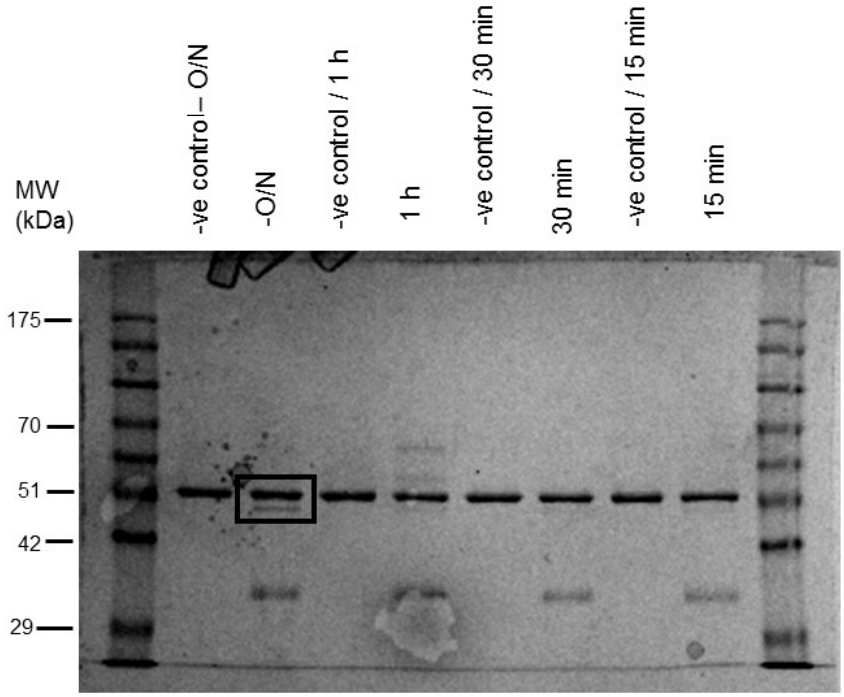

Figure 4.2 His-tag cleavage. Recombinant MAL (5 μg/μL) was incubated with thrombin (0.01 Units/μL) for 15 min, 30 min, 1h, and overnight at room temperature. The negative control lanes contain no thrombin. Cleavage occurs after overnight digestion for only a small fraction of the protein. Bands corresponding to thrombin bands appear at ~36 kDa. The box indicates partial cleavage after the overnight incubation.

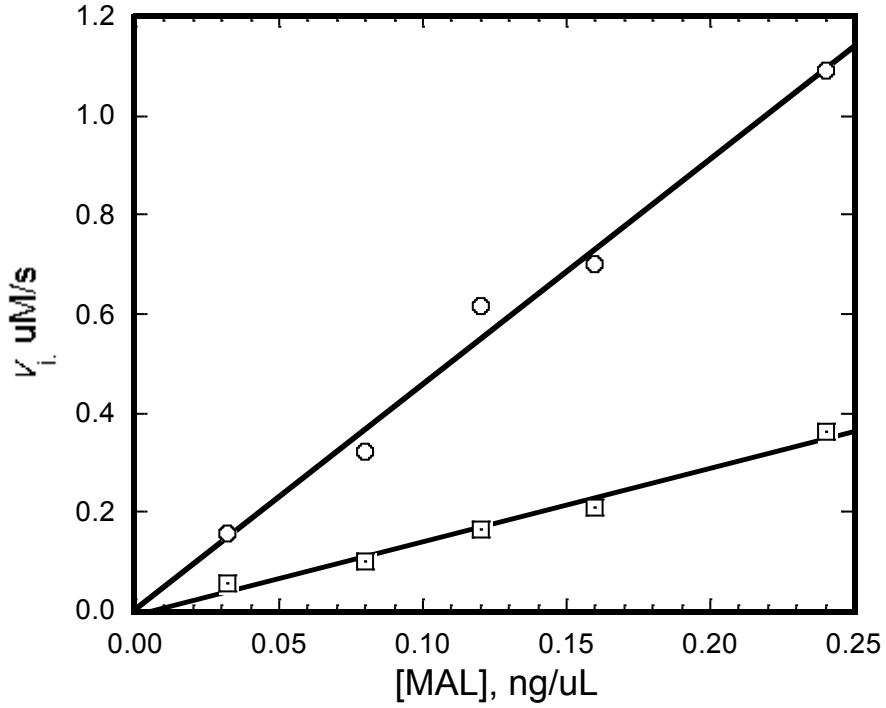

Figure 4.3 Determination of the MAL concentration that gives a linear time course. The MAL-catalyzed reaction was measured at different MAL concentrations (0.24 – 0.02 ng/μL) with DL-*threo*-methylaspartate concentrations of 10.0 mM (○) and 0.30 mM (□).

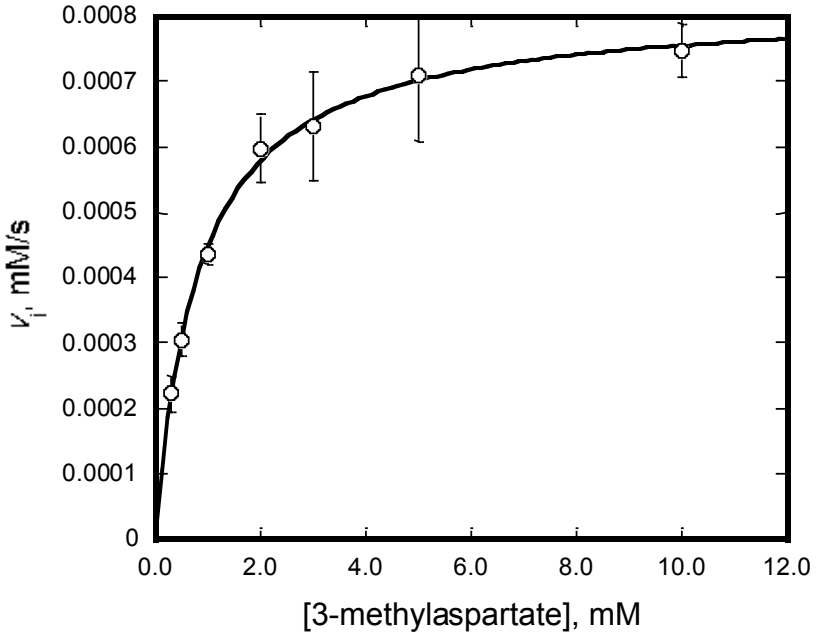

Figure 4.4 Michaelis-Menten plot for MAL. The kinetic parameters of recombinant MAL were determined using direct UV-vis spectrophotometry and k_{cat} was found to be 250 ± 22 s^{-1}, K_m to be 0.98 ± 0.16 mM, and k_{cat}/K_m to be 261 ± 41 $mM^{-1}s^{-1}$.

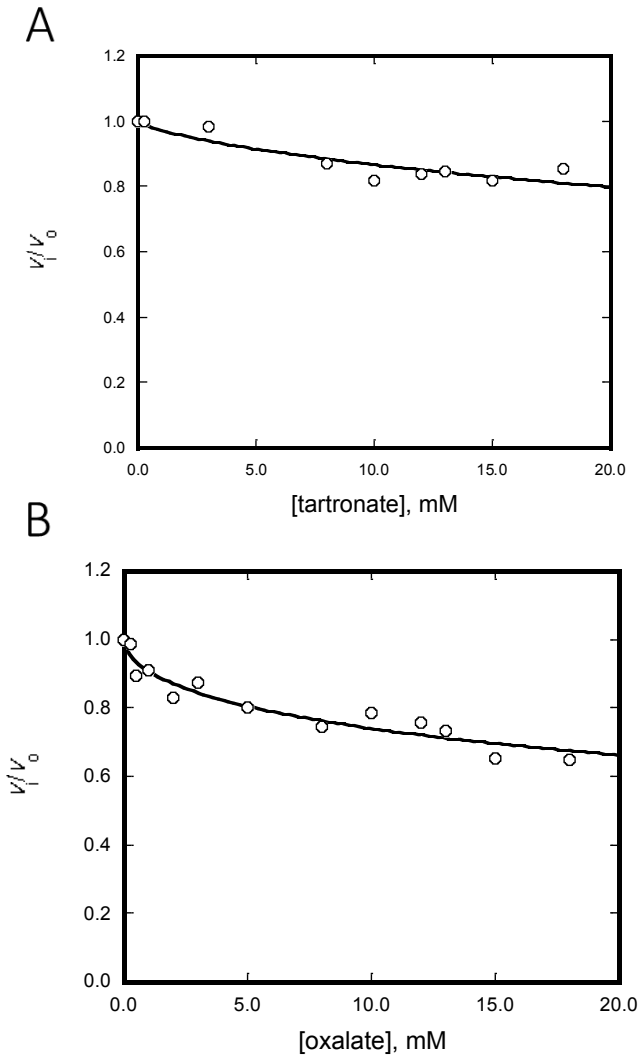

Figure 4.5 Inhibition by the "minimal" ligands tartronate and oxalate. IC_{50} studies with tartronate (A) and oxalate (B) were carried out with a concentration of DL-*threo*-methylaspartate equal to 1.0 mM. (A) Inhibition by tartronate revealed that the IC_{50} value, obtained by extrapolation, was ~ 136 ± 114 mM and $n = 0.7 \pm 0.3$. (B) Inhibition by oxalate gave an IC_{50} value, obtained by extrapolation, equal to 70 ± 22 mM and $n = 0.54 \pm 0.08$.

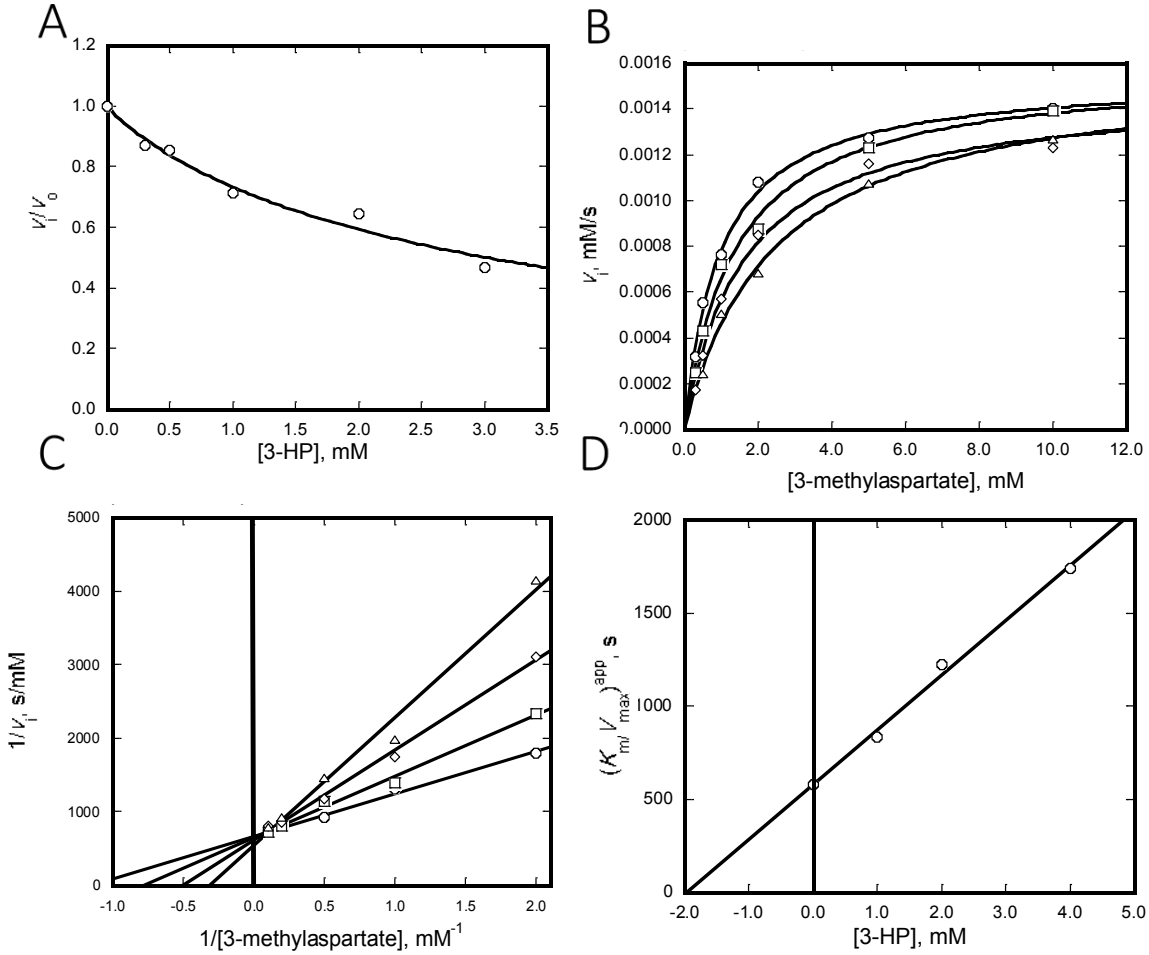

Figure 4.6 Inhibition studies of MAL by 3-HP. (A) A representative IC_{50} plot for the inhibition of MAL by 3-HP. The concentrations used were 1.0 mM for DL-*threo*-methylaspartate and 0.3-10.0 mM for 3-HP. The IC_{50} value was found to be 4 ± 1 mM and $n = 0.9 \pm 0.3$ (B) A representative Michaelis-Menten plot for the inhibition of MAL by 3-HP. The concentrations of DL-*threo*-methylaspartate were (0.3-10.0 mM) and for 3-HP were 0 mM (○), 1.0 mM (□), 2.0 (◊) and 4.0 mM (Δ). (C) A representative Lineweaver-Burk (LB) plot showing competitive inhibition of MAL by 3-HP. 3-HP concentrations are 0 mM (○), 1.0 mM (□), 2.0 mM (◊), and 4.0 mM (Δ). (D) A representative plot for K_m/V_{max} against inhibitor concentration where the x-intercept is $-K_i$ and thus, $K_i = 1.8 \pm 0.2$ mM.

4.3.3 Mass Spectrometry Results for Lys Modification

The active site Lys 331 (underlined) is present in the AGHVVQI<u>K</u>TPDLGGVNNIADAILYCNK peptide (AG-peptide, residues 324-350). For the control sample, the AG-peptide (monoisotopic, MH^{4+}, *m/z* = 720.88 Da) showed no modification of the active site Lys 331 (**Figure 4.7**) and (**Figure 4.8**). The "trapping" sample showed a modification of 88 Da to the AG-peptide (monoisotopic, MH^{4+}, *m/z* = 742.89 Da), corresponding to a covalent modification of Lys 331 in the active site due to formation of Schiff base with 3-HP and the subsequent reduction of the imine by $NaCNBH_3$ (**Figure 4.7**) and (**Figure 4.9**).

A

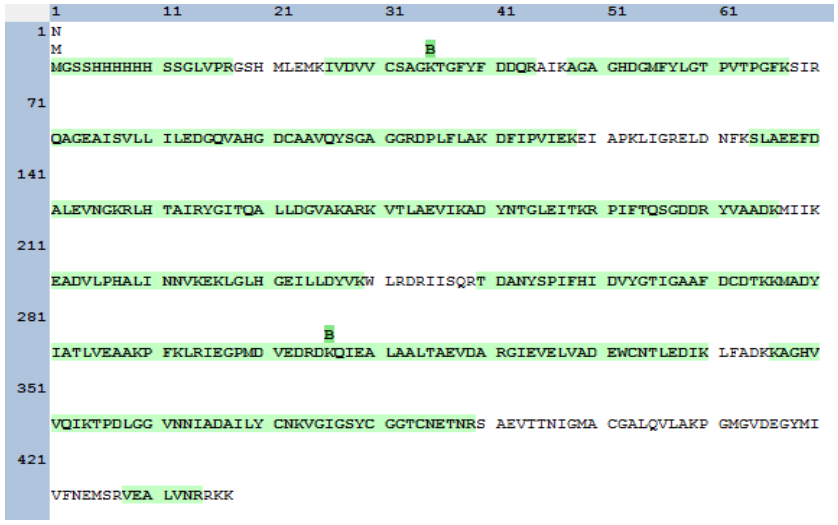

B

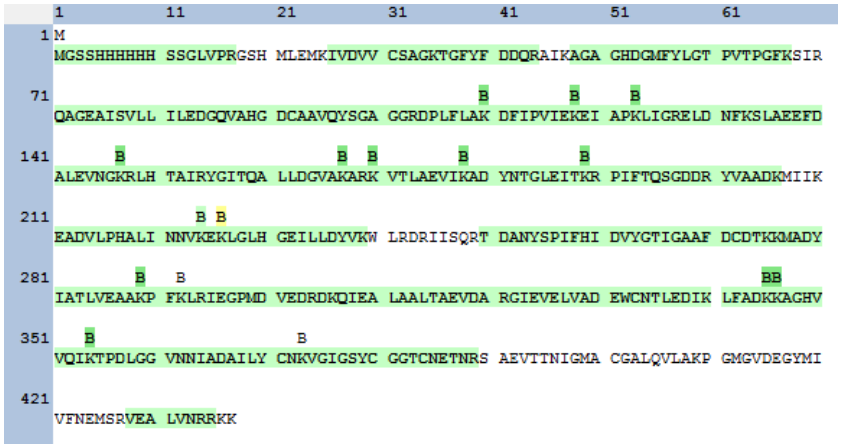

Figure 4.7 The sequence of the recombinant MAL as identified by MS. The figure shows the full sequence of the recombinant MAL as an N-terminal fusion protein with a His_6-tag. The highlighted residues are those that were identical to the database search to determine the identity of the protein. The modified residues have letters above them where B indicates modification by 3-HP (88-Da adduct), M indicates Met-loss and acetylation (N-terminus), and N indicates Met-loss (N-terminus). The highlight color of these letters indicates the modification site probability, where green is 100%-99%, light green is 99%-75%, and yellow is 75%-45%. (A) The sequence of recombinant MAL from the control sample shows no modification of the Lys 331 in the active site. (B) The sequence of recombinant MAL from the "trapping" sample shows modification with 3-HP forming an 88-Da adduct. It also shows off-target and surface modification by 3-HP with formation of additional 88-Da adducts. (The first 23 amino acid residues correspond to the His_6-tag and linker region.)

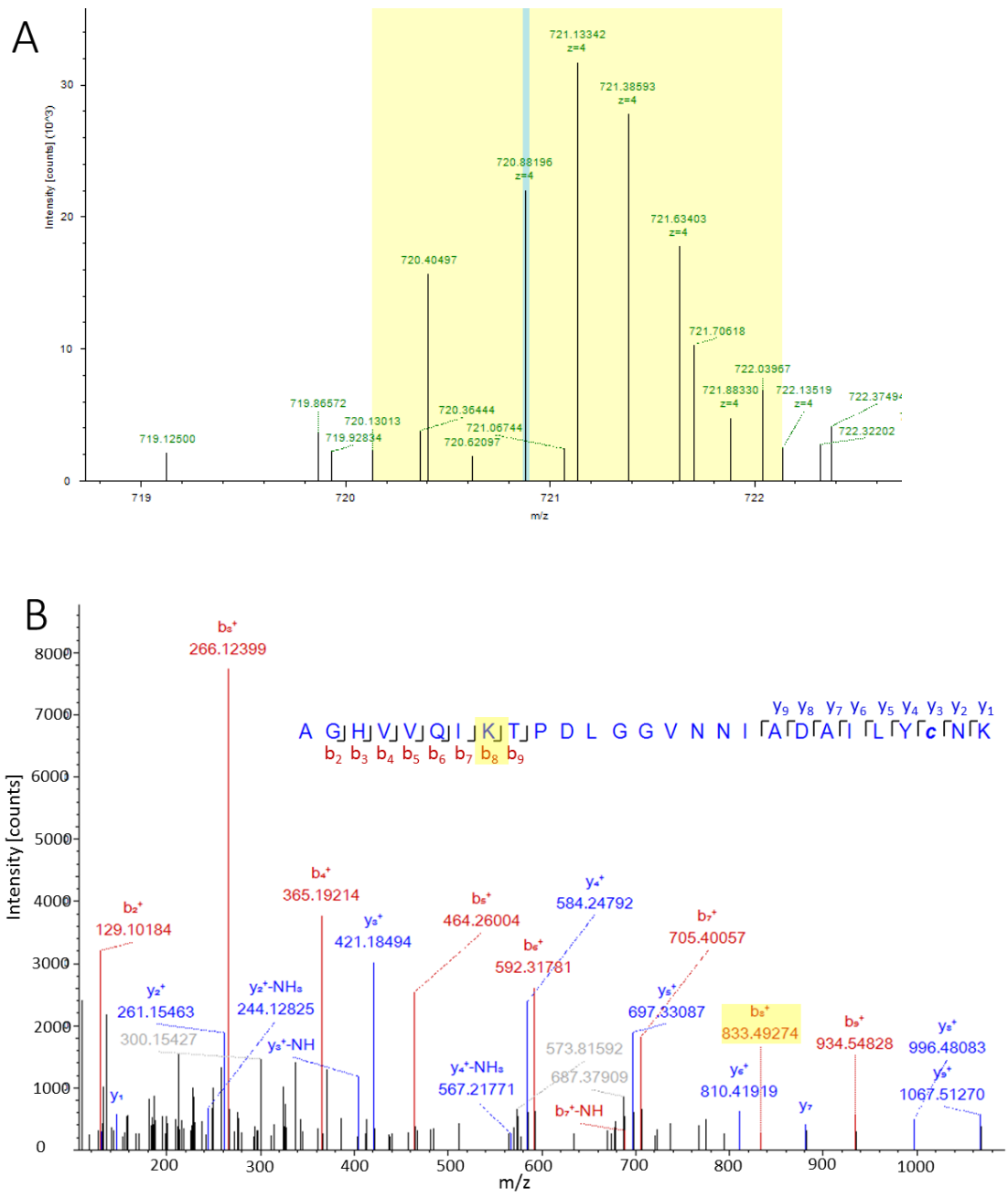

Figure 4.8 Mass spectrometry results for the control sample. (A) The precursor isotope pattern spectrum (MS1 spectrum) for the control sample shows no modification of the AG-peptide by 3-HP (monoisotopic, MH^{4+}, m/z = 720.88 Da). (B) The fragment match spectrum (MS/MS spectrum) shows no modification of Lys 331 present in the b_8 ion.

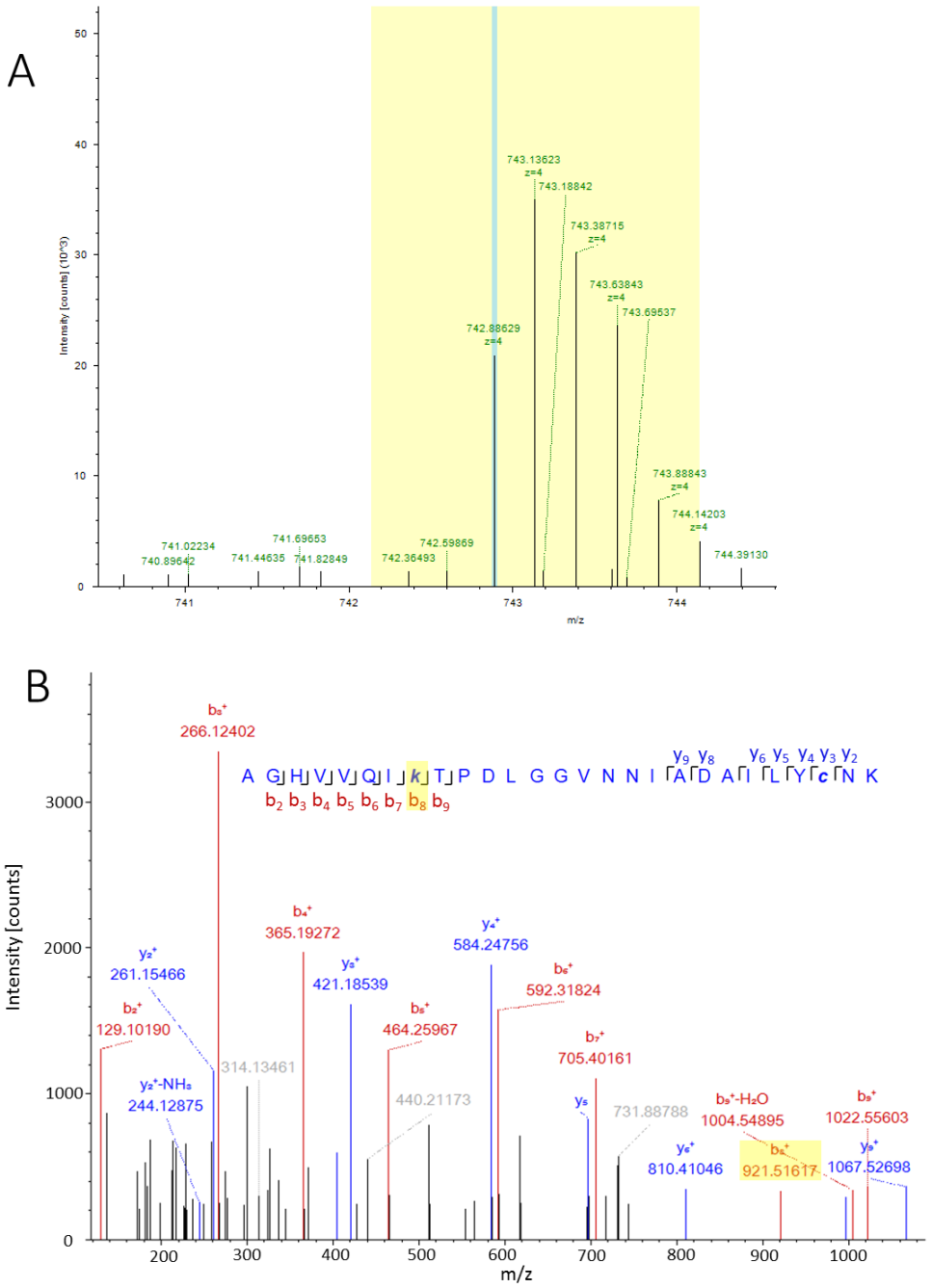

Figure 4.9 Mass spectrometry results for the "trapping" sample. (A) The precursor isotope pattern spectrum (MS1) shows a modification of 88 Da by 3-HP (monoisotopic, MH^{4+}, m/z = 742.88Da). (B) The fragment match spectrum (MS/MS spectrum) shows an 88 Da modification of Lys 331 present in the b_8 ion (the modified residue is italicized.)

4.4 DISCUSSION

The N-terminal His_6-tag appeared to be resistant to cleavage, which is likely due to the folding of the N-terminus with the tag in such a way that hinders the access of thrombin to the cleavage site. This was not anticipated at the start of the cloning trials since no crystal structure has been reported for *Fv*MAL. The pET-15b expression vector was employed because of the ease of purification of the recombinant protein using Ni^{2+}-affinity chromatography. Vectors which encode a C-terminal tag might be employed to overcome this cleavage problem. SDS-PAGE for the thrombin cleavage trials shows a second protein with a molecular weight of ~ 38 kDa, corresponding to thrombin which was not removed from the reaction mixture (**Figure 4.2**).

Bearne and co-workers have shown that the activity of MAL has a dependence on K^+ concentration (K_m^{app} = 3.3 ± 0.8 mM) and no dependence on Na^+ and thus, NaOH was used in all pH adjustments of the substrate and inhibitor solutions for use in the assays (Bearne *et al*., 2001). Bearne and co-workers also reported the use of BSA (0.01% in the final assay solution); however, this value was increased to 0.1% in the final assay solution in the present study in order to stabilize the protein for the time period of the assays and prevent its adsorption to the surfaces of glassware. The kinetic assays with MAL showed that the recombinant protein is active and that the kinetic values are on the same order of magnitude as those reported by Bearne and co-workers (Bearne *et al*., 2001). However, the values are not experimentally equal to those reported previously. The recombinant MAL had a higher (~ 2×) turnover number (250 ± 22 s^{-1}) as compared to that reported previously (105 s^{-1}), which could be attributed to the higher concentration of BSA used here as compared to that used by Bearne and co-workers (2001), resulting in more stability leading

to the observed higher k_{cat} value. The K_m reported here (0.98 ± 0.16 mM) is on the same order of magnitude (~ 2× higher) as that reported by Bearne and co-workers (0.51 ± 0.04 mM), which might be due to the presence of the His_6-tag (Bearne *et al*., 2001). Overall, similar values for the enzyme efficiency (literature value = 205 mM^{-1} s^{-1} (Bearne *et al.*, 2001) *c.f.* experimental value = 261 ± 41 mM^{-1} s^{-1}) were obtained.

The IC_{50} experiments revealed that inhibition by both tartronate (IC_{50} ~ 136 mM) and oxalate (IC_{50} ~ 70 mM) was very weak. Consequently, the IC_{50} studies were conducted only once for each compound.

The crystal structure of MAL from *C. amalonaticus* with the substrate in the active site reveals that the substrate chelates the Mg^{2+} via its carboxylate group (Raj *et al*., 2009). This may explain why tartronate was a very weak inhibitor of MAL. If tartronate exhibits the same mode of binding, the distal carboxylate group will be positioned far from the active site residues and thus preventing bridging of the two Brønsted acid-base catalysts as is observed when tartronate is bound at the active site of MR (Nagar *et al*., 2014). Accordingly, we anticipated that the shorter oxalate might bind in the active site of MAL in a way that allows one of the carboxylate groups to chelate the Mg^{2+} and the other to bridge the Brønsted acid-base catalysts (**Figure 4.10**). However, oxalate was a very weak inhibitor of MAL as well. In addition, looking at the binding pose of the substrate in the active site and the stabilizing interactions it has with other active site residues, as discussed previously in section **2.4 Discussion**, it is possible that the 2-OH group of tartronate and the distal carboxylate group of oxalate will be positioned where the 3-methyl group of 3-methylaspartate is typically located. This places the more polar group in a less solvent-accessible pocket, which would largely destabilize the binding of the minimal ligands

(Asuncion *et al*., 2002; Levy *et al*., 2002). Also, the distal carboxylate group of tartronate would now occupy the site that normally accommodates the 2-NH_3^+ group of the substrate, which should not favor binding of a negatively charged carboxylate group. This again leads to the destabilization of tartronate binding relative to that of the substrate (Asuncion *et al*., 2002; Levy *et al*., 2002). Thus, it can be concluded that both tartronate and oxalate do not possess sufficient binding determinants for interaction with the active site residues as compared to the substrate. Once again, tartronate exhibits different inhibition properties than those observed with MR, TarD, and TGD to further illustrate that tartronate is sensitive to the subtle changes in the active site structure of different members of the ENS.

Inhibition studies by 3-HP revealed that 3-HP is a competitive inhibitor of MAL, binding with an affinity (K_i = 1.8 ± 0.2 mM) ~ 2× lower than the binding affinity of the substrate (K_m = 0.98 ± 0.16 mM). 3-HP exhibits very good binding to MAL, as a competitive inhibitor and this binding interaction is similar to that observed with MR, in which 3-HP is also bound at the active site; however, in the latter case, 3-HP was found to be an irreversible inhibitor (Nagar *et al*., 2015). As previously discussed in section **2.4 Discussion**, in case of MR, 3-HP underwent the initial half-reaction (Nagar *et al*., 2015). Again, mass spectrometry experiments were conducted to determine if 3-HP reacts with Lys 331 in the active site to form a Schiff base. Two samples were prepared and two possibilities were anticipated as discussed in section **2.4 Discussion** (**Scheme 2.4**). The control sample showed no modification by 3-HP, whereas the "trapping" sample showed formation of an 88-Da adduct with Lys 331, indicating that 3-HP is able to access the active

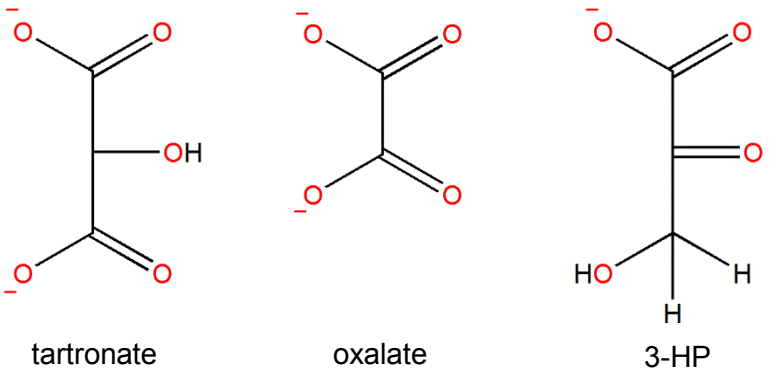

Figure 4.10 The proposed "minimal" ligands for MAL. Tartronate, oxalate, and 3-HP were expected to be minimal ligands for MAL. Tartronate and oxalate were expected to chelate the Mg^{2+} in the active site as well as bridge the two Brønsted acid-base catalysts; however, they did not exhibit binding. 3-HP was expected to form a Schiff base with the Lys residue in the active site, which was observed.

site and form a Schiff base with Lys 331 followed by reduction of the imine by $NaCNBH_3$ present in the "trapping" sample. Both samples showed modification of the cysteine residue in the AG-peptide due to carbamidomethylation as discussed in section **3.4 Discussion**. These results are consistent with the kinetic data and suggest that 3-HP exhibits a difference in the mode of its inhibition of MAL relative to MR. Consideration of the mechanism of the MAL-catalyzed reaction would suggest that His 194, the *R*-specific base, is protonated when (2*S*,3*S*)-3-methylaspartate is used as a substrate and that the Lys 331, the *S*-specific base, would exist in its unprotonated state to catalyze the initial α-proton abstraction. Thus, it might be that either a conformational change accompanying substrate binding or the initial half-reaction catalyzed by Lys 331 alters the active site architecture to shift the equilibrium towards protonation of His 194. Accordingly, it is possible that when 3-HP forms a Schiff base with the Lys 331 in the active site, this leads to a similar conformational change that enforces protonation of His 194. Consequently, the proton abstraction that "traps" 3-HP in the active site cannot occur as it does in the case of MR. Thus, 3-HP appears to be able to detect subtle changes in the active site architecture (i.e., possibly the protonation state of the active site Brønsted acid-base catalyst) of members of the ENS.

CHAPTER 5 PRELIMINARY INVESTIGATION OF THE METAL ION BINDING SITE OF D-TARTRATE DEHYDRATASE

5.1 INTRODUCTION

TarD is reported to require a divalent metal ion for catalysis as discussed in section **1.2.1.2 Structure and Active Site Architecture of TarD**. Typically, like other enzymes of the ENS, the divalent metal ion is Mg^{2+} which is stabilized in the active site through 6 interactions forming an octahedral coordination sphere. Three of these interactions are with the active site acidic residues Asp 213, Glu 239, and Glu 265 while the remaining sites are occupied by either water molecule or ligand interactions. This chapter describes preliminary experiments to gain insight into the Mg^{2+}-binding site of TarD through assessment of the absolute requirement for a divalent metal ion and through site-directed mutagenesis of the three acidic residues (D213N, E239Q, and E265Q).

5.2 MATERIALS & METHODS

5.2.1 General

D-Tartrate, β-nicotinamide adenine dinucleotide reduced disodium salt (NADH), malic dehydrogenase from porcine heart, and semicarbazide hydrochloride were purchased from Sigma-Aldrich Canada, Ltd. (Oakville, ON). Assays were conducted using an Agilent 8453 UV-visible spectroscopy system. DNA oligonucleotide primers were purchased from Integrated DNA Technologies (Coralville, IA). Restriction endonucleases were purchased from New England Biolabs (Ipswich, MA).

5.2.2 Experiments to Obtain the Apo-Enzyme

Wild-type TarD was expressed and purified as previously described in section **2.2.3 Expression and Purification of TarD Recombinant Protein**. To free TarD of Mg^{2+} (i.e., apo-enzyme), purified enzyme was subjected to exhaustive dialysis against EDTA in several different experiments. For the first experiment, the dialysis of the purified protein was against assay buffer (50 mM K^+-Hepes, pH 7.50) containing 10 mM EDTA for 16 h with two changes of the buffer (500 mL each) followed by dialysis against assay buffer (50 mM K^+-Hepes, pH 7.50) for 30 h with 3 changes of the dialysis buffer (500 mL) each. The activity of the enzyme was then assessed using the continuous coupled assay, as described previously in section **2.2.4.1 Continuous Coupled Assay**, where the reaction mixture contained the exhaustively-dialyzed TarD (2.6 ng/μL), D-tartrate (25 mM), MDH (10 Units/mL), NADH (0.16 mM), and assay buffer (50 mM K^+-Hepes, pH 7.50) in a total volume of 1 mL. The decrease in absorbance was followed at 340 nm, 25 °C in a 1-cm quartz cuvette. The same assay protocol was also used for assessing enzymatic activity after subsequent dialysis experiments. After assessment of the activity of the dialyzed enzyme from the first experiment, the same enzyme was re-dialyzed (experiment 1-cont.) see **Table 2** in the **5.3 Results** section. The enzyme was again dialyzed against the assay buffer (50 mM K^+-Hepes, pH 7.50) containing 10 mM EDTA for 24 h with three changes of buffer (500 mL each) followed by dialysis against the assay buffer (50 mM K^+-Hepes, pH 7.50) for 24 h with three buffer changes (500 mL each). The enzymatic activity was then assessed as described above. To three new portions of purified enzyme, three more experiments of exhaustive dialysis were conducted where the three new portions were subjected to dialysis against assay buffer (50 mM K^+-Hepes, pH 7.50) containing 50 mM,

250 mM, or 500 mM EDTA, for experiments 2, 3, and 4, respectively, for 24 h with three buffer changes (500 mL each), except for experiment 4 where 4 buffer changes were conducted (500 mL each). This was followed by dialysis against the assay buffer (50 mM K^+-Hepes, pH 7.50) for 24 h and three buffer changes (500 mL each), except for the last trial where 4 buffer changes were conducted (500 mL each). After each experiment, the enzymatic activity was assessed as described above.

5.2.3 Mutational Analysis of the Metal Ion-Binding Site of TarD

5.2.3.1 Site-Directed Mutagenesis

PCR-based site-directed mutagenesis was performed using the pET-15b-TarD plasmid as a template to generate the TarD variants D213N, E239Q, and E265Q using the QuickChange Site-directed Mutagenesis Kit (Stratgene, La Jolla, CA) following the manufacturer's instructions. For the E239Q-TarD, KAPA HiFi HotStart Ready Mix (KAPA Biosystems, D-Mark Biosciences – Toronto, ON) was used following the manufacturer's protocol. The forward and reverse primers for amplification of the open reading frame were: forward primer (5' - CTGTTCTGGTAC**CAG**GAGGTCGGCG – 3') and reverse primer (5' - CGCCGACCTC**CTG**GTACCAGAACAG – 3'), where the underlined bases correspond to the codon encoding the amino acid changed and the mutated base is shown in boldface. The amplification was conducted using an S1000 Thermal Cycler from BIO-RAD Laboratories (Mississauga, ON) and the parameters were as follows: initial denaturation at 95 °C for 30 s, 35 cycles of 98 °C for 20 s for denaturation, 58 °C for 75 s for annealing, 72 °C for 72 s for extension, and 72 °C for 144 s for final extension. For the D213N-TarD, Phusion High-Fidelity DNA Polymerase from New

England Biolabs (Ipswich, MA) was used for the PCR amplification following the manufacturer's protocol. The forward and reverse primers for amplification of the open reading frame were designed to be partially-overlapping: forward primer (5' - CGTC**A**AC GCCAACGGCCGCTTCAAC – 3') and reverse primer (5' - GTTGGC GT**T** GACGGCGAGCTGCGC – 3'), where the underlined bases correspond to the codon encoding the amino acid changed and the mutated base is shown in boldface. The parameters for the amplification were as follows: initial denaturation at 98 °C for 30 s, 30 cycles of 98 °C for 10 s for denaturation, 65.7 °C for 30 s for annealing, 72 °C for 200 s for extension, and 72 °C for 10 min for final extension. For the E265Q-TarD, Phusion High-Fidelity DNA Polymerase from New England Biolabs (Ipswich, MA) was used for the PCR amplification following the manufacturer's protocol. The forward and reverse primers for amplification of the open reading frame were: forward primer (5' - GGCGACAGGC **CAA** AACCTGTTCAGC – 3') and reverse primer (5' - GCTGAACAGGTTT **G** GCCTGTCGCC – 3'), where the underlined bases correspond to the codon encoding to the amino acid changed and the mutated base is shown in boldface. The parameters for the amplification were as follows: initial denaturation at 98 °C for 30 s, 30 cycles of 98 °C for 10 s for denaturation, 64 °C for 30 s for annealing, 72 °C for 200 s for extension, and 72 °C for 10 min for final extension. For all mutants, the PCR products were subjected to overnight digestion by Dpn1 at 37 °C followed by gel purification using QIAquick Gel Extraction Kit (QIAGEN) (Toronto, ON). Competent *E. coli* DH5α cells were transformed with the pET-15b-D213N-TarD, pET-15b-E239Q-TarD, and pET-15b-E265Q-TarD plasmids and glycerol stocks were prepared and stored at –20 °C. The sequences of the open reading frame were verified through commercial DNA sequencing

(Robarts Research Institute, London, ON) to ensure that no unwanted mutations had been introduced.

5.2.3.2 Expression and Purification of the Mutants

Competent *E. coli* BL21 (DE3) cells were also transformed with the pET-15b-D213N-TarD, pET-15b-E239Q-TarD, and pET-15b-E265Q-TarD plasmids and glycerol stocks were prepared and stored at –80 ºC. The protein expression was examined with and without IPTG induction and for incubation periods of 6, 20 and 48 h to find the optimal expression conditions for E239Q-TarD and for incubation period 24 h to find the optimal expression conditions for D213N-TarD and pE265Q-TarD mutants. E239Q-TarD was then overexpressed by inoculation of two starter cultures, each containing 5 mL sterile LB, 50 μg/mL ampicillin, and 10 μL of the glycerol stock, followed by incubation overnight at 37 °C with continuous shaking at 250 rpm. The starter cultures were then added to 1 L of sterile LB broth containing 50 μg/mL of ampicillin. This was incubated for 48 h (without isopropyl *β*-D-1-thiogalactopyranoside (IPTG) induction) at 37 °C with continuous shaking at 250 rpm (Yew *et al*., 2006). The cells were harvested afterwards by centrifugation at 4000 × g for 10 min at 4 °C. The cell pellet was re-suspended in 30 mL of ice-cold binding buffer (1 M NaCl, 20 mM Tris-HCl, 5 mM imidazole, pH 7.9) and then sonicated on ice with 5 × 10 s bursts and 1 min cooling times between bursts, or longer if needed, using a Branson Sonifier 250. The cell lysate was then clarified by ultracentrifugation at 40,000 × *g* for 30 min at 4 °C. The supernatant was subsequently passed through a Ni^{2+}-charged His-bind resin-packed column (10 mL columns packed to 2.5 mL) at 4 °C. The column was subsequently washed with 25 mL binding buffer, 15 mL wash buffer (1 M NaCl, 20 mM Tris-HCl, 60 mM imidazole, pH 7.9), and 7 mL strip buffer (0.5 M NaCl, 20 mM Tris-

HCl, 100 mM EDTA, pH 7.9). The purified protein eluted in the strip buffer. Purity was confirmed using 12% acrylamide SDS-PAGE followed by staining of the protein bands with Coomassie blue R-250. The protein was then dialyzed against the assay buffer (50 mM K^+- Hepes, 10 mM $MgCl_2$, pH 7.5) for 18 h at 4 °C with three buffer changes (500 mL each) (Sambrook, 1989; Yew *et al*., 2006).

5.2.3.3 Activity Assay

The activity of the E239QTarD mutant was assessed using the continuous coupled assay as described in section **2.2.4.1 Continuous Coupled Assay**; however, the concentration of the D-tartrate was increased up to 20 mM, which is 1000× higher than the measured K_m value (~ 0.02 mM). The concentration of the enzyme was also increased up to 0.37 μg/μL, which is ~ 150 × higher than the concentration used in the previously described assays (2.6 ng/μL) in **2.2.4 Kinetic and Inhibition Assays of Recombinant TarD**.

5.3 RESULTS

5.3.1 Exhaustive Dialysis Experiments

The results from the exhaustive dialysis experiments are shown in **Table 2**. The % activity retained was calculated from the measured initial rate of the wild-type TarD after exhaustive dialysis using the continuous coupled assay relative to the previously determined V_{max} using the same assay (0.21 ± 0.02 μM/s). Each measurement was done only once.

Table 2 Results from the exhaustive dialysis trials with wild-type TarD.

experiment	[EDTA], mM	total $t_{dialysis}$, h	v_i, µM/s	% activity retained
1	10	46	0.13	65
1 cont.	10	+ 48 (92)	0.1	47
2	50	48	0.07	32
3	250	48	0.16	46
4	500	48	0.05	28

5.3.2 Expression and Purification of the TarD mutants

Recombinant E239Q-TarD was obtained with high purity as shown by the 12% SDS-polyacrylamide gel (**Figure 2.11**). However, D213N-TarD and E265Q-TarD were not expressed when cultures were grown for 24 h with and without IPTG induction (**Figure 5.2**).

5.3.3 Measurement of the Kinetics of E239Q-TarD

E239Q-TarD mutant appeared to be inactive.

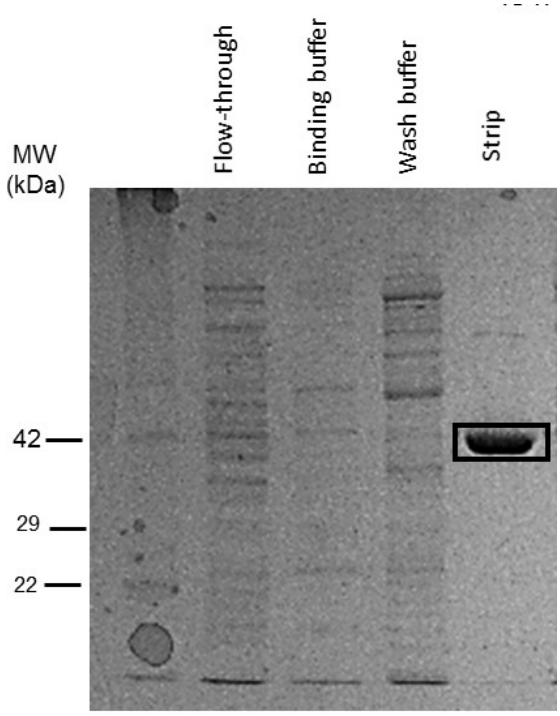

Figure 5.1 The purified recombinant E239Q-TarD. The gel shows the different fractions resulting from the protein purification. Recombinant E239Q-TarD elutes in the strip fraction with high purity.

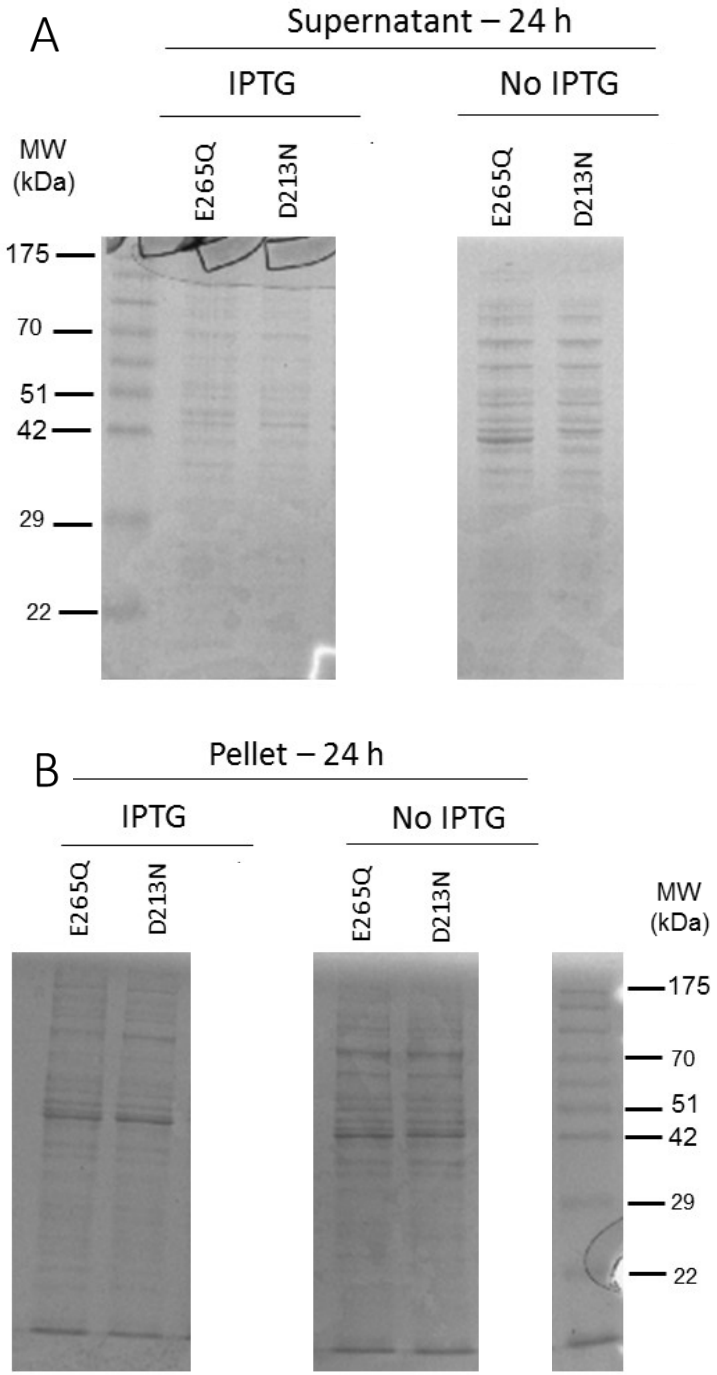

Figure 5.2 Overexpression trial for the TarD variants D213N and E265Q. The gels show the attempt to overexpress the TarD variants D213N and E265Q for 24 h at 25 °C and 250 rpm with and without addition of IPTG. Samples from both the (A) supernatant and (B) pellet were examined. The gels show no evidence of overexpression of the mutants. (The hidden parts of the gel contained samples corresponding to a different mutant that is not discussed here.)

5.4 DISCUSSION

In order to gain more insight into the metal binding site of TarD, we wanted to obtain the apo-enzyme through exhaustive dialysis as previously described for MR (Fee, Hegeman, & Kenyon, 1974). Most surprisingly, TarD showed activity even after dialysis against EDTA concentrations up to 0.5 M, indicating that EDTA was not able to remove Mg^{2+} from the active site. The % activity remaining was obtained by comparing the initial rate measured after exhaustive dialysis under saturating concentrations of substrate to the V_{max} value obtained from the Micahelis-Menten plots, in which case, the enzyme was dialyzed only for 16 h. Despite this lack of a proper control experiment, the fact that TarD still retains its activity after exhaustive dialysis is very interesting since MR loses all activity under similar conditions (Fee *et al*., 1974). This observation is in contrast to that observed by Rode and Giffhorn who used gel filtration to (apparently) free TarD from Mg^{2+}. Unfortunately, these authors did not report the activity of their enzyme preparation after gel filtration; only activities in the presence of other metal ions were reported (Rode & Giffhorn, 1982). Thus, to further pursue this, site-directed mutagenesis was used to obtain the TarD variants E239Q, E265Q, and D213N, where the residues mutated are the residues that chelate Mg^{2+} in the active site of TarD (**Figure 1.1 - Panel B**). E239Q-TarD had no activity even after varying the enzyme and substrate concentrations indicating that this mutation, however subtle, led to either disruption of the Mg^{2+}-binding site or another structural perturbation that obviated the activity of the enzyme. To further investigate these hypotheses, incubation of E239Q-TarD with elevated Mg^{2+} concentrations should be conducted, and CD spectroscopy could be employed to examine the secondary structure of the mutant, although the perturbation may still not be detected. For the TarD variants

D213N and E265Q, overexpression was not observed; however, further investigation of the expression level is required, e.g., purification without overexpression may be possible, as was observed with the E239Q mutant.

CHAPTER 6 CONCLUSIONS AND FUTURE RECOMMENDATIONS

Members of the enolase superfamily share the same overall structure; however, there are subtle differences in the active site architectures of the individual enzymes. In chapters 2-4, it was discussed how the use of the "minimal" ligands tartronate and 3-HP proved to be efficient tools for the detection of these differences. Tartronate exhibited weaker binding with TarD and TGD compared to that observed for MR which could be attributed to the difference in the positions of the Brønsted acid-base catalysts. Tartronate also showed very weak binding to MAL mainly due to the difference in the way the ligand binds to the Mg^{2+}, which takes place through the carboxylate group rather than through the glycolate moiety as it does for other members of the MR subgroup.

The "minimal" ligand 3-HP was able to access the active sites of all three enzymes and modify the Lys residue acting as the Brønsted base catalyst (Lys 184 in TarD, Lys 197 in TGD, and Lys 331 in MAL), and unlike its behavior with MR where it was an irreversible inhibitor, it behaved as a competitive inhibitor. In case of MR, the Schiff base formed between 3-HP and Lys 166 was followed by a deprotonation reaction assumed to be catalyzed by the Brønsted base catalyst, His 297, that led to "trapping" 3-HP in the active site of MR. Here, I suggest that the absence of this deprotonation event in the enzymes I have examined is due to the following: (1) In the case of TarD, the Brønsted base catalyst His 322, when acting on D-tartrate, is present in its conjugate acid form, which might result in its inability to catalyze the deprotonation reaction similar to that observed with MR. (2) For TGD, the Brønsted acid-base catalysts Lys 197 and His 328 are both likely present initially in the deprotonated form and then once a reaction happens with the

Brønsted base catalyst Lys 197, there might be a conformational change that favors conversion of the Brønsted base catalyst His 328 to its conjugate acid form. This would result in the inability of His 328 to perform the deprotonation reaction that would "trap" 3-HP in the active site. (3) For MAL, the Brønsted acid catalyst His 194 is likely always present as its conjugate acid and, thus, once again, the deprotonation reaction that would have "trapped" 3-HP in the active site cannot occur. Comparing the aforementioned observations to what is observed with MR, the following can be suggested: (1) In case of MR, the ability of His 297 to perform the deprotonation that "traps" 3-HP in the active site can be attributed to one of two possibilities, either His 297 exists in an equilibrium between its protonated and deprotonated states with the latter form acting as a Brønsted base catalyst after the reaction between Lys 166 and 3-HP, or the reaction of 3-HP with Lys 166 perturbs the pK_a of His 297 in favor of the deprotonated state. (2) In case of TarD, TGD, and MAL, it is possible that the Brønsted acid catalysts His 322, His 328, and His 194 either exist in an equilibrium between their protonated and deprotonated states with the equilibrium favoring the protonated state, or the binding of 3-HP to the active site does not induce conformational changes that alter the protein environment and thus, no perturbation of their respective pK_a values takes place. Glycerate was not found to be a ligand for either TarD or TGD, and D-arabinonate was not found to be a ligand for TGD.

In terms of the reported kinetic assays, the end-point assay developed for following the TarD-catalyzed reaction proved to be valid for that purpose, although using it for the K_i determination proved to be extremely time consuming. The CD-based assay developed for following the TGD-catalyzed reaction proved to be valid and convenient for conducting kinetic and inhibition assays.

Future recommendations for this project are as follows: (1) For TarD, repeating the mass spectrometry experiments, both the control and "trapping" samples, is recommended to further confirm the results obtained, especially the 86 Da adduct observed in the "trapping" sample. The time-dependence of the inhibition of TarD with 3-HP should be further investigated to see if the formation of an 86 Da adduct, as observed in the "trapping" sample, is a time-dependent phenomenon. It would also be interesting to conduct the hydrogen-deuterium exchange experiments with glycerate for longer incubation periods, using higher enzyme concentrations and using a standard to determine if it is a (partial) substrate. (2) For MAL, a C-terminal tag could be employed as an alternative.

The second project discussed preliminary investigations of the binding site of Mg^{2+} in TarD where TarD was shown to retain some of its activity after exhaustive dialysis against high concentrations of EDTA. Possibly, EDTA might not be able to access the active site of TarD or the binding affinity for Mg^{2+} is quite high. Site-directed mutagenesis of the acidic residues chelating the Mg^{2+} ion in the active site were conducted. The E239Q variant was found to be inactive and the D213N and E265Q variants were not overexpressed.

In the future, it might be informative to conduct the activity assays for E239Q-TarD in the presence of greater concentrations of $MgCl_2$ (up to 20 mM). It is also important to examine the secondary structure of the mutant protein using CD spectroscopy to determine whether the observed lack of activity is due to structural changes in the protein; although, this technique is limited in this capacity. X-Ray crystallography would be a very useful tool as well to assess structural perturbations. For D213N and E265Q mutants, it is not clear why the vectors did not respond to induction by IPTG which is similar to what was

observed for E239Q mutant and wild type TarD in this work and the work described previously by Gerlt and co-workers (Yew *et al*., 2006). However, it may still be possible to purify the mutant enzymes using metal ion affinity chromatography.

REFERENCES

Akiva, E., Brown, S., Almonacid, D. E., Barber, A. E., Custer, A. F., Hicks, M. A, Babbitt, P. C. (2014). The structure-function linkage database. *Nucleic Acids Research*, *42*, 521–530.

Asuncion, M., Blankenfeldt, W., Barlow, J. N., Gani, D., & Naismith, J. H. (2002). The structure of 3-methylaspartase from *Clostridium tetanomorphum* functions via the common enolase chemical step. *Journal of Biological Chemistry*, *277*(10), 8306–8311.

Babbitt, P. C., Hasson, M. S., Wedekind, J. E., Palmer, D. R. J., Barrett, W. C., Reed, G. H., Gerlt, J. A. (1996). The enolase superfamily: A general strategy for enzyme-catalyzed abstraction of the α-protons of carboxylic acids. *Biochemistry*, *35*(51), 16489–16501.

Bearne, S. L., White, R. L., MacDonnell, J. E., Bahrami, S., & Grønlund, J. (2001). Purification and characterization of β-methylaspartase from *Fusobacterium varium*. *Molecular and Cellular Biochemistry*, *221*(1-2), 117–126.

Cannan, R. K., & Kibrick, A. (1938). Complex formation between carboxylic acids and divalent metal cations. *Journal of the American Chemical Society*, *60*(10), 2314–2320.

Davies, D. D., & Kun, E. (1957). Isolation and properties of malic dehydrogenase from ox-heart mitochondria. *Biochemical Journal*, *66*(2), 307–316.

De Villiers, M., Veetil, V. P., Raj, H., De Villiers, J., & Poelarends, G. J. (2012). Catalytic mechanisms and biocatalytic applications of aspartate and methylaspartate ammonia lyases. *ACS Chemical Biology*, *7*(10), 1618–1628.

Doudoroff, M., & MacGee, J. (1954). A new phosphorylated intermediate in glucose oxidation. *The Journal of Biological Chemistry*, *210*(2), 617–626.

Fee, J. A., Hegeman, G. D., & Kenyon, G. L. (1974). Mandelate racemase from *Pseudomonas putida*. Subunit composition and absolute divalent metal ion requirement. *Biochemistry*, *13*(12), 2528–2532.

Gasteiger, E., Gattiker, A., Hoogland, C., Ivanyi, I., Appel, R. D., & Bairoch, A. (2003). ExPASy: The proteomics server for in-depth protein knowledge and analysis. *Nucleic Acids Research*, *31*(13), 3784–3788.

Gerlt, J. A, & Babbitt, P. C. (2001). Divergent evolution of enzymatic function: Mechanistically diverse superfamilies and functionally distinct suprafamilies. *Annu. Rev. Biochem.*, *70*, 209–246.

Gerlt, J. A., Babbitt, P. C., Jacobson, M. P., & Almo, S. C. (2012). Divergent evolution in enolase superfamily: Strategies for assigning functions. *Journal of Biological Chemistry*, *287*(1), 29–34.

Gerlt, J. A., Babbitt, P. C., & Rayment, I. (2005). Divergent evolution in the enolase superfamily: The interplay of mechanism and specificity. *Archives of Biochemistry and Biophysics*, *433*(1), 59–70.

Gerlt, J. A., & Gassman, P. G. (1993). Understanding the Rates of Certain Enzyme-Catalyzed Reactions: Proton abstraction from carbon acids, acyl-transfer reactions, and displacement reactions of phosphodiesters. *Biochemistry*, *32*(45), 11943–11952.

Gerlt, J. A., Kozarich, J. W., Kenyon, G. L., & Gassman, P. G. (1991). Electrophilic catalysis can explain the unexpected acidity of carbon acids in enzyme-catalyzed reactions. *Journal of the American Chemical Society*, *113*(25), 9667–9669.

Goda, S. K., Minton, N. P., Botting, N. P., & Gani, D. (1992). Cloning, sequencing, and expression in *Escherichia coli* of the *Clostridium tetanomorphum* gene encoding *β*-methylaspartase and characterization of the recombinant protein. *Biochemistry*, *31*, 10747–10756.

Gottlieb, H.E., Kotlyar, V., & Nudelman, A. (1997). NMR chemical shifts of common laboratory solvents as trace impurities. *J. Org. Chem*., *62*, 7512-7515.

Guthrie, J.P., & Kluger, R.. (1993). Electrostatic stabilization can explain the unexpected acidity of carbon acids in enzyme-catalyzed reactions. *J. Am. Chem. Soc.*, *115*, 11569.

Levy, C. W., Buckley, P. A., Sedelnikova, S., Kato, Y., Asano, Y., Rice, D. W., & Baker, P. J. (2002). Insights into enzyme evolution revealed by the structure of methylaspartate ammonia lyase. *Structure*, *10*(1), 105–113.

Nagar, M., Lietzan, A. D., Maurice, M. S., & Bearne, S. L. (2014). Potent inhibition of mandelate racemase by a fluorinated substrate-product analogue with a novel binding mode. *Biochemistry*, *53*, 1169–1178.

Nagar, M., Wyatt, B. N., St. Maurice, M., & Bearne, S. L. (2015). Inactivation of mandelate racemase by 3-hydroxypyruvate reveals a potential mechanistic link between enzyme superfamilies. *Biochemistry*, *54*(17), 2747–2757.

Ohkusa, T., Okayasu, I., Ogihara, T., Morita, K., Ogawa, M., & Sat. (2003). Induction of experimental ulcerative colitis by Fusobacterium varium isolated from colonic mucosa of patients with ulcerative colitis. *Gut*, *52*, 79–83.

Pollard, J. R., Richardson, S., Akhtar, M., Lasry, P., Neal, T., Botting, N. P., & Gani, D. (1999). Mechanism of 3-methylaspartase probed using deuterium and solvent isotope effects and active-site directed reagents: Identification of an essential cysteine residue. *Bioorganic and Medicinal Chemistry*, *7*(5), 949–975.

Raj, H., Weiner, B., Veetil, V. P., Reis, C. R., Quax, W. J., Janssen, D. B., Peolarends, G. J. (2009). Alteration of the diastereoselectivity of 3-methlaspartate ammonia lyase by using structure-based mutagenesis. *ChemBioChem*, *10*(13), 2236–2245.

Rakus, J. F., Fedorov, A. a, Fedorov, E. V, Glasner, M. E., Vick, J. E., Babbitt, P. C., Gerlt, J. A. (2007). Evolution of enzymatic activities in the enolase superfamily : D -mannonate dehydratase from No V *Osphingobium aromaticivorans*. *Biochemistry*, *46*(V), 12896–12908.

Rakus, J. F., Kalyanaraman, C., Fedorov, A. A., Fedorov, E. V., Mills-Groninger, F. P., Toro, R., Gerlt, J. A. (2009). Computation-facilitated assignment of the function in the enolase superfamily: A regiochemically distinct galactarate dehydratase from *Oceanobacillus iheyensis*. *Biochemistry*, *48*(48), 11546–11558.

Rode, H., & Giffhorn, F. (1982). Ferrous- or cobalt ion-dependent D-(-)-tartrate dehydratase of *Pseudomonads*: Purification and properties. *Journal of Bacteriology*, *151*(3), 1602–1604.

Sambrook, J. F. (1989). *Molecular cloning: a laboratory manual.* Cold Spring Harbor N.Y.: Cold Spring Harbor Laboratory.

Segel, I. H. (1975). *Enzyme Kinetics*. John Wiley & Sons, Inc., New York.

Shevchenko, A., Tomas, H., Havlis, J., Olsen, J. V, & Mann, M. (2007). In-gel digestion for mass spectrometric characterization of proteins and proteomes. *Nature Protocols*, *1*(6), 2856–2860.

Yew, W. S., Fedorov, A. a, Fedorov, E. V, Wood, B. M., Almo, S. C., & Gerlt, J. A. (2006). Evolution of enzymatic activities in the enolase superfamily : D -Tartrate dehydratase from *Bradyrhizobium japonicum*. *Biochemistry*, *45*(49), 14598–14608.

Yew, W. S., Fedorov, A. A., Fedorov, E. V., Almo, S. C., & Gerlt, J. A. (2007). Evolution of enzymatic activities in the enolase superfamily : L-Talarate/galactarate dehydratase from *Salmonella typhimurium* LT2. *Biochemistry*, *46*(33), 9564–9577.